QUANTUM THERMAL MACHINES IN COUPLED SPIN SYSTEMS

Ph.D. Thesis

by

Chayan Purkait

Department of Physics
Indian Institute of Technology Ropar
Rupnagar, Punjab 140001, India
March 2024

Quantum thermal machines in coupled spin systems

A thesis submitted

in partial fulfilment of the requirements

for the degree of

DOCTOR OF PHILOSOPHY

by

Chayan Purkait

(2018PHZ0001)

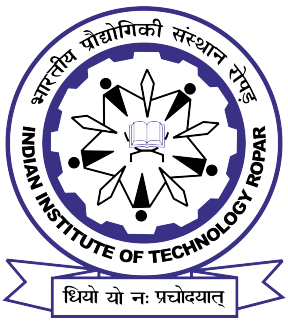

DEPARTMENT OF PHYSICS

INDIAN INSTITUTE OF TECHNOLOGY ROPAR

March 2024

To all my well-wishers

Declaration of Originality

I hereby declare that the work presented in the thesis titled **Quantum thermal machines in coupled spin systems** is the result of my own research carried out under the supervision of Dr. Asoka Biswas, Associate Professor, Department of Physics, Indian Institute of Technology Ropar. To the best of my knowledge, it is an original work, both in terms of research content and narrative, and has not been submitted or accepted elsewhere, in part or in full, for the award of any degree, diploma, fellowship, associateship, or similar title of any university or institution. Further, due credit has been attributed to the relevant state-of-the-art and collaborations with appropriate citations and acknowledgements, in line with established ethical norms and practices. I also declare that any idea/fact/source stated in my thesis has not been fabricated/falsified/misrepresented. All the principles of academic honesty and integrity have been followed. I fully understand that if the thesis is found to be unoriginal, fabricated, or plagiarized, the Institute reserves the right to withdraw the thesis from its archive and revoke the associated Degree conferred. Additionally, the Institute also reserves the right to appraise all concerned sections of society of the matter for their information and necessary action (if any). If accepted, I hereby consent for my thesis to be available online in the Institute's Open Access repository, inter-library loan, and the title & abstract to be made available to outside organizations.

Signature

Name: Chayan Purkait
Entry Number: 2018PHZ0001
Program: PhD
Department: Physics
Indian Institute of Technology Ropar
Rupnagar, Punjab 140001

March 2024

Acknowledgement

On this occasion, I would like to thank and express my sincere gratitude to the people who have selflessly supported me throughout my PhD journey.

First of all, I would like to thank my supervisor Dr. Asoka Biswas for giving me the opportunity to pursue my doctoral studies under her supervision. The present work would not have been possible without her guidance. I am deeply grateful to her for her insightful guidance, continuous support, and motivation throughout my PhD process. I would also like to express my deepest gratitude to Dr. Shubhrangshu Dasgupta for sharing his extensive knowledge of the subject and providing invaluable guidance.

I want to thank my doctoral committee members Dr. Mukesh Kumar, Dr. Saurav Bhattacharya and Dr. Arvind Kumar Gupta for their support and periodic evaluation of my work over the last five years of my PhD journey. I thank MHRD and IIT Ropar for supporting my doctoral studies with an institute fellowship. I am grateful to Anshu Vaid, a Physics Department staff member who helped me throughout and for the enjoyable time we spent in my PhD.

During this wonderful journey, I met some wonderful seniors like Suman Chand, Deepak Tomar, Basanta Kumar Paria, Rudra Narayan Sahoo and Shahariar Sarkar. I appreciate their constant guidance along with the good time we spent together, which helped me tremendously throughout my journey. I am especially thankful to Suman Da for many suggestions and interesting discussions. From him, I was inspired to work in the fascinating field of quantum thermodynamics. Also, I met some good people like Suman Das, Debarshi Saha, Suman Pradhan, Subhajit Saha and Mainak Pal who later became my friends. They made my journey easy and memorable. I express my sincere thanks and love to them from the bottom of my heart. My M.Sc. friends Manoj Kumar Kar and Biswarup Sengupta deserve my love and thanks. Furthermore, my childhood friends Amit Purkait and Dibyendu Ghosh. Also, I would like to thank my colleagues and lab mates Devender Garg, Chetan Waghela, Manju Maan, Nancy Ghangas, Jatin Ghildiyal and S R Rathnakaran for all the fun and many constructive conversations with them.

I would like to mention a few of my teachers Prof. Swapan Mandal and Dr. Amitava Bandyopadhyay in the Department of Physics at Visva Bharati, where I pursued my M.Sc. degree. Their excellent teaching methods sparked my interest in quantum optics and allied disciplines. Also, I would like to thank all the good teachers I was lucky to have on my entire journey.

In my life, I would not be where I am today without my family, especially my mother, father, and elder sister, who have shown me unconditional love and support. Thank you for believing in me and giving me a chance. You are the driving force behind all of this.

If I have forgotten to acknowledge anyone, please accept my thanks.

Chayan Purkait

Ropar, March 2024

Certificate

This is to certify that the thesis titled **Quantum thermal machines in coupled spin systems**, submitted by **Chayan Purkait (2018PHZ0001)** for the award of the degree of **Doctor of Philosophy** of Indian Institute of Technology Ropar, is a record of bonafide research work carried out under my guidance and supervision. To the best of my knowledge and belief, the work presented in this thesis is original and has not been submitted, either in part or full, for the award of any other degree, diploma, fellowship, associateship or similar title of any university or institution.

In my opinion, the thesis has reached the standard of fulfilling the requirements of the regulations relating to the Degree.

Signature of the Supervisor

Name: Dr. Asoka Biswas
Department: Physics
Indian Institute of Technology Ropar
Rupnagar, Punjab 140001

March 2024

Abstract

Classical thermodynamics deals with systems that contain many particles as long as they remain in equilibrium. Because of the existence of many particles, heat and work fluctuations are negligible with respect to their mean values. On the other hand, in the recent few years, people have been interested in studying the thermodynamics of quantum systems, even at the level of a single spin or an atom, with technological advances in the control and measurement of quantum systems and recent research interest in quantum devices. Also, apart from the academic need, novel quantum technologies can be created by harnessing quantum thermodynamic features. The study in quantum thermodynamics aims to develop a novel thermodynamic framework, that goes beyond conventional thermodynamics, the inclusion of non-equilibrium dynamics, and accounts for finite-size effects and explores the possible advantages of non-classical features, namely entanglement and quantum coherence, of the system. A major study in quantum thermodynamics involves quantum thermal machines (QTMs), primarily whether these machines can outperform their classical counterparts by exploiting quantum properties or other quantum mechanical behaviour in QTMs' performance.

In a so-called reciprocating heat-work cycle of a standard QTM, the coupling between the system and the heat baths is switched off and on, during the work extraction stage and the heating or cooling stage, respectively. In our work, we have focused on two different types of QTMs, namely, the Stirling engine and the Otto engine, and studied how their various stages can be implemented using a few-spin chain. We explore how spin-spin interaction can affect the operation and performance of these QTMs. We investigate how the cycle behaves as different thermal machines depending on the cycle parameters.

We study the performance of quantum Stirling machines near a quantum critical point in a two-spin working system, in which the nearest neighbour interaction of the Heisenberg-XX type couples the spins. We show how this system can exhibit a QPT which is examined by the measure of entanglement and correlation.

We show that at the QCP, the engine efficiency and the coefficient of performance of the refrigerator attain corresponding values of their Carnot counterparts, along with maximum work output. We analyze how such enhancement can be attributed to the non-analytic behaviour of spin-spin correlation and entanglement near the QCP.

We study quantum Otto thermal engines with a two-spin working system coupled by anisotropic interaction. Also, we consider two scenarios of fueling the engines, one

by a heat bath and another by non-selective quantum measurements. We investigate how a measurement-based QOE behaves differently from a standard QOE in finite time. We introduce the case of a QOE operating with a local spin working system. We discuss different thermodynamic figures of merit of local QOE operation. We aim to find the role of anisotropy in the performance of various HEs operating in various timeframes. We discuss the effect of quantum internal friction that arises due to finite-time unitary time evolution processes. We show that for anisotropic interaction, the efficiency of a measurement-based and local spin engine oscillates in finite times. Therefore, for a suitable choice of timing of the unitary processes in the short time regime, the engine can have a higher work output and less heat absorption, such that it works more efficiently than a quasi-static engine. We analytically show that this oscillation comes into the picture through an interference-like effect between two probability amplitudes. Finally, we discuss the case of an always-on heat bath.

Keywords: Quantum Thermodynamics; Quantum Thermal Machine; Quantum Stirling heat engine and refrigerator; Quantum Otto engine; Heisenberg XY model; Quantum phase transition; Quantum Measurement; Open quantum system.

Thesis Based on List of Papers

1. Chayan Purkait and Asoka Biswas, *Performance of Heisenberg-coupled spins as quantum Stirling heat machine near quantum critical point*, Physics Letters A 442 128180 (2022)

2. Chayan Purkait and Asoka Biswas, *Measurement-based quantum Otto engine with a two-spin system coupled by anisotropic interaction: Enhanced efficiency at finite times*, Phys. Rev. E 107, 054110 (2023).

3. Chayan Purkait, Suman Chand and Asoka Biswas, *Anisotropy-assisted thermodynamic advantage of a local-spin thermal machine*, preprint arXiv:2309.04757

Contents

List of Figures

Chapter 1

Introduction

1.1 Classical thermodynamics

Water, wind and animals could convert one form of motion into another form. In the 18th century, with the invention of the steam engine, heat could be converted into mechanical motion. Therefore, an exciting possibility opened up that was different from others fundamentally. It not only led to the industrial revolution in human civilization but also created a novel area of study in science: thermodynamics. Newtonian mechanics developed to describe heavenly bodies' motion. Unlike that, thermodynamics emerged for a more practical reason, to explain motion generation from heat. Thermodynamics began with the study of heat and motion generated by it. Later on, this merged with the larger perspective of energy studies and the transformation of one form into another. Thermodynamics is developed into a theory that describes changes in matter states. The motion produced by heat is caused by certain changes in matter states [3, 4, 5].

Thermodynamics witnessed the rise and decline of many theories. It also survived the big physics revolutions in the 19th century. Einstein's take on thermodynamics: **"It is the only physical theory of universal content, which I am convinced, that within the framework of applicability of its basic concepts will never be overthrown."**

Every theory consults thermodynamics for advice and adheres to thermodynamic concepts, so it is consistent with thermodynamic laws. The thermodynamic laws make no hypotheses about the microscopic or small-scale details of matter. It is concerned only with the macroscopic or large-scale properties of matter which makes it different from other theories. Among all the physical laws, the laws of thermodynamics affect our everyday lives the most. It finds application in refrigerators, power plants, boats, spacecraft, aircraft, cars, wind turbines, food processing, and the human body. Also, thermodynamic tools have been widely used to study the physics of massive black holes.

1.1.1 Laws of classical thermodynamics

The thermodynamic laws provide the framework for understanding thermodynamic processes all around us. We use a part of the universe to conduct our studies, known as the 'system'. The rest of the part, also referred to as the universe, which excludes the system, is called the 'environment'. In thermodynamic terminology, this environment is also known as a reservoir or bath. This bath is assumed to be very large with an infinite heat capacity (for a heat bath), such that its property does not change with interaction with a system.

A system can be classified as closed, open, or isolated, based on how matter and energy are transferred between the system and its environment. In an isolated system, neither matter nor energy can be transferred between the system and its environment. In a closed system, energy (in the form of heat or work) can be transferred between the system and its environment, but matter cannot enter or leave the system. Whereas, open systems exchange matter and energy with their environment.

In the following, we describe the four laws of classical thermodynamics. Depending on them, we can define various physical quantities like temperature, energy and entropy for a thermodynamic system at thermal equilibrium.

Zeroth Law :

The exchange of energy and/or matter between two or more systems eventually leads to a thermal equilibrium of the systems. In this case, all systems have the same temperature, and this temperature is spatially uniform within each system. The thermal equilibrium of system A with a second system B, and the B with a third system C, implies that C is in thermal equilibrium with A. This is often referred to as the Zeroth Law. Hence, the systems in equilibrium have a spatially uniform and well-defined temperature [3, 4, 5].

First Law :

In today's world, the quest for energy is one of the most essential endeavours. For all thermodynamic systems of different types, energy represents an extensive property. The energy of a system can be measured against a reference state whose energy is assumed to be zero. If a system can lift a weight that means it has a certain amount of energy. The more energy it has, the more weight it can lift. This criterion applies to all types of energy.

A system can store energy in three ways. The kinetic and potential energy come under macroscopic forms. So to change them, the system must change position or

velocity. However, all microscopic forms of energy storage are included in internal energy. However, internal energy comes under microscopic forms of energy storage. The change in the internal energy of a system does not arise from displacement. Instead, it arises from changes in its temperature, pressure, and electrical state.

Also, energy can be exchanged from a system or to a system in two ways, in the form of heat (Q) or work (W). Heat transfer is an uncontrollable form of energy transfer, that occurs on a microscopic level, not associated with macroscopic displacement. Work is the form of the transfer of energy due to some external control parameters viz., for a change in magnetization $\vec{M}$, $dU = \vec{B}.d\vec{M}$ where $\vec{B}$ represents the magnetic field, or change in volume V, it becomes for a $dU = -PdV$, which is a controllable form of energy transfer, without any temperature difference across the boundary of a closed system.

In thermodynamics, the first law represents the conservation of energy. It states that the change in the internal energy of a closed system is given by the sum of work done and heat transferred to it. Mathematically this can be stated as

$$dU = \delta Q + \delta W, \tag{1.1}$$

where δQ and δW represent the heat and work, respectively, infinitesimally. Non-exact differentials are represented here by δ and correspond to path dependence i.e., they are not state functions. Therefore, heat and work do not represent observables [3, 4, 5, 6].

Entropy and Second Law of thermodynamics :

The concept of a reversible cycle and heat engine was introduced by Sadi Carnot. This cycle is known as the Carnot cycle. After a detailed investigation of a reversible heat engine performance, he reached a conclusion, known as Carnot's theorem. This states that a reversible engine delivers maximum efficiency, which is given by

$$\eta = 1 - \frac{Q_2}{Q_1} = 1 - \frac{T_2}{T_1}, \tag{1.2}$$

where T_1 and T_2 represent the temperatures of the cold and hot baths, respectively, in absolute value. If an ideal reversible heat engine absorbs Q_1 amount of heat from a hot bath at temperature T_1 and releases Q_2 amount of heat to a cold bath at temperature T_2, we can write, from **Eq. 1.2**,

$$\frac{Q_1}{T_1} = \frac{Q_2}{T_2}. \tag{1.3}$$

Actually, all real-life heat engines need to operate in finite time cycles to produce a finite amount of power. Because of that, they operate irreversibly due to the existence of heat flow across a temperature gradient. This makes them less efficient. We get lower efficiency from them than from a heat engine which functions reversibly, i.e.

$$\eta' = 1 - \frac{Q_2}{Q_1} \leq 1 - \frac{T_2}{T_1}, \tag{1.4}$$

which implies in the case of irreversible processes $T_2/T_1 \leq Q_2/Q_1$. Therefore, the inequality for a cycle with irreversibility is given by

$$\frac{Q_1}{T_1} < \frac{Q_2}{T_2}. \tag{1.5}$$

The generalizations of the expressions (**Eq. 1.3, 1.4**, **1.5**) were made by Rudolf Clausius for an arbitrary cycle. By considering an arbitrarily closed loop as consisting of many tiny Carnot cycles, he arrived at

$$\oint \frac{dQ}{T} = 0, \tag{1.6}$$

where heat absorption by the system is given by $\mathrm{d}Q \geq 0$ and heat release by the system is given $\mathrm{d}Q \leq 0$.

From **Eq. 1.6**, Clausius showed that in a reversible process, a new function S can be defined that depends only on the initial and final states. For a system if A and B are the states before and after a process, and if S_A and S_B represent the function at those states, then we have

$$S_\mathrm{B} - S_\mathrm{A} = \int_\mathrm{A}^\mathrm{B} \frac{\mathrm{d}Q}{T} \text{ or } \mathrm{d}S = \frac{\mathrm{d}Q}{T}. \tag{1.7}$$

In 1865, Clausius first introduced this new quantity, which he called entropy.

For a system which follows an arbitrary cycle, and also consists of irreversible processes, Clausius got

$$\oint \frac{\mathrm{d}Q}{T} \leq 0, \tag{1.8}$$

where equalities hold for reversible processes and inequalities hold for irreversible processes.

Ultimately, in a cyclic process, the changes in the entropy of a system are summarized as follows:

$$\begin{array}{ll} \text{Cyclic reversible process:} & \mathrm{d}S = \frac{\mathrm{d}Q}{T}, \oint \mathrm{d}S = \oint \frac{\mathrm{d}Q}{T} = 0 \\ \text{Cyclic irreversible cycle:} & \mathrm{d}S > \frac{\mathrm{d}Q}{T}, \oint \mathrm{d}S = 0, \quad \oint \frac{\mathrm{d}Q}{T} < 0 \end{array} \tag{1.9}$$

These mathematical relations can be understood in this way, at the end of a cyclic process, the entropy of the system does not change irrespective of the reversible or irreversible nature of the processes because, at the end of the cycle, it returned to its initial state. This signifies that, in an irreversible cycle the system releases more heat to the outside. This is because, in an irreversible process, mechanical energy is generally transformed into heat. This increases entropy on the outside of the system.

Combining above all relations, Clausius inequality is expressed as:

$$\mathrm{d}S \geq \frac{\mathrm{d}Q}{T}, \tag{1.10}$$

This is the mathematical form of the Clausius version of the second law of thermodynamics.

In nature, no system undergoes a cyclic process and returns to its initial state without increasing its environment's entropy. The future is distinguished from the past by the irreversible nature of every natural process which increases entropy. Therefore, the second law of thermodynamics shows an arrow of time [3, 4, 5].

Third Law :

The above mathematical formalism enables us to determine only changes in entropy. The absolute value of entropy can't be determined, but it can only be calculated with an additive constant. Walther Nernst formulated a law in 1906 that states that the entropy of all systems approaches zero as the temperature becomes zero:

$$S \Rightarrow 0 \text{ as } T \Rightarrow 0.$$

This law is called the Third Law in thermodynamics. This law allows us to determine entropy's absolute value. However, the physical foundation of this law is in the behaviour of matter at low temperatures, which can only be understood through quantum mechanics [3, 4, 5].

1.1.2 Classical Thermal Machines

Heat is a form of energy that remains distributed among all degrees of freedom. In contrast, work is a form of energy that is not distributed among all the degrees of freedom in the system. As a result, heat cannot be used as a form of energy. On the other hand, work remains concentrated in a few degrees of freedom, so that energy can be utilized. Despite the different energy sources around us, we get most of our energy in the form of heat. So, to make it useful we need heat engines [3, 4, 5, 7].

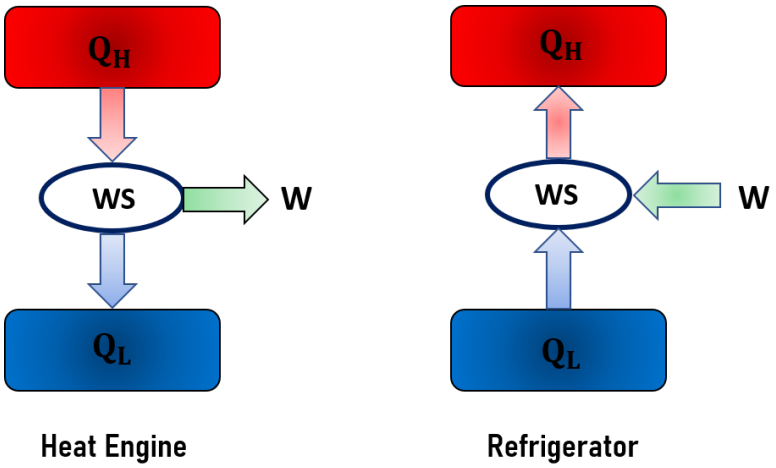

Figure 1.1: Schematic diagram of thermal machines

A heat engine is a system that converts heat into work, whereas a refrigerator system converts work into heat. A heat engine is a device that does some amount of work (W_{net}) on its surroundings at the cost of heat (Q_{in}) absorbed by it. Normally, thermal machines operate in thermodynamic cycles, which is essential to operate them continuously. If we supply heat or work to these thermal machines, they will do their jobs [6]. According to Carnot's analysis 'a motive force can be generated if there exists a temperature difference'. An engine that uses heat flows between two heat baths that have different temperatures to produce work. A portion of energy, in the form of usable energy such as mechanical work, from the flow of heat from a hot bath to a cold bath is attracted by heat engines [5]. Whereas, a refrigerator cools down the temperature of a targeted body with the help of a work supply from the outside.

A thermal machine (heat engine or refrigerator) consists of a working medium and two heat baths, one acting as a heat source and one as a heat sink. Schematic diagrams of thermal machines are shown in **Fig. 1.1**. For a heat engine operation, $Q_H > 0$ amount of heat is absorbed from a hot bath at temperature T_H by the heat engine to perform $W > 0$ amount of work on its surroundings. It finally releases $Q_L < 0$ amount of heat to a heat sink at temperature T_L. In that case, heat engine efficiency can be defined as the engine's ability to transform heat into work. An engine's efficiency can be mathematically represented as follows:

$$\eta = \frac{W}{Q_H} = \frac{Q_H - |Q_L|}{Q_H}. \tag{1.11}$$

For the refrigerator operation, $Q_L > 0$ amount of heat is absorbed from a cold bath at temperature T_L with the help of $W > 0$ amount of work from the outside. It finally releases $Q_H < 0$ amount of heat to a hot bath at temperature T_H. The

merit of the performance of a refrigerator can be defined as the ability to extract heat from the cold body by using external work. The coefficient of performance (COP) of a refrigerator can be mathematically presented as follows:

$$\eta = \frac{|Q_L|}{W} = \frac{|Q_L|}{Q_H - |Q_L|}. \tag{1.12}$$

The other two types of operation of a thermodynamic cycle are accelerator and heater. The cycle acts as a thermal accelerator when heat flows in the natural direction, i.e. $Q_H > 0$ and $Q_H < 0$, with the help of work is done ($W > 0$) on the system [8, 9]. The cycle operates as a heater when the system releases heat to both the hot and cold heat baths, i.e. $Q_H < 0$ and $Q_L < 0$, with the assistance of work done ($W > 0$) on the system [8, 9].

Depending on the nature of the thermodynamic cycles the working substances go through, there are various reciprocating thermal machines. The different types of thermodynamic cycles are described below.

Carnot Cycle

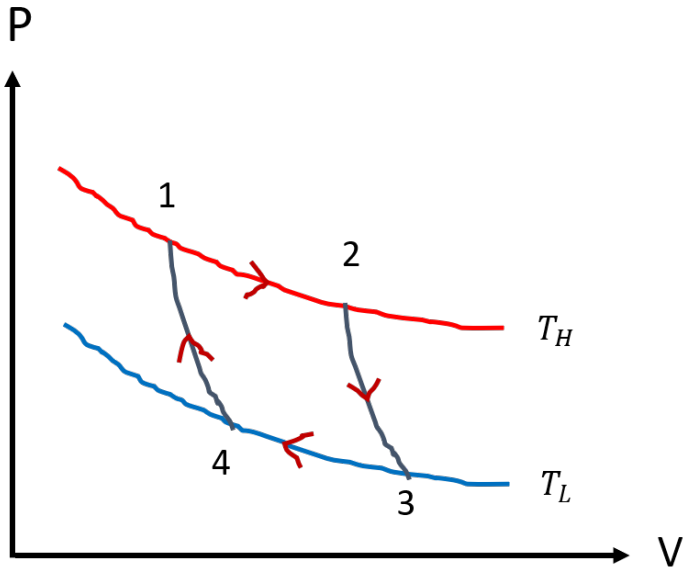

Figure 1.2: Carnot cycle on a pressure (P) versus volume (V) plane. The strokes $1 \to 2$ and $3 \to 4$ are isothermal and the $2 \to 3$ and $4 \to 1$ are adiabatic processes.

In the Carnot cycle, there are two adiabatic and two isothermal processes. Heat is exchanged between a working substance and a heat bath in an isothermal process. Also, an external control parameter, mainly the volume, of the system is slowly varied such that the system maintains thermal equilibrium with the bath. So, the

system's temperature remains fixed in this process. In an adiabatic process, there is no exchange of heat between a system and a heat bath, so in this process, the system's entropy remains constant. So, this represents an isentropic process. A schematic diagram of the Carnot cycle is shown in **Fig. 1.2**. The Carnot cycle is an idealised reversible cycle. In reality, we can't build a heat engine that follows the Carnot cycle.

Otto Cycle

In an Otto cycle, there are two isochoric and two adiabatic processes. In an isochoric process, the external control parameter, here mainly the volume, remains fixed but heat is exchanged between the system and a heat bath. The schematic diagram of an Otto cycle is shown in **Fig. 1.3**. The Otto engine is a practical version of heat engines. This is an internal combustion engine.

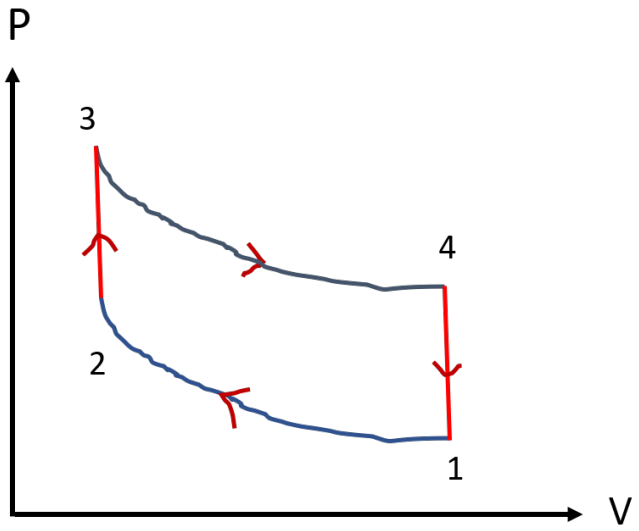

Figure 1.3: Otto cycle on a pressure (P) versus volume (V) plane. The strokes $1 \rightarrow 2$ and $3 \rightarrow 4$ represent adiabatic processes, while the strokes $2 \rightarrow 3$ and $4 \rightarrow 1$ represent isochoric processes.

Stirling Cycle

In a Stirling cycle, there are two isothermal and two isochoric processes. The schematic diagram of a Stirling cycle is shown in **Fig. 1.4**. Stirling heat engine is an external combustion engine.

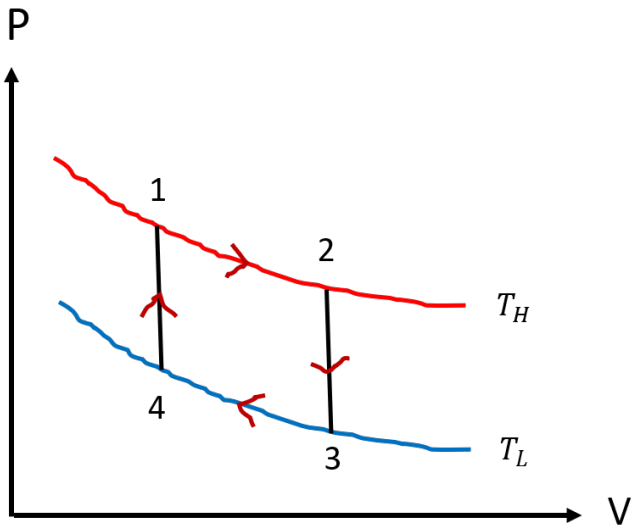

Figure 1.4: Stirling cycle on a pressure (P) versus volume (V) plane. The strokes $1 \rightarrow 2$ and $3 \rightarrow 4$ are isothermal and the $2 \rightarrow 3$ and $4 \rightarrow 1$ are isochoric processes.

1.2 Stochastic Thermodynamics

In classical thermodynamics, the thermodynamic behaviour of large complex systems, consisting of many microscopic particles, is described by a few macroscopic quantities including heat, work and entropy. With the consideration of smaller and smaller system sizes, fluctuations in these quantities (work, heat, and entropy fluctuate, but energy, volume, and the number of particles do not fluctuate) can't be neglected and become increasingly relevant. These are tackled in stochastic thermodynamics [10]. Also, stochastic thermodynamics describes the non-equilibrium behaviour of systems using (non-equilibrium) statistical mechanics [11]. The study of fluctuations in thermodynamic quantities gives us the discovery of fluctuation theorems like universal relations [10].

1.2.1 Information and Thermodynamics

The second law of thermodynamics has fallen into existential crises several times in the past. Most notable is when its validity was challenged by a thought experiment proposed by Maxwell. Today, this is referred to as Maxwell's Demon [12, 13, 14]. This created a path for discovering the link between thermodynamics and information.

In the thought experiment [12, 13, 14, 15], Maxwell imagined a box that contained two compartments, which were filled with gas. Gas particles are in thermal equilibrium and move randomly, although the gas temperature fixes their mean

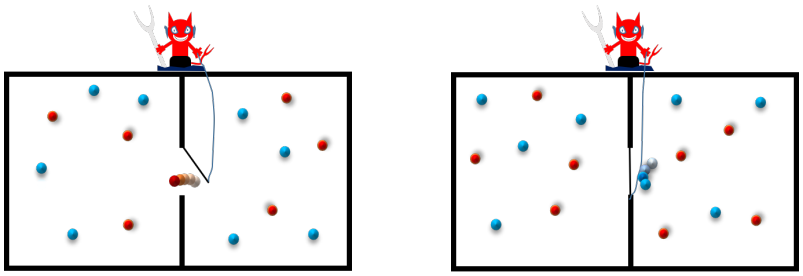

Figure 1.5: Schematic diagram of Maxwell's demon. Source: [1]

velocity. Maxwell considered that there was a partitioned wall that connected two compartments and a window on the wall. The window had a handle to open it. A demon, also known as Maxwell's demon, has the ability to monitor individual particles and is set to operate the window. It opens the window to particles moving fast from the right side of the box and coming slowly from the left side of the box. Consequently, the particles in the left compartment will have a higher velocity than the average and the particles in the right compartment will have a lower velocity. Therefore, the left compartment will have a higher gas temperature than the right compartment. Using the temperature difference between these two compartments a heat flow can be generated and work can be extracted from there. Therefore, the demon can decrease the system's total entropy and energy can be extracted "for free", which violates the second law. Here, it is assumed that the handle is frictionless so that the demon can move the handle without performing any work himself.

After several years of this paradox proposal, a significant step towards solving this was taken by Szilard. Based on the idea of Maxwell's demon, he proposed a thought experiment. Today it is known as the Szilard engine [16, 12, 13, 14], which is a minimal version of Maxwell's proposal.

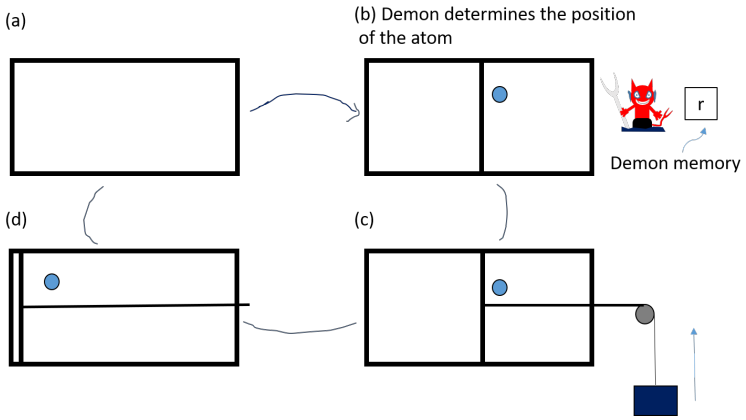

Figure 1.6: Schematic diagram of Szilard engine. Source: [2]

He considered a cylinder containing a single-molecule gas and a heat bath

attached to the cylinder. In the beginning, to split the cylinder volume into two equal portions, a demon puts a piston in the middle of the cylinder. Therefore, the probability of finding the molecule on either side of the piston is 1/2. Then a measurement is performed by the demon to determine on which side of the piston the molecule is located. Based on the outcome of the measurement, a string is attached to the piston on the same side of the molecule. To the open end of the string, a hanging weight is attached. Here, the weight is small enough, therefore collisions of the molecule drive the piston in the opposite direction of the hanging weight. This makes lifting the weight, which does a work W against gravity. The piston is removed when it reaches the end of the cylinder, therefore the whole volume of the cylinder is occupied by the single-molecule gas and the cycle can be started again. Thus, the net result of the cycle is, in the isothermal reversible expansion there takes place a complete conversion of the heat absorbed Q from the heat bath into work W_{ext} as long as there is no cost associated with insertion and removal of the piston (because these operations can be performed reversibly). The work done in this process

$$W = \int dW = \int_{\frac{V_0}{2}}^{V_0} PdV = \int_{\frac{V_0}{2}}^{V_0} \frac{k_B T}{V} dV = k_B T \ln 2.$$

As the one-molecule gas returns to the same initial state after a complete cycle i.e., $\Delta S_{gas} = 0$. But, as the gas absorbs heat from the heat bath, the bath entropy is decreased by an amount $k_B \ln 2$, which yields $\Delta S_{total} < 0$. Therefore, the machine appears to violate the second law: "A heat engine operating in a cycle can completely covert the heat absorbed from a heat bath to mechanical work".

Szilard tried to recover the second law by arguing that for the reduction in the bath's entropy, the entropy in other parts of the system must increase for compensation. Later Brillouin tried to explain that it is the act of measurements, i.e. acquisition of information [17, 12, 13, 14], which leads to an increase in entropy. So, to extract work of a certain amount, there must be the same amount of cost has to be compensated by increasing the entropy. This was the first proposal on the link between thermodynamics and information.

The paradox was finally resolved by Charles Bennett, who linked Landauer's bound and Maxwell's demon [18, 19]. According to him, the demon retains a memory about the location of the one-molecule gas (left or right of the piston) in the cylinder. Therefore, to close the cycle successfully, the memory needs to be reset (or erased). Further, he argued that the acquisition of information by measurements i.e., any computation can be carried out reversibly, without costing any energy[18, 19].

In a separate study by Landauer [20, 12, 13, 14], he formulated the minimal energy cost for memory erasing in a computer. According to this, the minimum energy cost (which is dissipated as heat) to erase one bit of information from a system, maintaining contact with a heat bath at temperature T, is given by $k_B T \ln 2$, this is referred to as Landauer's bound. To maintain a constant amount of internal energy in the working system, this amount of energy must be compensated by an invested work of equal amount $W_{eras} = Q_{eras}$.

Bennett introduced Landauer's erasure principle in his proposal. To start the next cycle we must erase the demon's memory, as it retains information from the preceding cycle [18, 19]. This costs energy and implies that no network is extracted in a complete cycle. From the perspective of entropy, the reduction in bath entropy is exactly compensated for by an increase in entropy when the demon memory is erased. Therefore, the total entropy change in a complete cycle is $\Delta S_{tot} = 0$. Thus, the second law is recovered.

1.3 Quantum Thermodynamics

The field of quantum technologies is rapidly progressing with the creation of smaller and smaller devices. Also, state-of-the-art technology gives us ultrafast experimental control over quantum systems. As a result of these developments, understanding quantum thermodynamics has become increasingly important. This demand pushes the limits of conventional thermodynamics to construct quantum thermodynamics [21, 22, 23, 24]. In addition to that, understanding the thermodynamics of quantum systems may also have an impact on uncovering novel technologies harnessing quantum thermodynamic features [21, 22, 23, 24].

Quantum thermodynamics studies how thermodynamic laws emerge from quantum mechanics and whether the laws are valid in systems which are far from equilibrium. The study is based on two separate but consistent physical theories, namely, thermodynamics and quantum mechanics, and shows how quantum phenomena affect heat engines and refrigerators. Quantum mechanics provides the dynamical framework for thermodynamics, providing a solid foundation for finite-time thermodynamics. This framework takes into consideration different exotic properties of the systems such as finite-size effects, non-equilibrium scenarios, and non-classical properties of the systems (quantum correlations, coherence) which we don't consider in traditional thermodynamics.

1.3.1 Quantum Version of the Laws of Thermodynamics

Zeroth Law

In macroscopic thermodynamics, the concept of thermal equilibrium is described as an equivalence relation between states under the Zeroth Law. The parameter temperature characterizes different equivalence classes.

A different scenario exists for thermodynamics at the microscopic level [25], due to quantum properties, such as quantum correlation. This gives us novel insights into thermodynamics. In general, it is considered that there is no correlation between the system and the bath in any thermodynamic process. However, correlations may appear during a process. System-environment correlation can violate the Zeroth law. In that case, we need a modification to the equilibrium concept beyond the well-known equivalence relation.

In a recent study [26], the authors showed a way to define the zeroth law in a generalized form in the case of system-environment correlation. As per them if work can't be extracted under entropy-preserving operations from any of pairs in a set of states $\{\rho_X\}_X$ then they are in mutual equilibrium with each other. This happens only when there is no correlation among all the parties X, and a thermal state is maintained by each of them at the same temperature.

The first law of thermodynamics under time-dependent Hamiltonians

In quantum thermodynamics, normally an external agent drives a system by an external control parameter $\lambda(t)$ of the system to extract work. Therefore, the system becomes time-dependent represented by a Hamiltonian of a time-dependent nature, where the control parameter's time dependence introduces time dependence in the system.

Now we will introduce the definition of work and heat for a time-dependent system. Then we will discuss the quantum version of the first law of thermodynamics with the help of these definitions.

Definition of heat, work and the first law of the thermodynamics :

Let us consider that a system is driven by an external agent, so it is represented by a time-dependent Hamiltonian $H(\lambda(t))$. The state of the system is represented by the density matrix $\rho(t)$ at time t. Also $U(t) = \mathrm{Tr}[\rho(t)H(\lambda(t))]$ represents the system's average internal energy at an instant. Therefore, the change in average

internal energy is given by

$$\Delta U = \mathrm{Tr}[\rho(\tau)H(\lambda(\tau))] - \mathrm{Tr}[\rho(0)H(\lambda(0))], \tag{1.13}$$

for a time interval $0 \leq t \leq \tau$. Again, from the derivative of the average internal energy $U(t)$ with respect to time t we can rewrite the **Eq. 1.13**, so we get

$$\begin{aligned} \Delta U &= \int_0^\tau dt \frac{d}{dt} \mathrm{Tr}[\rho(t)H(\lambda(t))] \\ &= \int_0^\tau dt \left(\mathrm{Tr}\left[\frac{d\rho(t)}{dt} H(\lambda(t))\right] + \mathrm{Tr}\left[\rho(t)\frac{dH(\lambda(t))}{dt}\right]\right). \end{aligned} \tag{1.14}$$

Now, we know that work is the form of energy which is transferred due to the variation of external control parameters of a system. Whereas heat transfer is associated with the change in system entropy, without any variation in the Hamiltonian of the system. Therefore, we can identify the contribution of work and heat to the total change in system energy as follows.

The average value of work and the average value of heat are given by [27, 15]

$$\begin{aligned} \langle Q \rangle &= \int_0^\tau dt\, \mathrm{Tr}\left[\frac{d\rho(t)}{dt} H(\lambda(t))\right], \\ \langle W \rangle &= \int_0^\tau dt\, \mathrm{Tr}\left[\rho(t)\frac{dH(\lambda(t))}{dt}\right]. \end{aligned} \tag{1.15}$$

Now, from **Eq. 1.14** and the definition of work and heat (**Eq. 1.15**), we can arrive at the first law of thermodynamics for quantum systems [27, 15]

$$\Delta U = \langle Q \rangle + \langle W \rangle. \tag{1.16}$$

Also, we can see from the definitions (**Eq. 1.15**, **1.13**) that the variation in system internal energy depends on the states at the beginning and final point only. In contrast, heat and work are process-dependent, therefore, the value of heat and work varies depending on which path is followed by the system due to the external control from $\lambda(0)$ to $\lambda(\tau)$. Therefore, the exact differential dU in an infinitesimal process divides into two parts, δQ and δW, which are not exact differentials. Therefore, in a cyclic process, where $\rho_0 = \rho_\tau$, and $\hat{H}\left(\lambda(\tau)\right) = \hat{H}\left(\lambda(0)\right)$, the change in internal energy $\Delta U = 0$, but heat and work, in general, are nonzero, gives rise to $W_{\mathrm{cyc}} = -Q_{\mathrm{cyc}}$ [27, 15].

Second Law

Consider a system S that interacts with a heat bath B, the inverse temperature of the bath is β. The total Hamiltonian of the system and bath is given by [27, 28]

$$H_{\text{tot}}(t) = H_{\text{S}}(t) + H_{\text{B}} + V_{\text{SB}}(t), \tag{1.17}$$

where $H_{\text{S}}(t)$ represents the driven system, H_{B} represents the bath and $V_{SB}(t)$ represent the interaction between them. Work done externally drives the system out of equilibrium, whereas a few classical parameters represent the external drive which introduces the time dependence in $H_{\text{S}}(t)$ and H_{B} is independent of time. Here we are assuming that there is a single heat bath and the external control is operated from the time 0 to τ.

We assume that the initial state of the driven system and the heat bath composite system is represented by a separable state

$$\rho(0) = \rho_{\text{S}}(0) \otimes \rho_{\text{B}}^{\text{eq}}, \quad \rho_{\text{B}}^{\text{eq}} := \frac{e^{-\beta H_{\text{B}}}}{\text{Tr}\left[e^{-\beta H_{\text{B}}}\right]},$$

where the heat bath is in the thermal equilibrium Gibbs state at an inverse temperature β. The time evolution of the composite system is governed by the Schrodinger equation. Then the composite system has the following final state: $\rho_{\text{SB}}(\tau) = U_{\text{SB}}\rho_{\text{SB}}(0)U_{\text{SB}}^{\dagger}$, where $U_{\text{SB}} = \text{T}\exp\left(-\frac{i}{\hbar}\int_0^\tau dt H_{\text{tot}}(t)\right)$ represents the time-evolution operator of unitary type and T represents the time-ordering operator.

Second law and relative entropy -

We consider that the von Neumann entropy $S(\rho) := -\text{Tr}[\rho \ln \rho]$ represents the entropy (nonequilibrium) of a system. Then, in the composite system (SB), the total entropy production in a non-equilibrium process is given by

$$\Sigma := \Delta S - \beta\langle Q\rangle, \tag{1.18}$$

where in the driven system the variation in von Neumann entropy is represented by $\Delta S := S\left(\rho_{\text{S}}(\tau)\right) - S\left(\rho_{\text{S}}(0)\right)$, and the heat absorption by the system is represented by [29, 28]

$$\langle Q\rangle := \text{Tr}\left[\rho_{\text{B}}^{\text{eq}} H_{\text{B}}\right] - \text{Tr}\left[\rho_{\text{B}}(\tau) H_{\text{B}}\right], \tag{1.19}$$

and the bath entropy change is given by $-\beta\langle Q\rangle$. The quantity Σ represents an important parameter that quantifies the irreversibility in non-equilibrium processes.

Again, we know that under a unitary transformation, the von Neumann entropy

remains unchanged, therefore for the composite system we can write [27]

$$\begin{aligned} S(\rho(\tau)) = S(\rho(0)) &= S\left(\rho_{\mathrm{S}}(0)\right) + S\left(\rho_{\mathrm{B}}^{\mathrm{eq}}\right) \\ &= S\left(\rho_{\mathrm{S}}(0)\right) - \mathrm{Tr}\left[\rho_{\mathrm{B}}^{\mathrm{eq}} \log \rho_{\mathrm{B}}^{\mathrm{eq}}\right]. \end{aligned} \tag{1.20}$$

Now, the variation in the driven system entropy using the **Eq. 1.20** is given by

$$\begin{aligned} \Delta S &:= S\left(\rho_{\mathrm{S}}(\tau)\right) - S\left(\rho_{\mathrm{S}}(0)\right) \\ &= S\left(\rho_{\mathrm{S}}(\tau)\right) - S(\rho(\tau)) - \mathrm{Tr}\left[\rho_{\mathrm{B}}^{\mathrm{eq}} \log \rho_{\mathrm{B}}^{\mathrm{eq}}\right] \\ &= -\mathrm{Tr}\left[\rho_S(\tau) \log \rho_{\mathrm{S}}(\tau)\right] + \mathrm{Tr}[\rho(\tau) \log \rho(\tau)] - \mathrm{Tr}\left[\rho_{\mathrm{B}}^{\mathrm{eq}} \log \rho_{\mathrm{B}}^{\mathrm{eq}}\right] \end{aligned} \tag{1.21}$$

Again, from the **Eq. 1.20**, we can get

$$\begin{aligned} \beta\langle Q\rangle &= \beta\left(\mathrm{Tr}\left[\rho_{\mathrm{B}}^{\mathrm{eq}} H_{\mathrm{B}}\right] - \mathrm{Tr}\left[\rho_B(\tau) H_{\mathrm{B}}\right]\right) \\ &= \mathrm{Tr}\left[\rho_B(\tau) \log e^{-\beta H_{\mathrm{B}}}\right] - \mathrm{Tr}\left[\rho_{\mathrm{B}}^{\mathrm{eq}} \log e^{-\beta H_{\mathrm{B}}}\right] \\ &= \mathrm{Tr}\left[\rho(\tau) \log \rho_{\mathrm{B}}^{\mathrm{eq}}\right] - \mathrm{Tr}\left[\rho_{\mathrm{B}}^{\mathrm{eq}} \log \rho_{\mathrm{B}}^{\mathrm{eq}}\right]. \end{aligned} \tag{1.22}$$

Now, if we put ΔS and $\beta\langle Q\rangle$ in **Eq. 1.18**, the total entropy production Σ can be connected to the quantum relative entropy $S(\rho\|\sigma) := \mathrm{Tr}[\rho \ln \rho] - \mathrm{Tr}[\rho \ln \sigma]$ [30, 31] which as follows:

$$\Sigma = S\left(\rho_{\mathrm{SB}}(\tau) \| \rho_{\mathrm{S}}(\tau) \otimes \rho_{\mathrm{B}}^{\mathrm{G}}\right). \tag{1.23}$$

As the quantum relative entropy is non-negative [28, 32], we get

$$\Sigma = \Delta S - \beta\langle Q\rangle \geq 0. \tag{1.24}$$

This represents the Clausius form of the second law of thermodynamics for quantum systems. This form is similar to the classical version of the second law of thermodynamics as shown in **Eq. 1.10**.

Also, we can connect entropy production to work extraction, and it is possible to derive a work extraction bound. In order to do that, we define nonequilibrium-free energy [33, 34, 35, 36] as

$$F(\rho; H) := \mathrm{Tr}[\rho H] - \beta^{-1} S(\rho), \tag{1.25}$$

which is analogous to the Helmholtz free energy $F = E - TS$ in macroscopic thermodynamics. Therefore, we have

$$\begin{aligned} \Delta F &:= F(\rho(\tau); H(\tau)) - F(\rho(0); H(0)) \\ &= \Delta U - \beta^{-1} \Delta S, \end{aligned} \tag{1.26}$$

where $\Delta S = S(\rho(\tau)) - S(\rho(0))$, ΔU is given in **Eq. 1.13**.

Again, from **Eq. 1.16** and **Eq. 1.18**, we have

$$\Sigma = \Delta S - \beta \Delta U - \beta \langle W \rangle, \tag{1.27}$$

using a negative sign for the work extraction. Therefore, the entropy production in terms of work extraction can be expressed as

$$\Sigma = -\beta(\Delta F + \langle W \rangle), \tag{1.28}$$

where we have used **Eq. 1.16**. Now, using the property that the entropy production can't be negative (**Eq. 1.24**), we have

$$\langle W \rangle \leq -\Delta F, \tag{1.29}$$

which gives a work extraction upper bound in a thermodynamic process known as the principle of maximum work. This represents another form of the second law of thermodynamics [27, 24].

Third Law

If the ground state energy level of a system is non-degenerate, the decrease in temperature of the system to zero makes its entropy tend to zero in equilibrium.

$$S_{\text{th}} \ \to 0 \text{ if } T \to 0K. \tag{1.30}$$

This is referred to as the third law in thermodynamics [37, 5]. For any thermodynamic state, the theorem defines the thermodynamic entropy on an absolute scale. Also, sometimes it is reformulated as, which was first pointed out by Nernst [38], for any process, in a cyclic finite number of cyclic operations and also at a finite time we can't achieve the absolute zero temperature.

In the quantum regime, many studies have been done on the third law of thermodynamics. The relation between two different formulations of this law has been studied [39, 40]. Many studies have been done on the Nernst theorem based on Ising models and lattice systems [41, 42], as well as the role of degeneracy, has been investigated. The dynamic form of the third law also has been studied from the perspective of quantum thermal machines [43, 44, 45, 46, 47]. Furthermore, the amount of energy needed to perform cooling operations and the reservoir size have been investigated from the perspective of the third law [40, 48, 49, 50, 51, 52].

1.3.2 Quantum Thermodynamic Processes

In **Sec. 1.1.2**, we have discussed how the classical thermodynamic processes are defined. There are mainly four main classical thermodynamic processes, isothermal, adiabatic, isochoric and isobaric processes. The classification is done depending on the different parameters viz., volume, temperature, pressure, and entropy that remain fixed during the execution of the processes. Now we will see how the quantum thermodynamic processes, quantum isothermal, quantum isochoric, quantum adiabatic, and quantum isobaric [53] are defined. The quantum thermodynamic processes are nothing but the quantum-mechanical analogue of the classical thermodynamic processes. Quantum thermodynamic processes are discussed briefly as follows.

Quantum Isothermal Process

In classical thermodynamics, if the temperature of a system remains constant throughout a process then it is called a classical isothermal process [5]. It is executed by connecting the system to a thermal bath and simultaneously changing a system parameter very slowly. So, this allows the system to retain the same temperature as that of the thermal bath by exchanging heat exchange with the bath throughout the process.

A quantum isothermal process [53] is a (quasi-static) process in which a quantum system maintains a fixed temperature with a quantum mechanical heat bath at a temperature T throughout the process. This process is carried out by changing an external control parameter of the system. This control parameter is changed very slowly such that in each instant of the process, the system maintains thermal equilibrium with the bath by exchanging heat. With changes in the external control parameter in this process the energy gaps in the system also change, so the system exchanges some amount of work (work is done by the system or work is done on the system depends on the change of sign of the system energy) with a work reservoir.

The heat transfer in this process is defined as $\delta Q = TdS$ and we can calculate the work done in this process by $\delta W = dF$, under the condition of the reversible isothermal process. Here, F represents the Helmholtz free energy defined as $F = U - TS$, and using these relationships we can calculate the work done in this process.

Quantum Isochoric Process

In a classical isochoric process [5] the volume of a system remains fixed, whereas the system exchanges heat with a heat bath. In this process, the pressure P and the temperature T of the system change, and the system reaches thermal equilibrium

with the heat bath at the end. As the volume is fixed throughout the process, there is no work exchange in this process.

Similarly, in a quantum isochoric process [53], external control parameters of a quantum system remain fixed, in other words, the energy gaps do not change. In this process, there is no work done as the energy gaps remain fixed. But, the system is coupled with a heat bath so it exchanges some amount of heat with the bath. This is manifested by the change in occupation probabilities P_n of the energy levels of the system, although the energy level spacing E_n remains the same:

$$\delta W = \sum_n P_n dE_n = 0.$$

But, the heat exchange of the system with the heat bath is given by

$$\delta Q = \sum_n E_n dp_n \neq 0.$$

The entropy S of the system changes with the change in occupation probabilities until it reaches thermal equilibrium with the heat bath. At the end of the process, the system state is represented by the Gibbs state.

Quantum Adiabatic Process

In classical thermodynamics, if the system entropy remains fixed in a process, it is said to be an adiabatic process. This means the classical adiabatic process is an isentropic process [5]. Also, from the second law (Clausius's version), we know that system entropy is linked with heat transfer. So, if there is no heat transfer between the system and its environment, it represents an isentropic process. In this process, all the changes in the system's internal energy are due to work exchange, according to the first law of thermodynamics.

To keep an analogy with the classical adiabatic process that the process should be isentropic, the adiabatic process in the quantum domain is defined as a unitary time evolution process in a system in which the external control parameter of the system is changed from one value to another value. This change should be slow enough to satisfy the generic quantum adiabatic condition [53]. Also, the system remains disconnected from its environment in this process. When the time evolution process is slow enough, there will be no transitions among the instantaneous eigenstates of the system. Let us suppose that the system initially, at time $t = 0$, is in an eigenstate $|n(0)\rangle$ of the starting Hamiltonian of the system. Then, the Hamiltonian is slowly changed with the aid of an external control parameter with respect to time. In this process, the system remains in the nth eigenstate $|n(t)\rangle$ of the instantaneous system

Hamiltonian following the quantum adiabatic theorem. This means the occupation probability at the instantaneous eigenstate $|n(t)\rangle$ will be the same as initially. As the occupation probabilities of the system energy levels do not change, which leads to no change in the system entropy in a quantum adiabatic process, like a classical adiabatic process.

As in this process, the system remains disconnected from the heat baths, there is no heat transfer between the system and the heat baths. But the change in the Hamiltonian leads to the change in energy level gaps, and the system exchanges some amount of work

$$\delta W = \sum_n P_n dE_n \neq 0,$$

the sign signifies the work done by the system on the system.

If we consider a situation where the process is fast, this process will not be a quantum adiabatic process. Because generally there will be internal excitations in the system, although there is no transfer of heat between the system and heat baths as the system is disconnected from heat baths, the process is considered to be a classical adiabatic process. However, there is no mandatory requirement for a classical adiabatic process that occupation probabilities should not change. In this sense, we can say that the classical adiabatic processes are more universal than the quantum adiabatic processes; basically, the quantum adiabatic processes are a subset of the classical adiabatic processes [53].

Heat and Work in quantum isochoric and adiabatic processes:

As in the quantum isochoric and adiabatic processes, either heat or work is exchanged by the system, therefore heat and work in these processes can be calculated just by taking the difference of internal energy of the system before and after the process.

In a thermodynamic process $A \rightarrow B$, if ρ_A and ρ_B represent the states of the system, and $U_A = Tr(H_A\rho_A)$ and $U_B = Tr(H_B\rho_B)$ represent the internal energies of the system at points A and B, respectively, then the quantity $U_B - U_A$ represents the work in an adiabatic process and heat in an isochoric process. Here H_A and H_B represent the Hamiltonian of the system at A and B, also in an isochoric process $H_B = H_A$. These formulas are more general and consider the off-diagonal terms of the density matrix.

1.3.3 Quantum Thermal Machines:

Learning from examples has been a major theme in thermodynamic studies since Carnot's pioneering work [5, 6]. This is also applicable to thermodynamics in the quantum domain, in which heat and work acquire concrete meaning. Quantum thermal machines (heat engines and refrigerators) provide us with a platform to study the basic principles of thermodynamics at the quantum level. Therefore, quantum thermal machines have been a major topic of study in quantum thermodynamics.

In **Sec. 1.1.2**, we have discussed the classical thermal machines where macroscopic working substances are used to perform thermodynamic tasks. On the contrary, in a quantum thermal machine (QTM), a well-defined quantum system as a working substance which is coupled to heat baths, is used to perform these thermodynamic tasks [21, 54]. Depending on the nature of the cycle the quantum thermal machines can be classified into two categories, the continuous cycle and the reciprocating cycle QTMs. In the continuous cycle machines, the system-bath interaction is always-on and there are no separate strokes/stages in the cycle, rather there is continuous coupling among the systems, heat baths and work reservoirs [55, 56, 57]. These models are autonomous quantum thermal machines and QTMs with periodically modulated working systems fall under this category. Another type of thermal machine is the reciprocating cycle where discrete strokes are present in the cycle, where the working system alternatively goes through heating/cooling with thermal baths and manipulation by an external control for work extraction/insertion processes [55, 56, 57]. The QHEs under these category are basically the quantum mechanical analogue of classical Otto, Carnot, and Stirling engines [53]. Therefore, the reciprocating cycle QTMs consist of several basic quantum thermodynamic processes such as the quantum isothermal, quantum adiabatic, and quantum isochoric processes. These quantum thermodynamics are discussed in **Sec. 1.3.2**. QTMs can be further classified based on whether any external driving is needed or not. QTMs with external driving or time-dependent fields or periodically modulated working system thermal come under this category. Another type is autonomous QTMs that operate without the help of any external control or time-dependent fields and can be modelled using the time-independent Hamiltonian.

Scovil and Schultz-DuBois first introduced the idea of a quantum thermal machine in 1959. They showed that a three-level maser (i.e., microwave amplification by stimulated emission of radiation) functions like a heat engine [58]. In their model, they considered a three-level system, where a hot is coupled between

the upper and lower energy levels, whereas a cold bath is coupled between the upper and intermediate energy levels. These heat baths are able to create a population inversion between the intermediate and ground energy levels. The population inversion leads to amplified light as work [56]. Also, they showed that the Carnot efficiency bound is the upper limit of the efficiency of the action of a maser. Quantum refrigerator for the purpose of pumping heat to a hot bath from cold by consuming power in a three-level system first proposed by Geusic, Schulz-DuBois, De Grasse and Scovil [59]. After a long time of these proposals, a dynamical picture of QHEs within an open quantum system framework was proposed by Alicki [60] and Kosloff [61]. In the last decade, tremendous experimental advances in nanoscale devices, circuit QEDs, superconducting circuits, and quantum many-body devices have expanded the interest of quantum thermal machines study, both theoretically and experimentally, into many areas of the modern study of quantum mechanics, including quantum information, quantum control, nonequilibrium quantum dynamics, quantum fluctuations, quantum many-body systems, thermoelectric devices, quantum transport phenomena, and more [21, 57, 62, 63].

In quantum thermodynamics, we address a few essential questions, which are described below, by analyzing various models of quantum thermal machines. These studies help us to understand thermodynamics in the quantum domain, particularly thermodynamic laws.

The microscopic scale raises several open questions [21]. In the field of quantum thermal machines some of which are given below.

- How are quantum thermal machines different from their classical counterparts in working principles?
- What is genuinely quantum about quantum thermal machines? Can quantum properties uplift the performance of thermal machines? How does quantum coherence or entanglement play a role?
- Is quantum supremacy possible? What advantages can we expect from the quantum nature of quantum thermal machines?
- What limits does thermodynamics impose on quantum devices, especially quantum thermal machines? Is the Carnot bound still valid for quantum thermal machines?
- How is the finite-time operation of a QTM different from its classical counterparts?

Furthermore, quantum thermal machines provide an excellent platform for studying the impact of quantum phenomena in non-equilibrium thermodynamics [62, 57, 55]. Also, the role of quantum fluctuation, strong coupling, and non-Markovianity in energy conversion can be studied through quantum thermal machines (heat engines and refrigerators).

Studying quantum thermal machines can provide many practical applications besides their fundamental perspective. In the era of quantum technology [64], it may find applications viz., cooling down a qubit [65], quantum state preparation [66], quantum thermometry [67] and quantum metrology [55], and many more. It has been shown that by analysing the work distribution in an Otto cycle we can distinguish between left and right-handed molecules [68]. Also, a QHE can be used for the charging purpose of a quantum battery or other work storage devices at the quantum domain [69].

Non-classical effects in the performance of quantum thermal machines

To find whether these so-called "quantum thermal machines" have quantum mechanical superiority, many studies have been done in this direction. QHEs may show unusual and exotic properties because of the quantum nature of working systems. It has been shown that in prototypical non-thermal QHEs which are fuelled by means of non-thermal baths, i.e., whose quantum states cannot be described by thermal Gibbs states, the efficiency can surpass known classical heat engine bounds. Exceeding conventional efficiency bounds appears to violate the second law. After that, several studies have shown that exceeding efficiency bounds is mainly due to special features of non-thermal baths, which contribute to additional sources of work. Actually, QHEs operating with these types of nonthermal baths, e.g., coherent and squeezed baths, harness additional resources than their thermal counterparts. It was revealed that these violations are only apparent and can be overcome by considering additional thermodynamic resources associated with the non-equilibrium nature of the heat baths, the performance of these machines is bounded by generalized bounds.

- **Quantum internal friction** - Normally QHEs function in quantum systems that have no commuting Hamiltonians at different times [70, 71, 72, 73, 74, 75, 76, 77, 78, 79]. This leads to the generation of quantum internal friction when a system is driven by an external control parameter in a unitarily time evolution process. Because of that nonadiabatic transitions are induced between the Hamiltonian instantaneous eigenstates. This results in a large amount of entropy production and irreversibility in engine operation, which degrades QHE performance [75, 76, 77, 78, 79].

- **Dynamical quantum lubricant** - It has been shown that quantum coherence can be used as a dynamical quantum lubricant. If a QOE is operated in a finite time, unitary time evolution processes and the isochoric heating process are executed in finite times. There is an interference effect between the residual quantum coherence after the incomplete isochoric heating process (thermalization) and the coherence generated in the next stroke of the finite-time unitary driving process. Due to this interference, oscillatory behaviour can be found and performance degradation due to quantum internal friction can be overcome [74].

- **Quantum Coherence as a resource** - Work and the corresponding efficiency in a QHE, assisted by Maxwell's demon, can be improved by a coherent demon [80]. Also, quantum coherence in a periodic feedback-driven HE can enhance efficiency

- **Non-thermal baths** - Scully et al. proposed a model of a photo-Carnot engine with a coherent bath. In this engine, a single-mode cavity field working system undergoes a Carnot cycle, where repetitive weak interactions of the working system with three-level identical atoms with degenerate ground states play as a heat bath. By introducing quantum coherence between two degenerate ground states, a thermalization temperature of the cavity field can be obtained which depends on the coherence. Using that quantum coherence, work is possible to extract from a single bath [81]. Also, a few studies, theoretically and experimentally, have shown that if a squeezed thermal bath is used for fueling a QOE instead of thermal baths, the engine efficiency can be increased above the Carnot limit by increasing the squeezing parameter [82, 83, 84].

- **The role of quantum correlation** - Entanglement can enhance cooling in an autonomous quantum refrigerator [85]. In a Szilard engine, the quantum mutual information of the correlated memory, consisting of two parts, can be used to generate work [86]. Quantum correlation has been proposed as a fuel for heat pumps. This is based on the principle that, if there is an initial correlation then energy can flow from a cold body to a hot body [87].

1.3.4 Working systems for quantum thermal machines

In recent years with the advances in experimental techniques, different types of quantum mechanical systems are being used to implement quantum heat engine models experimentally. Recent theoretical proposals for quantum heat engines include quantum dots [88, 89], spin chain [90, 63, 91], trapped ions, optomechanical

setups [92, 93, 94, 95, 96], and superconducting qubits, two-level system [8, 97, 98], hybrid light-matter systems [99, 100, 100, 101, 102, 103], Josephson junction [104], particles in a box [105, 106, 107, 101], harmonic oscillators [83, 108, 109, 110], Bose-Einstein condensate system [111], Dirac particles [112, 113], photosynthetic reaction center [114], coupled qubits [115, 116, 117], PT-symmetric non-Hermitian system [118], superconducting resonator [119, 120], three-level systems [121, 122, 81], cavity QED [123, 81, 124, 125], cold bosonic atoms [126], many body localization [127] etc. Experimental implementation of quantum heat engines includes trapped ions [128, 129, 130, 131, 132], ensemble of nitrogen-vacancy centers [133], ultracold atoms [134, 135, 136], NMR setup [137, 138], tunnel field-effect transistor (TFET) [139], quantum dots [140, 88], photonic system [141] etc. Furthermore, nowadays quantum heat engines and refrigerators are being tested experimentally on cloud-based quantum computers [142, 143, 144].

In this thesis, we will consider spin chain systems as the working system for thermal machine operation.

Heisenberg coupled spin chain systems:

Let us consider a 1D spin chain system where the spins are coupled by the Heisenberg coupling of the nearest neighbour interaction type. The most general Hamiltonian of a 1D Heisenberg coupled spin chain system in a transverse magnetic field of strength B is represented by [145, 146]

$$H_{XYZ} = \sum_{j=1}^{N-1} \left(J_x S_j^x S_{j+1}^x + J_y S_j^y S_{j+1}^y + J_z S_j^z S_{j+1}^z \right) + B \sum_{j=1}^{N} S_j^z, \tag{1.31}$$

where J_i, $S^i = \frac{\hbar}{2}\sigma^i$, and σ_i $(i \in x, y, z)$ represent the exchange interaction constant, spin operators, and the Pauli matrices along the x, y and z directions respectively. Now depending on the values of the coupling constants, the above Heisenberg spin chain model can be classified into XXZ model if $J_x = J_y \neq J_z$, XXX model if $J_x = J_y = J_z$. For $J_z = 0$, this represents a XY model if $J_x \neq J_y$ and XX model if $J_x = J_y$. The speciality of this type of Hamiltonian is that they can be built in the laboratory using state-of-the-art quantum technology viz., ion trap, NMR or superconducting qubits.

Now for Heisenberg anisotropic XY interaction, the Hamiltonian is represented

by [145, 146]

$$\begin{aligned} H_{XY} &= \sum_{j=1}^{N-1} \left(J_x S_j^x S_{j+1}^x + J_y S_j^y S_{j+1}^y\right) + B \sum_{j=1}^{N} S_j^z \\ &= \frac{J}{2} \sum_{j=1}^{N-1} \left[(1+\gamma) S_j^x S_{j+1}^x + (1-\gamma) S_j^y S_{j+1}^y\right] + B \sum_{j=1}^{N} S_j^z, \end{aligned} \tag{1.32}$$

where the anisotropy $\gamma \in (0,1)$ and $\gamma J = J_x - J_y$ is the ansiotropy in the in-plane interaction, where $J_x = (1+\gamma)\frac{J}{2}$ and $J_y = (1-\gamma)\frac{J}{2}$. The $\gamma = 0$ represents the isotropic XY interaction in a transverse magnetic field and $\gamma = 1$ represents the transverse Ising spin Hamiltonian.

In our work, we will particularly focus on the two-spin case where the number of total spins in a spin chain is $N = 2$. Let's consider a system of two-spin coupled by an anisotropic XY interaction (with anisotropy parameter $0 \leq \gamma \leq 1$) of Heisenberg type in a transverse magnetic field B. The Hamiltonian that describes this system can be written as (in the unit of $\hbar = 1$ and considering other multiplication factor as 1) [147, 145]

$$\hat{H} = B\left(\hat{\sigma}_1^z + \hat{\sigma}_2^z\right) + J\left[(1+\gamma)\hat{\sigma}_1^x \hat{\sigma}_2^x + (1-\gamma)\hat{\sigma}_1^y \hat{\sigma}_2^y\right], \tag{1.33}$$

where J represents the coupling strength two-spin. In the limiting case of γ, we obtain the isotropic XX interaction Hamiltonian when $\gamma = 0$ and the Ising spin Hamiltonian when $\gamma = 1$.

1.3.5 Model of a bath

Now we will describe the model of a thermal bath which consists of an infinite number of modes with a continuum of frequencies. The dynamics of a two-spin system coupled by anisotropic interaction under a bosonic thermal bath is described by a Lindblad master equation, in interaction picture which can be obtained as [148, 82, 147]

$$\begin{aligned} \frac{\partial \hat{\rho}}{\partial t} =& i[\hat{\rho}, \hat{H}(t)] + \sum_{i=1,2} [\Gamma(n_i+1)(\hat{X}_i \hat{\rho} \hat{X}_i^+ - \frac{1}{2}\hat{X}_i^+ \hat{X}_i \hat{\rho} - \frac{1}{2}\hat{\rho}\hat{X}_i^+ \hat{X}_i) \\ &+ \Gamma n_i (\hat{X}_i^+ \hat{\rho} \hat{X}_i - \frac{1}{2}\hat{X}_i \hat{X}_i^+ \hat{\rho} - \frac{1}{2}\hat{\rho}\hat{X}_i \hat{X}_i^+)], \end{aligned} \tag{1.34}$$

where we have considered only one spin of the coupled two-spin system interacting with a heat bath at temperature T to maintain the simplicity of the master equation. The sum over i represents the number of transitions in the system under the heat

bath, and the thermal photon number distribution at the transition frequencies in the bath are $n(\omega_i) = \left[\exp\left(\frac{\hbar\omega_i}{kT}\right) - 1\right]^{-1}$. Here, Γ is the coupling constant between the system and the bath. Similarly, we can consider that each spin interacts with the bath.

The jump operators associated with each system operator X [149, 148]:

$$X(\omega) = \sum_{\epsilon' - \epsilon = \omega} |\epsilon\rangle \langle\epsilon| X_\beta |\epsilon'\rangle \langle\epsilon'|,$$

where $\{|\epsilon\rangle\}$ is the basis of the eigenvectors of the system Hamiltonian H. Therefore, the jump operators of the system $\hat{X}_i$ and the respective transition frequencies, when only the first spin interacts with the heat bath by σ^x operator, are given by

$$\begin{aligned} \hat{X}_1 &= \tfrac{1}{2}\left(\tfrac{B+K-\gamma J}{\sqrt{K^2+BK}}\ |\psi_1\rangle\langle\psi_3| + \tfrac{B-K+\gamma J}{\sqrt{K^2-BK}}\ |\psi_0\rangle\langle\psi_2|\right), \quad \hbar\omega_1 = 2K + 2J \\ \hat{X}_2 &= \tfrac{1}{2}\left(\tfrac{B+K+\gamma J}{\sqrt{K^2+BK}}\ |\psi_2\rangle\langle\psi_3| + \tfrac{B-K-\gamma J}{\sqrt{K^2-BK}}\ |\psi_0\rangle\langle\psi_1|\right), \quad \hbar\omega_2 = 2K - 2J. \end{aligned} \tag{1.35}$$

These operators satisfy the relations $[\hat{H}, \hat{X}_i] = -\omega_i \hat{X}_i$ and $[\hat{H}, \hat{X}_i^\dagger] = \omega_i \hat{X}_i^\dagger$.

1.3.6 Other topics in quantum thermodynamics

Apart from the study of quantum thermal machines, people also work on many other important topics under which quantum thermodynamics that we discuss below.

Thermodynamic resource theories:

Fundamental laws of nature often appear as restrictions. These laws include that nothing in a vacuum can travel faster than light, no energy can be created out of nothing, and there is no perpetual motion. To investigate the impact of such constraints on the physical systems evolution a mathematical framework is developed known as the resource theory.

The resource theory of quantum entanglement is the most well-known application of this approach [150, 151, 152]. Then it emerges that thermodynamics can benefit from this type of theory developed to study entanglement [151, 152]. In thermodynamics, the first and second laws act as fundamental constraints. Because of these laws, total energy remains conserved and the complete conversion of heat to work is forbidden in thermodynamic processes. In this context, a question to ask is: if these laws restrict any thermodynamic process, what constitutes a resource?

Within the framework of resource theories, these questions can be addressed. Thus, resource theories used for quantifying and managing resources are based on

information-theoretic frameworks. All resource theories consist of three essential components [15, 151, 152, 153]

- A set S of free states that are freely accessible,
- A set C of allowed quantum operations closed under S and
- A set R of resource states that cannot be created by S and C alone.

Therefore, the only way to access states that are not in S is through resource states. All resource theories differ based on what is considered to be allowed operations, free states, and resources in them.

Given the allowed operations and free states, someone can ask: what are the states that may be reached by manipulation of a quantum state ρ, by using the allowed operations and free states mentioned above? This puts forth another aspect of resource theories which is the state conversion conditions, determine that by using the allowed operations and free states which resource states can be converted into each other. According to these conditions, if a specific function f, which obeys a partial order, decreases $f(\rho) \geq f(\rho')$ in a transition, then the transition is possible $\rho \to \rho'$. These functions are known as resource monotones [15, 151, 152, 153].

In the thermodynamic resource theory, the Gibbs thermal states at temperature T represent the free states. and allowed operations which, are called thermal operations, are represented by partial traces and energy-preserving unitaries, all non-thermal states represent the resources. Therefore, under the allowed operations [15, 151, 152, 153]

$$\mathcal{T}(\rho) = \mathrm{Tr}_B \left(U_{AB} \left(\rho_A \otimes \rho_{B,\beta} \right) U_{AB} \right),$$

where a thermal state is represented by $\rho_{B,\beta}$ at an inverse temperature $\beta = 1/k_B T$ and also $[U_{AB}, H] = 0$, where U_{AB} represents an energy preserving unitary.

Also, the monotones in the thermodynamic resource theory are determined by the quantum free energy [153, 154]:

$$F(\rho) = \mathrm{Tr}\left[H_S \rho\right] - kT_B S(\rho)$$

We define the free energy difference between a general state ρ and a thermal state by ρ_β $\Delta F(\rho) := F(\rho) - F(\rho_\beta)$. Then it can be shown that $\Delta F(\rho)$ is a monotone under thermal operations. In order to show that we can check that $\Delta F(\rho) = kT_B S(\rho \| \rho_\beta)$, where the quantum relative entropy is represented by $S(\rho \| \rho_\beta) = \mathrm{Tr}\left[\rho (\log \rho - \log \rho_\beta)\right]$. Under quantum operations the contractiveness

of relative entropy and the relation $\mathcal{T}(\rho_\beta) = \rho_\beta$ gives

$$\Delta F(\mathcal{T}(\rho)) = kT_B S\left(\mathcal{T}(\rho)\|\rho_\beta\right) = kT_B S\left(\mathcal{T}(\rho)\|\mathcal{T}\left(\rho_\beta\right)\right) \leq kT_B S\left(\rho\|\rho_\beta\right) = \Delta F(\rho)$$

Using the mathematical framework, mentioned above, of resource theory of quantum thermodynamics, developed in quantum information theory, the basic questions of thermodynamics are revisited [152, 154].

Quantum fluctuation relations:

The classical laws of thermodynamics, which apply to large systems, are ignorant of the constituent particles of the systems of interest. For these large systems, there can be variations in thermodynamic quantities viz., heat or work. However, typically the fluctuations in these quantities are so small with respect to the mean values that those fluctuations are negligible. These laws hold on average. But, when the system size scales down to the microscopic scale e.g., a stretched RNA molecule, the thermodynamic quantities will also scale down. Their thermodynamic quantities (work and heat) become stochastic quantities. In that case, fluctuations in thermodynamic quantities are non-negligible compared to their mean values [21, 155].

To describe such situations, fluctuations must be included in non-equilibrium thermodynamic descriptions. This was first achieved in stochastic thermodynamics. In this framework, at the stochastic trajectory level, it is also possible to state a first law like energy conservation for microscopic systems. Also, entropy can be defined at this level. Furthermore, fluctuation theorems (FT) like universal relations were discovered through the study of fluctuations in thermodynamic quantities such as work, heat and entropy. These theorems pose constraints on fluctuating quantities statistics. FT generalizes the second law, which applies to equilibrium and out-of-equilibrium systems, and to systems of a few particles that are not within the thermodynamic limit. Based on the detailed FT, different types of FT can be obtained in a unified manner. Particularly, by measuring nonequilibrium work we can determine equilibrium free energy through Jarzynski equality and the Crooks FT. These fluctuation theorems apply to classical small systems viz., molecular motors, biomolecules, and colloidal particles.

In the quantum regime, with thermal fluctuation quantum fluctuation is also present due to quantum systems' inherent randomness. Various fluctuation theorems have been reformulated for quantum systems in quantum thermodynamics. Serious issues arise when we deal with quantum systems regarding the quantum nature

of work and heat. Here we can also define quantum trajectories, but to monitor quantum systems we require measurements of the system. Quantum measurements cause back-actions in the system. Projective measurements at the beginning and end of a process of interest are used in most extensions of fluctuation theorems to the quantum domain. This framework is known as the two-measurement protocol (TMP).

1.4 Structure of the thesis

In **Chapter 1** we present the introduction of thermodynamics and quantum thermodynamics. First, we discuss the laws of classical thermodynamics and different classical thermal machines. We explore the role of information in thermodynamics. Then, we discuss how the laws of thermodynamics emerge from a quantum mechanical context. This discussion introduces some fundamental thermodynamic quantities viz., heat, work and entropy. Also, we discuss different subtopics of quantum thermodynamics. In our work, we explore quantum thermodynamics through the study of different QTM models. Therefore, we elaborately discuss what are QTMs and different quantum thermodynamic processes viz., isothermal, adiabatic, isochoric and isobaric, to explore various models of QTMs viz., quantum Carnot, Stirling and Otto thermal machines. Finally, we introduce coupled spin systems as a working substance for thermal machines.

In **Chapter 2** we study the performance of quantum Stirling machines near a quantum critical point in a two-spin working system, in which the nearest neighbour interaction of the Heisenberg-XX type couples the spins. We show how this system can exhibit a QPT which is studied by the measure of entanglement and correlation. We investigate how the cycle behaves as different thermal machines depending on the parameters of the cycle. We study how these thermal machines behave near the QCP. Further, we explore how two spins perform as a thermal machine in the presence of a third spin, when all three spins are in thermodynamic equilibrium and exhibit a quantum Stirling cycle.

In **chapter - 3**, we explore a quantum Otto thermal engine with a two-spin working system coupled by anisotropic interaction, defined by a parameter γ. We study how anisotropy plays a fundamental role in the performance of the quantum Otto engine (QOE) operating in different timeframes. We discuss the effect of quantum internal friction that arises due to the finite-time unitary time evolution processes. We also discuss the effects of incomplete thermalization on engine performance. Further, we study the QOE with a local spin working system. We discuss different thermodynamic figures of merit of the local operation of a QOE.

Specifically, in finite-time operation, we show that the efficiency oscillates with respect to the time of the unitary processes of the global system.

In **chapter 4**, we study the performance of a measurement-based quantum Otto engine (QOE) with the same working system as the chapter. Non-selective quantum measurements fuel the engine. We investigate how a measurement-based QOE behaves differently from a standard QOE in finite time. We show that for anisotropic interaction, the efficiency of the engine oscillates in a finite time. Therefore, for a suitable choice of timing of the unitary processes in the short time regime, the engine can have a higher work output and less heat absorption, such that it works more efficiently than a quasi-static engine. We find a connection between a local spin QOE and a measurement QOE by showing that the oscillatory nature of the efficiency comes from the same origin of interference-like effects. Finally, we discuss the case of an always-on heat bath.

In **chapter - 5**, we conclude our work and try to give the future direction of work.

Chapter 2

Critical point behaviour of a quantum Stirling machines

In the previous chapter, we discussed the basic ideas and tools of quantum thermodynamics and various aspects of the subject. More specifically, we have discussed in detail about QTMs and their implementation. In this chapter, we show the implementation of a reciprocating cycle quantum sterling engine in a coupled spin system.

2.1 Motivation

In this chapter, we focus on the quantum thermal machines using Stirling cycles. Classical Stirling engines are of external combustion type, in which the working fluid is heated passively using a combustion-based heat source. In last few years, the quantum version of the Stirling cycle is also getting attention [156, 157, 158, 159, 160, 161, 162, 163, 164, 165, 166, 167, 168, 169, 170]. This becomes interesting, as the size of the machines does not matter any more, at the quantum level. It has been shown [159, 160] that the energy level degeneracy can be used as a resource to generate work and the engines can achieve the Carnot efficiency under specific conditions of temperatures of the baths. Quantum Stirling cycle has been studied from the perspective of the uncertainty relation as well [169]. Its efficiency can be enhanced beyond that of a quantum Carnot engine, with the aid of a regenerator [156]. A model of an endoreversible entangled quantum Stirling engine using two coupled spins as a working medium has been investigated for finite-time operation [157]. Also in various studies, finite-time analysis of the quantum Stirling cycle has been done [171, 172, 173, 174].

We first investigate whether any sharp nonanalytic behaviour can be found in a few-spin systems, which is far away from the thermodynamic limit, as one approaches absolute zero. Here we will consider the level crossing of the ground states as a signature of QPT which follows from the extended Ehrenfest classification of phase transitions [175, 176, 177]). This is an example of the first-order transition as

the first-order derivative of the ground state energy with respect to the control parameter becomes discontinuous at the critical point. Next, we will explore if such nonanalyticity can enhance the performance of thermal machines near the QCP for few-spin systems, similar to that obtained for systems in thermodynamic limit (e.g., as described in [178, 158, 179, 180, 181, 182, 183, 184]).

A few-spin systems can show a QPT when it remains in thermal equilibrium. In this chapter, we focus on a few spin-based quantum thermal machines using the Stirling cycle which consists of two isothermal and two isochoric processes. Classical Stirling engines are of external combustion type, in which the working fluid is heated passively using a combustion-based heat source. Despite the size limitation, the Stirling engines are more versatile in nature as they can be used with any heat source, and also deliver heat-to-work conversion with comparably high efficiency [185]. This becomes interesting, as the size of the machines does not matter any more, at the quantum level. We aim to investigate how such an engine behaves near a quantum critical point in a two-spin working system, in which the spins are coupled by the nearest neighbour interaction of Heisenberg XX-type and show a QPT when it remains in thermal equilibrium. Further, we explore how coupling to a third spin affects the performance of these cycles.

2.2 Model of working System

Let us consider two spin-1/2 particles that are coupled to each other by the Heisenberg XX exchange interaction, with a strength J. In the presence of a homogeneous external magnetic field B, applied along the z axis. The Hamiltonian of this system is given by (in the unit of $\hbar = 1$):

$$H = J(\sigma_1^x \otimes \sigma_2^x + \sigma_1^y \otimes \sigma_2^y) + \frac{B}{2}(\sigma_1^z \otimes \mathbb{1} + \mathbb{1} \otimes \sigma_2^z) \,, \tag{2.1}$$

Please note that the Hamiltonian is time-independent here. In this chapter, we will study the system in antiferromagnetic configuration, i.e., for $J > 0$. The eigenvalues E_n and corresponding eigenvectors $|\psi_n\rangle$ $(n \in 1, 2, 3, 4)$ for this Hamiltonian can be written in the two-qubit computational basis $\{|11\rangle, |10\rangle, |01\rangle, |00\rangle\}$ as

$$\begin{aligned} E_1 &= -B \qquad |\psi_1\rangle = |00\rangle \,, \\ E_2 &= -J \qquad |\psi_2\rangle = \tfrac{1}{\sqrt{2}}(|01\rangle - |10\rangle), \\ E_3 &= J \qquad |\psi_3\rangle = \tfrac{1}{\sqrt{2}}(|01\rangle + |10\rangle), \\ E_4 &= B \qquad |\psi_4\rangle = |11\rangle \,. \end{aligned} \tag{2.2}$$

Please note that depending on the relative value of B and J, either $|\psi_1\rangle$ (if $B > J$) or $|\psi_2\rangle$ (for $B < J$) becomes the ground state. Therefore, by controlling the magnetic field externally, one can change the ground-state properties of the system.

2.2.1 Internal energy and entropy of the system in the thermal state:

At thermal equilibrium with a heat bath at a temperature T, the state of the system can be represented by the Gibbs State which is given by (in the unit of $k_B = 1$)

$$\rho = \frac{e^{-H/T}}{Z} = \sum_n P_n \left|\psi_n\right\rangle \left\langle\psi_n\right| \ ,$$

where $P_n = \exp(-E_n/T)/Z$ is the occupation probability of the eigenstate $|\psi_n\rangle$ and $Z = \sum_n \exp(-E_n/T)$ is the partition function.

The internal energy of the system is given by the expectation value of the Hamiltonian and can be calculated as

$$U = \mathrm{Tr}(\rho H) = \sum_n P_n E_n = -\frac{2}{Z}\left(B \sinh\frac{B}{T} + J \sinh\frac{J}{T}\right) \ , \tag{2.3}$$

where $Z = 2\left(\cosh\frac{B}{T} + \cosh\frac{J}{T}\right)$ is the partition function. The von Neumann entropy of the system is given by

$$S = -\mathrm{Tr}(\rho \ln \rho) = -\sum_n P_n \ln P_n = \frac{U}{T} + \ln Z \ . \tag{2.4}$$

2.2.2 Quantum Phase Transition

Quantum phase transition (QPT) in a system refers to a nonanalyticity in the ground state properties at absolute zero ($T \to 0$) in the thermodynamic limit, which signifies here the number N of constituent particles is infinitely large. The QPT involves changes in the ground-state properties at a critical value of a non-thermal control parameter (e.g., the strength of the control field) at absolute zero temperature [186]. This critical value of the external control parameter is known as the quantum critical point (QCP). In QPTs, it is the quantum fluctuations which are responsible for taking the system from one phase to another, in contrast to the thermal fluctuations at a finite temperature that are responsible for the classical phase transitions (CPT), which dominate in the above-absolute-zero phase transitions. Typically, nonanalyticity emerges when the number of particles in the system is increased i.e. when one approaches the thermodynamic limit [187, 188, 189, 190, 191, 192, 193].

In fact, at such a limit, correlations among these particles become long-range and sharp features in the phase transition profile are observed [189].

Please refer to Eq. 2.2, where it can be seen that, at a critical value of the magnetic field ($B_C = J$), there occurs a ground state energy level crossing. As this gives rise to a discontinuity in the first-order derivative of the ground state energy, it can referred to as a QPT of first-order [186, 194, 195, 196].

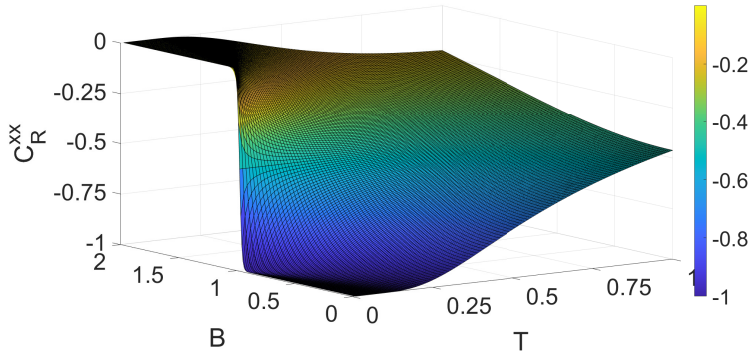

Figure 2.1: Variation of the xx-correlation function of two spins at thermal equilibrium as a function of temperature T and magnetic field B. We have chosen the coupling constant $J = 1$ throughout this chapter.

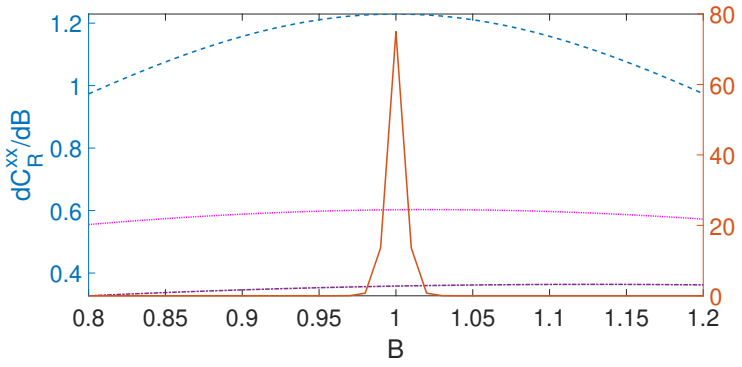

Figure 2.2: Variation of the first order derivative of the xx-correlation of thermal equilibrium state at the temperatures $T = 0.0033$ (solid line, brown), $T = 0.2033$ (dashed line, light blue), $T = 0.4033$ (dotted line, pink), and $T = 0.6033$ (dash-dotted line, violet), respectively. For the solid line, the scale of the y-axis is shown on the right side, while for the remaining plots, it is shown on the left side.

2.2.3 Spin-spin correlation and entanglement: Quantum Phase Transition

Due to the coupling between the two spins, spin-spin correlations and entanglement arise, even at thermal equilibrium [197, 198, 199, 200]. At a critical point, the correlation among the participating subsystems becomes long-range in the

thermodynamic limit. This suggests that spin-spin correlation can be a marker of the QPT in our model also. On the other hand, in the information-theoretic approach to QPT, different measures of entanglement are used for the identification of quantum phase transition [201, 198, 202, 203, 197, 200, 199, 204]. Below, we investigate how entanglement and correlation can be used to detect a quantum critical point when the system is in thermal equilibrium.

Correlations:

The correlation function of two spins is defined as [198]

$$C_R^{kk} = \langle \sigma_1^k \sigma_2^k \rangle - \langle \sigma_1^k \rangle \langle \sigma_2^k \rangle ,$$

where $k \in x, y, z$. The expectation value is taken over the state of the system. For the state of the system in thermal equilibrium, these functions take the forms

$$\begin{aligned} C_R^{xx} &= C_R^{yy} = \frac{-\sinh \frac{J}{T}}{\cosh \frac{B}{T} + \cosh \frac{J}{T}}. \\ C_R^{zz} &= \frac{\sinh \frac{B}{T} - \cosh \frac{J}{T}}{\cosh \frac{B}{T} + \cosh \frac{J}{T}} - \left[\frac{\sinh \frac{B}{T}}{\cosh \frac{B}{T} + \cosh \frac{J}{T}} \right]^2 . \end{aligned} \tag{2.5}$$

A plot of the xx-correlation function as a function of the magnetic field (B) and temperature (T) is shown in **Fig. 2.1**. In this plot, any non-zero value of the correlation functions represents a correlated state. It is clear from this plot that as $T \to 0$, the correlation exhibits a very sharp change around the critical point $B = J$. This signals the existence of a first-order QPT. We found that the yy- and zz-correlation also exhibit similar behaviour in the neighbourhood of the critical point. The transition becomes sharper as the temperature decreases and the first order derivative of the correlation functions with respect to the external control parameter (here the magnetic field) diverges at the critical point [see **Fig. 2.2**] [203]. Mathematically, at the quantum critical point ($T = 0, B = B_c = J$), the correlation functions become nonanalytic functions of B and a quantum phase transition takes place [200].

Entanglement:

Similar behaviour can also be found in the variation of the entanglement between the spins in terms of concurrence [200, 205], which is given by

$$c(\rho) = \max \left\{ 0, \sqrt{\lambda_1} - \sqrt{\lambda_2} - \sqrt{\lambda_3} - \sqrt{\lambda_4} \right\}$$

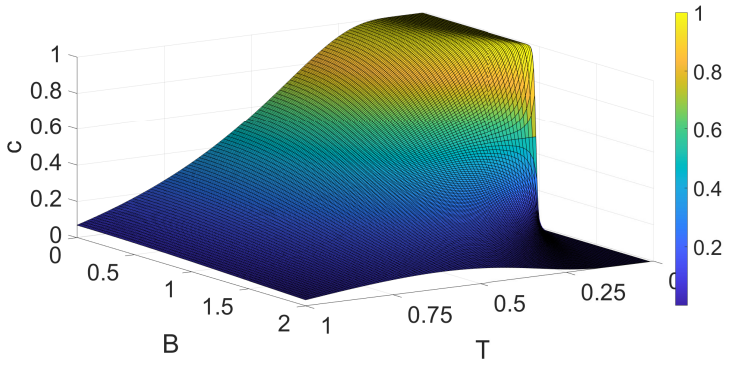

Figure 2.3: Variation of concurrence of two spins at thermal equilibrium as a function of temperature (T) and magnetic field (B). We have chosen $J = 1$.

where λ_i are the eigenvalues of the matrix $\rho\,(\sigma_1^y \otimes \sigma_2^y)\,\rho^*\,(\sigma_1^y \otimes \sigma_2^y)$ arranged in descending order and ρ^* is the complex conjugate of ρ. We get the expression of the concurrence as

$$c = \frac{\sinh \frac{J}{T} - 1}{\cosh \frac{J}{T} + \cosh \frac{B}{T}}. \tag{2.6}$$

If $c = 0$, this refers to a separable state, while for the maximally entangled Bell states, c becomes unity. A plot of concurrence as a function of the magnetic field B and the temperature T is displayed in **Fig. 2.3**. It is clear that as T decreases, the concurrence exhibits a faster decrease in the neighbourhood of $B = J$ (the critical point). This means that the concurrence exhibits nonanalytical behaviour around this critical point, as $T \to 0$. Such a sharp change in concurrence from 1 to 0 (i.e., from a maximally entangled state to a separable state) is a signature of the first-order QPT. In fact, this can be attributed to the change in the ground state from $|\psi_2\rangle$ to $|\psi_1\rangle$.

Thus, the concurrence and the correlation can be considered as order parameters (which distinguish between two phases in a phase transition) to identify QPT in the two-spin system, described via the Hamiltonian (**Eq. 2.1**) [198].

2.3 Implementation of different stages of the quantum Stirling cycle

The quantum Stirling cycle, in analogy with its classical counterpart, consists of four stages: two quantum isothermal and two quantum isochoric processes (see **Fig. 2.4**). A description of the four stages of the cycle is given below. Note the coupling constant J is kept fixed, as it depends upon the distance between the two spins and cannot be dynamically changed in a given spin architecture.

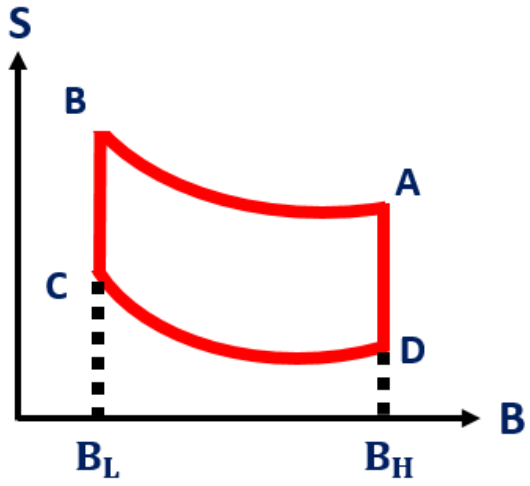

Figure 2.4: Schematic diagram of the different stages of a Stirling cycle on the entropy-magnetic field plane. A description is added to the text.

Isothermal stage ($A \rightarrow B$): The system is coupled with a heat bath at a temperature T_H and the magnetic field is changed quasistatically from B_H to B_L such that the system maintains thermal equilibrium with the bath at each point in that process. During this process, heat is exchanged between the system and the bath, while the system also exchanges a certain amount of work with an external work reservoir. The heat exchanged can be calculated in terms of the change in entropy of the system, which is, in turn, associated with the change in energy of the system, and is given by

$$Q_{AB} = T_H(S_B - S_A) = U_B - U_A + T_H \ln \frac{Z_B}{Z_A} \,, \tag{2.7}$$

where S_A and S_B represent the entropies of the system at points A and B respectively. U_A and U_B represent the internal energies at A and B respectively. Also, $Z_A = 2(\cosh\frac{B_H}{T_H} + \cosh\frac{J}{T_H})$ and $Z_B = 2(\cosh\frac{B_L}{T_H} + \cosh\frac{J}{T_H})$ are the partition functions at points A and B respectively.

Isochoric stage ($B \rightarrow C$): In the second stage, the coupling to a heat bath of lower temperature $T_L (< T_H)$ is switched on, while the magnetic field is kept fixed at B_L. During this stage, heat is exchanged between the system and the bath and at the end of the stage, the system reaches thermal equilibrium with the cold bath at the temperature T_L. No work is done on or by the system, as the magnetic field remains fixed. Therefore, the change in the internal energy of the system contributes to the heat transfer between the system and the bath contributes only. This is given by

$$Q_{BC} = U_C - U_B \,, \tag{2.8}$$

where U_C represent the internal energy of the system at point C.

Isothermal stage ($C \to D$): The third stage is similar to the first one. The only differences are that in this case, the system is coupled with another heat bath at the temperature T_L and the magnetic field is reversed from B_L to B_H. The heat transfer between the system and the bath can be written as

$$Q_{CD} = T_L(S_D - S_C) = U_D - U_C + T_L \ln \frac{Z_D}{Z_C} , \tag{2.9}$$

where S_D and S_C represent the entropies of the at points D and C. U_D represents the internal energy at D. Also, $Z_C = 2(\ \cosh \frac{B_L}{T_L} + \cosh \frac{J}{T_L}\ )$ and $Z_D = 2(\ \cosh \frac{B_H}{T_L} + \cosh \frac{J}{T_L}\ )$ are the partition functions at points C and D of **Fig. 2.4**.

Isochoric stage ($D \to A$): In the final stage, the system is coupled to the hotter heat bath at a temperature T_H again, while the magnetic field is kept fixed at B_H. No work is done on or by the system, as the magnetic field remains fixed. Similar to the previous isochoric process (the second stage), the heat transfer is given by

$$Q_{DA} = U_A - U_D . \tag{2.10}$$

Thermodynamic quantities in a complete cycle:

In a complete cycle, heat transfer between the system and the hot bath at the temperature T_H is therefore given by

$$Q_H = Q_{AB} + Q_{DA} = U_B - U_D + T_H \ln \frac{Z_B}{Z_A} . \tag{2.11}$$

Similarly, the heat exchange with the cold bath at the temperature T_L becomes

$$Q_L = Q_{BC} + Q_{CD} = U_D - U_B + T_L \ln \frac{Z_D}{Z_C} . \tag{2.12}$$

According to the first law of thermodynamics, the total change of energy of the system in a complete cycle is zero $W_{AB} + W_{CD} + Q_H + Q_L = 0$, where W_{AB} and W_{CD} represent the works in the AB and CD isothermal processes. So, the work done in a complete cycle can be written as

$$W = -(W_{AB} + W_{CD}) = Q_H + Q_L = T_H \ln \frac{Z_B}{Z_A} + T_L \ln \frac{Z_D}{Z_C} . \tag{2.13}$$

We are using the following sign convention of the thermodynamic quantities: a positive (negative) value of Q refers to the absorption (release) of heat by the system and a positive (negative) value of W corresponds to work done by (on) the

system. Therefore, for a heat engine, we have $Q_H > 0$, $Q_L < 0$, and $W > 0$, i.e., the system absorbs some amount of heat Q_H from the hot bath, a part Q_L of which is released to the cold bath and the rest is used to deliver a certain amount of work W. Similarly, when performing as a refrigerator, $Q_H < 0$, $Q_L > 0$, and $W < 0$, such that Q_L amount of heat is absorbed by the system and W amount of work is done on the system. This energy input is released as Q_H amount of heat to the hot bath. Here we assumed that the internal energy of a system does not change in a complete heat cycle.

The efficiency of the heat engine cycle is given by

$$\eta = \frac{W}{Q_H} = \frac{Q_{AB} + Q_{BC} + Q_{CD} + Q_{DA}}{Q_{AB} + Q_{DA}} , \tag{2.14}$$

while the coefficient of performance (COP) of the refrigeration cycle is given by

$$\epsilon = \frac{Q_L}{\mid W \mid} = \frac{Q_{BC} + Q_{CD}}{\mid Q_{AB} + Q_{BC} + Q_{CD} + Q_{DA} \mid} . \tag{2.15}$$

2.4 Performance analysis of thermal machines

2.4.1 Numerical observations

Operation of the cycle as various thermal machines:

To identify the operation of the cycle as different thermal machines, we plot the thermodynamic quantities heat Q_H exchanged with the hot bath, that Q_L with the cold bath, and the work done W in **Fig. 2.5** and **Fig. 2.6**.

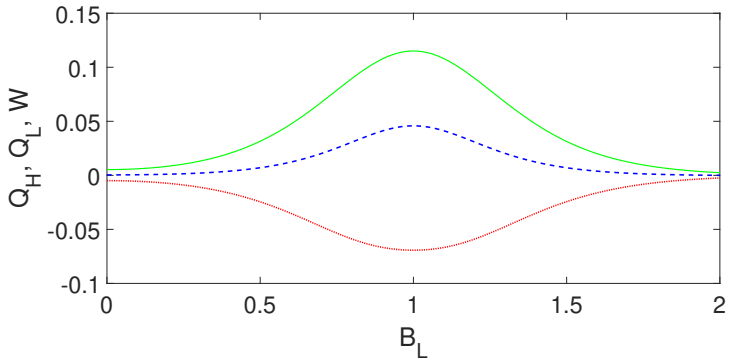

Figure 2.5: Variation of heat exchange by the system with the hot bath, Q_H (solid line, green), that with the cold bath, Q_L (dotted line, red) and the work done W (dashed line, blue) as a function of B_L when $J = 1$, $B_H = 2$, $T_H = 0.166$ and $T_L = 0.1$. In all the figures, we have used a unit system where $\hbar = 1$, $k_B = 1$ and all parameters are made dimensionless with respect to J for the two-spin system.

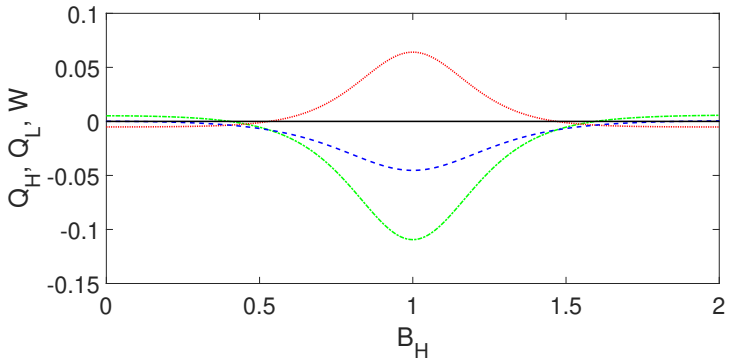

Figure 2.6: Variation of the heat exchange by the system with the hot bath, Q_H (dash-dotted line, green), that with the cold bath, Q_L (dotted line, red) and the work done W (dashed line, blue) as a function of B_H when $J = 1$, $B_L = 0.066$, $T_H = 0.166$ and $T_L = 0.1$. The solid black line represents the zero line.

It can be seen from **Fig. 2.5** that the system works as a heat engine over the entire range of the parameter B_L ($< B_H$), as $Q_H, W > 0, Q_L < 0$ in this range. More importantly, it delivers maximum work when B_L becomes nearly equal to the coupling constant J. On the other hand, from **Fig. 2.6**, it is clear that the system works as a refrigerator, though not over the entire range of the parameter B_H ($> B_L$). Rather, there exists a narrower range of values B_H for such an operation. In this case, also, the cycle gives better performance in terms of heat absorption, heat release and work done when B_H becomes equal to the coupling constant J. This range of B_H for the operation of the refrigerator cycle decreases with the increase in B_L. Note that all the quantities Q_H, Q_L and W are negative, when the B_H becomes nearly equal to 0.5 and 1.5 (see **Fig. 2.6**). This means that work is to be done on the system to drive heat flows into both the heat baths. This type of thermal machine therefore does not become useful due to high energy cost and we will only focus on the parameter domain in which the thermal machine works either as a heat engine or a refrigerator.

Clearly, the two-spin system can be made through a heat engine cycle or a refrigerator cycle by a suitable choice of the parameters B_L, B_H and J of the cycle. For $B_L \approx J$, the system delivers maximum work as a heat engine, while for $B_H \approx J$, it performs as a refrigerator.

Performance of the heat engine and refrigerator:

Now we will study the performance of the thermal machines. We find that the efficiency of the heat engine reaches Carnot efficiency at $B_L = J$ for very low temperatures of the heat baths. The Carnot efficiency for the present choice of the bath temperatures is given by $\eta_C = 1 - T_L/T_H = 0.4$. The efficiency gradually falls

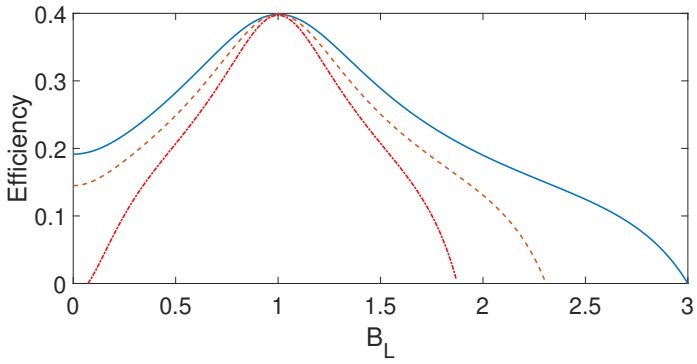

Figure 2.7: Variation of the efficiency as a function of B_L for different values of B_H and bath temperatures: $T_H = 0.25$, $T_L = 0.15$ and $B_H = 3$ (solid line, light blue); $T_H = 0.19$, $T_L = 0.11$ and $B_H = 2.3$ (dashed line, brown); $T_H = 0.15$, $T_L = 0.09$ and $B_H = 1.87$ (dash-dotted line, red) when $J = 1$. Note that the Carnot efficiency for all the cases is $\eta_C = 0.4$, which is achieved when $B_L = J = 1$.

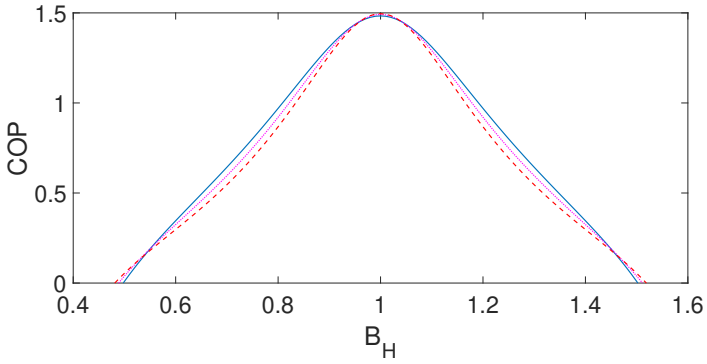

Figure 2.8: Variation of the COP as a function of B_H for different values of B_L and bath temperatures: $T_H = 0.125$, $T_L = 0.075$ and $B_L = 0.05$ (solid line, light blue); $T_H = 0.114$, $T_L = 0.068$ and $B_L = 0.045$ (dotted line, pink); $T_H = 0.104$, $T_L = 0.06$ and $B_L = 0.04$ (dashed line, red) for $J = 1$. Note that the Carnot COP for all the cases is $\epsilon_C = 1.5$, which is achieved when $B_H = J = 1$.

when B_L deviates from its critical value J [see **Fig. 2.7**]. Similarly, the COP of the refrigerator reaches that for a Carnot refrigerator, given by $COP_C = T_L/(T_H - T_L) = 1.5$, when B_H becomes equal to a critical value J [see **Fig. 2.8**]. Note that according to the first law of thermodynamics, the COP can be greater than unity.

2.4.2 Theoretical analysis of obtaining the Carnot limit of efficiency and COP

Now we will theoretically analyze how the efficiency and the COP can reach the respective Carnot limits at the QCP point.

For heat engine:

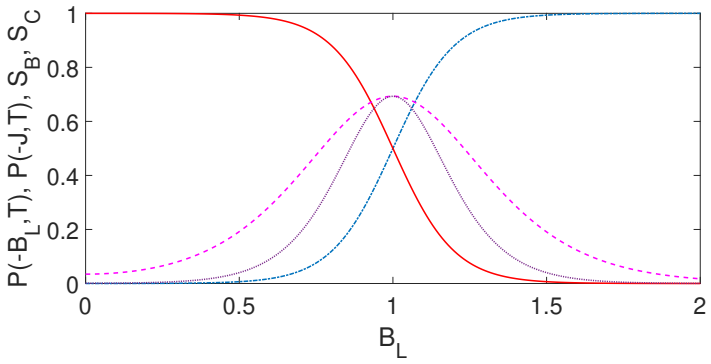

Figure 2.9: Variation of the entropy at the point B of the cycle S_B (dashed line, pink) and at C of the cycle S_C (dotted line, violet) as a function of B_L when $B_H = 2$, $J = 1$, $T_H = 0.166$ and $T_L = 0.1$. Variation of the population of the energy levels $P(-J,T)$ (solid line, red) and the $P(-B_L,T)$ (dash-dotted line, light blue) as a function of B_L are also shown.

Now in the DA arm of the cycle, when $B_H \gg J$, under low temperature population of the ground state $|\psi_1\rangle$ is obtained as

$$P_1(B_H,T) = \frac{\exp(B_H/T)}{\exp(B_H/T) + \exp(-B_H/T) + \exp(-J/T) + \exp(J/T)} \approx 1 \, .$$

Most of the population remains in the ground state. This means that the von Neumann entropies of the system, at the points A and D of the cycle become negligible: $S_A(B_H,T_H), S_D(B_H,T_L) \approx 0$. Therefore, the heat transfer of the system with the hot bath in the isochoric process from D to A is given by

$$\mathrm{Q}_{D\Lambda} = U_A - U_D = \sum_{i=1}^{4} P_i^A E_i^A - \sum_{i=1}^{4} P_i^D E_j^D \approx E_1^A - E_1^D = 0. \tag{2.16}$$

With all these, the efficiency of the heat engine becomes

$$\eta = \frac{T_H S_B + U_C - U_B - T_L S_C}{T_H S_B} \, . \tag{2.17}$$

Now if the BC arm of the cycle is placed at the QCP, $B_L = J$, the entropies of the system at points B and C of the cycle become equal: $S_B \approx S_C \approx \ln 2$ (see **Fig. 2.9**). Also, the internal energies of the system at these points become equal: $U_B \approx U_C \approx -B_L$. Using these values, from the **Eq. 2.17**) we retrieve the efficiency of the heat engine at the QCP, which is the same as the Carnot efficiency:

$$\eta = 1 - \frac{T_L}{T_H} \, . \tag{2.18}$$

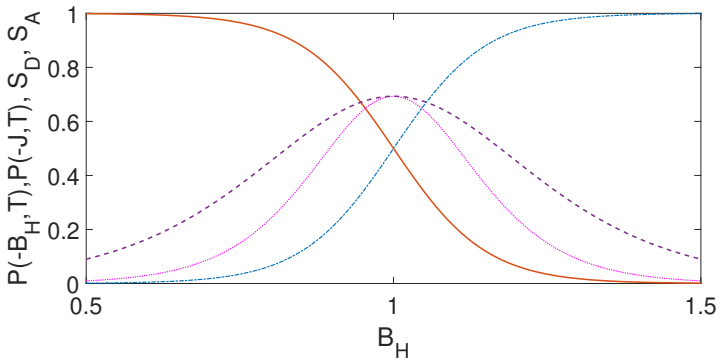

Figure 2.10: Variation of the entropy at the point D of the cycle S_D (dotted line, pink) and at A of the cycle S_A (dashed line, violet) as a function of B_H when $B_L = 0.05$, $J = 1$, $T_H = 0.125$ and $T_L = 0.075$. Variation of the population of the energy levels $P(-J,T)$ (solid line, red) and $P(-B_H,T)$ (dash-dotted line, light blue) as a function of B_H are also shown.

So, the efficiency of the quantum Stirling engine approaches the Carnot efficiency at the quantum critical point, B_L is equal to J, under the condition that B_H is much larger than J at very low temperatures of the baths compare to J.

For refrigerator:

Similarly, for the refrigerator cycle, in the BC arm of the cycle, when $J \gg B_L$, under low-temperature population in the ground state, $|\psi_2\rangle$ is obtained as

$$P_2(J,T) = \frac{\exp(J/T)}{\exp(B_L/T) + \exp(-B_L/T) + \exp(-J/T) + \exp(J/T)} \approx 1 \ .$$

Thus, when the magnetic field is maintained at a constant value B_L (the evolution from B to C in **Fig. 2.4**), the system is prepared in the ground state. Therefore, it possesses negligible entropy and the heat exchanged during this isochoric stage is also negligible. Then the COP of the refrigerator cycle becomes

$$\epsilon = \frac{T_L S_D}{|T_L S_D - T_H S_A + U_A - U_D|} \ . \tag{2.19}$$

Now if the DA arm of the cycle is placed at the QCP $B_H = J$, similar to the case of the heat engine, the entropies of the system at points D and A of the cycle become equal, i.e., $S_D \approx S_A \approx \ln 2$ (see **Fig. 2.10**). Also, the internal energies of the system at points D and A become equal: $U_D \approx U_A \approx -B_H$, such that $Q_{BC} \approx 0$. With all these values, the COP of the refrigerator cycle at the QCP is obtained as

$$\epsilon = \frac{T_L}{T_H - T_L} \ , \tag{2.20}$$

which is the same as the Carnot COP. So, the COP of the Stirling refrigerator approaches the Carnot COP at the QCP $B_H = J$ under the conditions $B_L \ll J$ at very low bath temperatures compared to J.

Work and efficiency extremization:

As we mentioned, the work and the efficiency become maximized at the QCP. However, for larger bath temperatures, this is not true. As long as these temperatures are much lower than the strength of the coupling constant J, the effect of the quantum phase transition dominates. In this situation, the population in each of the degenerate ground states $|E_{1,2}\rangle$ remains at 50%. However, for larger temperatures ($T_{L,H} \sim J$), the excited states $|E_{3,4}\rangle$ also get populated, Then, the work and the efficiency do not get maximized at the QCP. This can be understood from the condition of zeros of the derivatives of W and η with respect to B_L. We get the following conditions at the QCP ($B_L = J$) from the derivative of work

$$\tanh\left(\tfrac{J}{T_L}\right) = \tanh\left(\tfrac{J}{T_H}\right) , \tag{2.21}$$

and from the derivative of efficiency

$$\begin{aligned} &\left[\tanh\left(\tfrac{J}{T_H}\right) - \tanh\left(\tfrac{J}{T_L}\right)\right] \times \\ &\left[T_H \ln\left(\tfrac{Z_B}{Z_A}\right) - J\tanh\left(\tfrac{J}{T_H}\right) + \tfrac{2}{Z_D}\left\{B_H \sinh\left(\tfrac{B_H}{T_L}\right) + J\sinh\left(\tfrac{J}{T_L}\right)\right\}\right] \\ &= (\tfrac{J}{T_H})\left[T_L \ln\left(\tfrac{Z_C}{Z_D}\right) - T_H \ln\left(\tfrac{Z_B}{Z_A}\right)\right] \mathrm{sech}^2(\tfrac{J}{T_H}) . \end{aligned} \tag{2.22}$$

Since, for $B_L = J$ and $T_L, T_H \ll J$ both the above equalities are satisfied [as $\tanh(J/T_L)$, $\tanh(J/T_H) \to 1$], the work and the efficiency become maximum at the QCP $B_L = J$. However, for larger T_L, T_H, such that $T_L, T_H \sim J$, they exhibit maximum at different values of B_L. This becomes clear from the work-efficiency plot in **Fig. 2.11**. As can be seen in **Fig. 2.11(c)** for $T_L = 0.4$ and $T_H = 0.666$, the efficiency becomes maximum at $B_L = 0.7747$ and the work becomes maximum at $B_L = 0.9807$, both far from the QCP.

Similar conditions can be obtained for the relation between the work W on the system during the refrigeration cycle and the corresponding COP at the critical point $B_H = J$. We find that the condition to minimize the W is the same as Eq. (2.21), while that to maximize COP can be written as (2.22), however with the following replacements: $T_L \leftrightarrow T_H$ and $B_H \leftrightarrow B_L$, with different expressions of the partition functions, namely, $Z_A = 4\cosh(J/T_H)$, $Z_B = 2\{\cosh(B_L/T_H) + \cosh(J/T_H)\}$, $Z_C = 2\{\cosh(B_L/T_L) + \cosh(J/T_L)\}$, and $Z_D = 4\cosh(J/T_L)$.

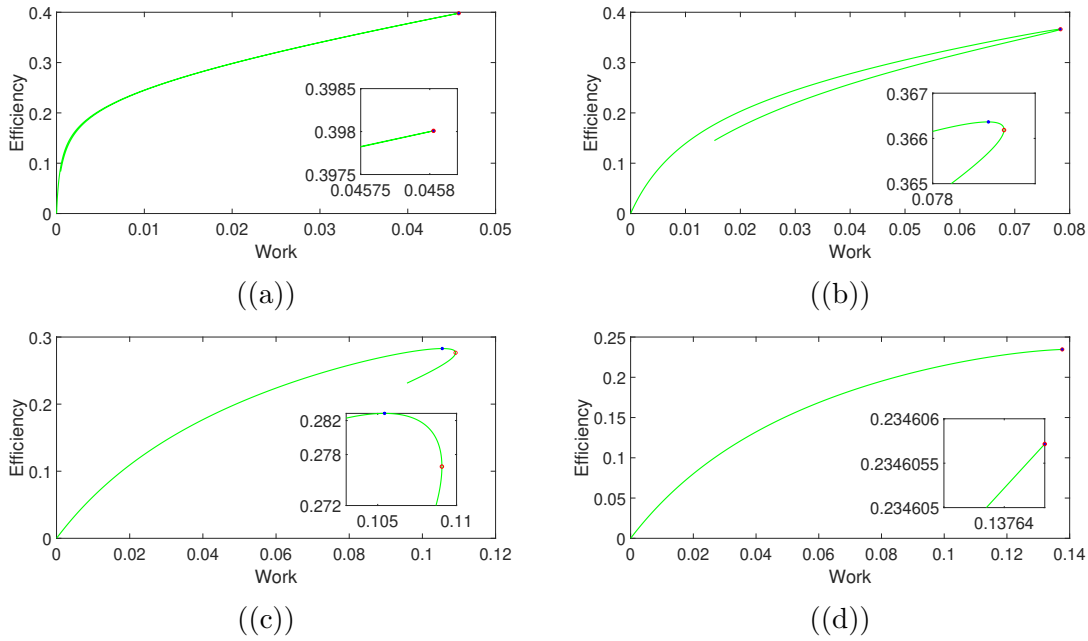

Figure 2.11: Variation of the efficiency with respect to the work, when B_L changes from 0 to 2 and the bath temperatures are (a) $T_H = 0.166$ and $T_L = 0.1$, (b) $T_H = 0.33$ and $T_L = 0.2$, (c) $T_H = 0.666$ and $T_L = 0.4$, (d) $T_H = 1$ and $T_L = 0.666$. The other parameters are $B_H = 2$ and $J = 1$. Black dot and red circles in the corresponding zoomed figures (in the inset) indicate the maximum efficiency and work, for (a) the same value $B_L = 0.9997$ (b) $B_L = 0.9947$ and $B_L = 1.0127$, respectively, (c) $B_L = 0.7747$ and $B_L = 0.9807$, respectively, and (d) the same value of $B_L = 0.0667$.

2.4.3 Relation of the thermodynamic quantities with correlation and entanglement

We will show now how the maximization of the work and efficiency at low temperatures of the baths are related to the entanglement at the QCP for the heat engine operation. Concurrences at points B and C of the cycle can be found as

$$c_B = \frac{\sinh\frac{J}{T_H} - 1}{\cosh\frac{J}{T_H} + \cosh\frac{B_L}{T_H}}, \text{ and } c_C = \frac{\sinh\frac{J}{T_L} - 1}{\cosh\frac{J}{T_L} + \cosh\frac{B_L}{T_L}}. \tag{2.23}$$

These two expressions become equal, for the low temperatures of the baths, $J \gg T_L, T_H$ and at the QCP $B_L = J$, as $\tanh(J/T_L) \sim \tanh(J/T_H) \to 1$ and $\mathrm{sech}(J/T_L) \sim \mathrm{sech}(J/T_H) \to 0$ in this limit. As we discussed before, in this limit, the work and the efficiency of the heat engine also get maximized. We have found that the concurrences become equal to 0.5 at the QCP [199]. This is because, in the process B$\to$ C the state of the system does not change, therefore, there is no heat exchange of the system with the bath in that process. This in turn gives rise to the maximization of work and efficiency at the quantum critical point. Further,

as we have seen from the **Fig. 2.3**, the concurrence sharply changes from one to zero across the QCP at $T \to 0$, corresponding to a change in the ground state of the system (from a maximally entangled state $|\psi_2\rangle$ to a separable state $|\psi_1\rangle$). This leads to a large derivative of the concurrences and to the enhancement of efficiency. On the contrary, at higher temperatures of the baths, the concurrences c_B and c_C do not become equal at the critical point, which in turn reduces the work and efficiency of the heat engine operation. Moreover, the system never becomes maximally entangled or fully separable, as clear from the values of concurrence at $B_L = 0$ and $B_L = 2$ [199] at higher temperatures.

Similar to the QHE operation, we can relate the maximization of COP with the equality of the concurrences at points D and A of the cycle:

$$c_D = \frac{\sinh \frac{J}{T_L} - 1}{\cosh \frac{J}{T_L} + \cosh \frac{B_H}{T_L}}, \text{ and } c_A = \frac{\sinh \frac{J}{T_H} - 1}{\cosh \frac{J}{T_H} + \cosh \frac{B_H}{T_H}}, \tag{2.24}$$

which become equal at the critical point [199], as there is no heat generation during the isochoric process D→A. This leads to the maximum COP. This also is related to the nonanalytic behaviour of the derivative of the correlation near the QCP when $T \to 0$.

Therefore we can conclude that for the Stirling cycle thermal machines, the sharp changes and equalization of the correlation functions near the QCP can similarly be related to the enhancement of efficiency and the COP.

2.4.4 Use of a regenerator in the cycle

The Stirling cycle generally operates with a regenerator, which is a substance that stores a non-zero heat output from the isochoric cooling process and is reused in the next isochoric heating process [206]. These heat inputs and outputs need to be accounted for in the calculation of efficiency.

In our case, the heat release and absorption in the two isochoric processes (Q_{BC} and Q_{DA}) remain zero under the physical conditions the cycle is being operated at the QCP, so there is no heat imbalance. Therefore, one does not require a heat regenerator in our case and the quantum Stirling cycle works reversibly at the QCP. Thus, we emphasize that a quantum Stirling cycle should be best operated at the QCP of the working system to achieve the best performance.

2.4.5 Experimental feasibility

Now to explore the possible experimental implementation of the present model of thermal machines using a coupled two-spin system we have to look at the state-of-the-art quantum technology [193]. We have to find a system where the coupling constant should be much larger than the possible achievable temperature in that system. The most suitable choice for this can be the superconducting circuits, in which the Heisenberg type of interaction between the qubits can be constructed. In this system, the coupling constant between two qubits can be a few hundred MHz and the external magnetic field can also be of the same order of magnitude [193, 207, 208]. Moreover, we can make the temperature of a superconducting circuit of the order of a few mK [209].

In order to have numerical estimates of potential work output and performance figures of merits, let us consider the temperature of the hot bath as $T_H = 0.2$ mK and that of the cold bath as $T_H = 0.1$ mK. Also, we consider that the coupling constant between two qubits is $J = 150$ MHz and the external magnetic fields are given by $B_L = J$ and $B_H = 2J$ for the cycle operation at the critical point. Using these parameters, we get the following values of the thermodynamic variables, namely, the total work done $W = 0.6867 k_B T_L = 9.4768 \times 10^{-28}$ Joule and heat transfer $Q_H = 1.38 k_B T_L = 19.044 \times 10^{-28}$ Joule, $Q_L = 0.6932 k_B T_L = -9.5669 \times 10^{-28}$ Joule, and the efficiency $\eta = 0.4976$, which is very close to the Carnot efficiency 0.5.

2.5 Thermal machines with three spins

Next, we consider a three-spin chain, in which each spin interacts with its nearest neighbour spin via Heisenberg XX exchange interaction. Such a model can be useful to understand the thermodynamic behaviour of the two spins when all three spins are in thermal equilibrium and undergo a quantum Stirling cycle. This kind of scenario also helps us to understand how a subsystem of a total system behaves as a thermal machine when the total system is operated in a Stirling cycle. In this Section, we will first analyze the performance of the three spins and then that of the first two spins.

It is expected that the two spins will exchange energy with both the baths and the third spin, therefore will not be in thermal equilibrium with the bath. So, it is a joint interplay of coupling to the baths and the third spin, that affects the thermal machine performance of the two spins as a working system. This is strictly different from other models, where the working system itself is in thermal equilibrium, and its interaction with any additional spin brings it out of equilibrium.

We note that this model can be extended to study internal heat current, work imbalance, and microscopic heat management. Such types of performance analysis of heat engines for a subsystem have been done previously for other engine cycles also [210, 211, 212, 213, 214, 184, 179].

2.5.1 Case of three spins

The Hamiltonian describing the evolution of three spins can be written as

$$H_{tot} = \frac{B}{2}(\sigma_1^z + \sigma_2^z + \sigma_3^z) + J_1(\sigma_1^+\sigma_2^- + \sigma_1^-\sigma_2^+) + J_2(\sigma_2^+\sigma_3^- + \sigma_2^-\sigma_3^+) \ , \tag{2.25}$$

where J_i represents the coupling strength between the ith and the $(i+1)$th spin ($i \in 1, 2$). The eigenvalues and the corresponding normalized eigenstates of this Hamiltonian are given by

$$\begin{aligned} &E_1^{tot} = -x_-, E_2^{tot} = x_+, E_3^{tot} = -x_+, E_4^{tot} = x_-, \\ &E_5^{tot} = -\frac{B}{2}, E_6^{tot} = \frac{B}{2}, E_7^{tot} = -\frac{3B}{2}, E_8^{tot} = \frac{3B}{2} \ , \end{aligned} \tag{2.26}$$

and

$$\begin{aligned} ket\phi_1 &= \frac{1}{\sqrt{2(J_1^2+J_2^2)}}(J_1 \left|100\right\rangle + \sqrt{J_1^2+J_2^2}\left|010\right\rangle + J_2\left|001\right\rangle) \ , \\ \left|\phi_2\right\rangle &= \frac{1}{\sqrt{2(J_1^2+J_2^2)}}(J_2 \left|110\right\rangle + \sqrt{J_1^2+J_2^2}\left|101\right\rangle + J_1\left|011\right\rangle) \ , \\ \left|\phi_3\right\rangle &= \frac{1}{\sqrt{2(J_1^2+J_2^2)}}(J_1 \left|100\right\rangle - \sqrt{J_1^2+J_2^2}\left|010\right\rangle + J_2\left|001\right\rangle) \ , \\ \left|\phi_4\right\rangle &= \frac{1}{\sqrt{2(J_1^2+J_2^2)}}(J_2 \left|110\right\rangle - \sqrt{J_1^2+J_2^2}\left|101\right\rangle + J_1\left|011\right\rangle) \ , \\ \left|\phi_5\right\rangle &= \frac{1}{\sqrt{J_1^2+J_2^2}}(-J_2 \left|100\right\rangle + J_1\left|001\right\rangle) \ , \\ \left|\phi_6\right\rangle &= \frac{1}{\sqrt{J_1^2+J_2^2}}(-J_1 \left|110\right\rangle + J_2\left|011\right\rangle) \ , \\ \left|\phi_7\right\rangle &= \left|000\right\rangle \ , \ \left|\phi_8\right\rangle = \left|111\right\rangle \ , \end{aligned} \tag{2.27}$$

where $x_\pm = \frac{B}{2} \pm \sqrt{J_1^2+J_2^2}$. In such a case, the QCP can be found when $E_7^{tot} = E_3^{tot}$, i.e., when $B = B_c = \sqrt{J_1^2+J_2^2}$. As the magnetic field increases from $B < B_c$ to $B > B_c$, the ground state changes from $\left|\phi_3\right\rangle$ to $\left|\phi_7\right\rangle$, indicating a QPT.

The state of the system, when in thermal equilibrium with a heat bath at a temperature T, can be written as (in a unit of $k_B = 1$)

$$\rho_{tot} = \sum_n P_n^{tot} \left|\phi_n\right\rangle \left\langle\phi_n\right| \ ,$$

where the occupation probabilities of the eigenstates $\left|\phi_n\right\rangle$ are $P_n = \exp(-E_n^{tot}/T)/Z$ and $Z = \sum_n \exp(-E_n^{tot}/T)$ is the partition function.

Now, let us first choose all the three coupled spins as the working system which

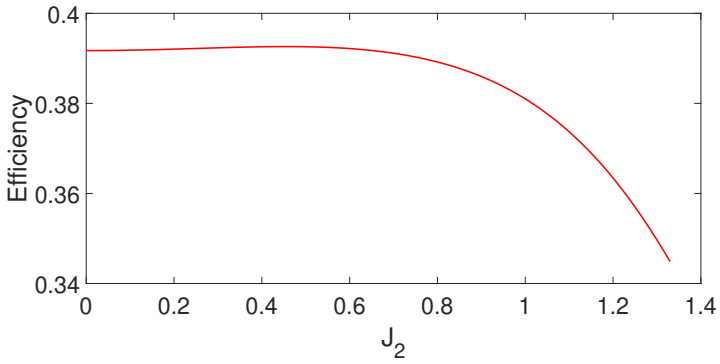

Figure 2.12: Variation of the efficiency of a 3-spin Stirling heat engine as a function of J_2, at the corresponding critical point $B_L = \sqrt{J_1^2 + J_2^2}$. The parameters chosen here are $J_1 = 1$, $B_H = 2$, $T_H = 0.166$ and $T_L = 0.1$. All the parameters are made dimensionless with respect to J_1 for three-spin system.

follows the same standard Stirling cycle as described for the two spins in the Sec. 4.2.1. We show in **Fig. 2.12** how the efficiency at the QCP behaves in a nonlinear fashion with change in J_2. It is clear that for larger J_2, both the work and the efficiency get reduced. More interestingly, when $J_2 = 0$, the 3-spin working system can be considered as if there are two coupled spins, along with a third spin, which is not directly coupled with the first two. In such a case, $B_L = J_1$ still represents the QCP and the system behaves as a heat engine, albeit with a reduced efficiency than a two-spin heat engine (without the presence of the third spin as in Sec.2.2). This reduction in the efficiency to a value below the Carnot limit at QCP can thus be attributed to the mere presence of the third spin, which is not *directly* coupled with two coupled spins. We found that due to the presence of the third spin, the heat absorbed from the hot bath gets reduced, without changing the amount of work done. It must be borne in mind that this uncoupled spin still remains coupled to the common heat baths, as the two other spins are, during the isochoric processes of the cycle. Thus, a third spin, even if not directly coupled, affects the engine performance of the three-spin working system.

2.5.2 Case of two spins as a working system

The above analysis is valid when we consider all the three spins constituting the working system of the heat engine. But, if we choose only the first two spins as the working system, while the third spin acts as an auxiliary one (but coupled to the common bath), the present model can be considered as a suitable test bed to understand the effect of this additional spin. A similar kind of work has been reported in [179], where two coupled ions play the role of the working system that undergoes a quantum Otto cycle. The performance of this engine is studied in the

presence of a third ion. Also, a non-conventional heat cycle has been studied using a two-level system as the working medium, which is coupled to a cavity mode. The dynamics of the qubit is obtained by taking the partial trace on the cavity's degrees of freedom [210]. There are also reports on engine performance of a single-qubit system, namely, for the quantum Otto cycle [211, 212, 213, 214] and quantum Brayton cycle [184], where the single qubit has been a part of a larger system. Let us start with the three coupled spins. In the following, at each stage of the

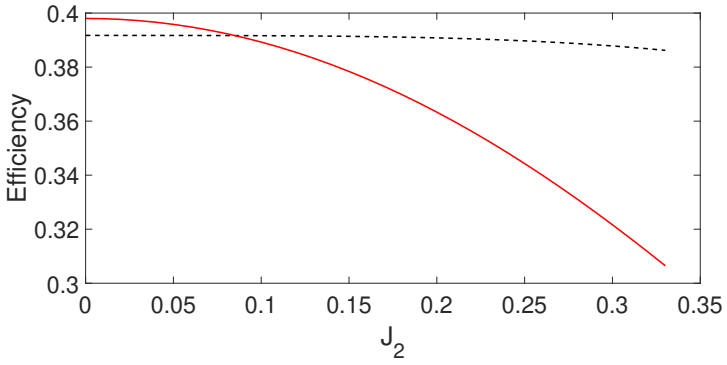

Figure 2.13: Variation of the efficiency of the heat engine with J_2, when (i) three spins are considered as a working system (solid line, red) and (ii) two-spin chosen to be the working system coupled with an auxiliary third spin (dashed line, black). The parameters chosen here are $B_L = J_1 = 1$, $B_H = 2$, $T_H = 0.166$ and $T_L = 0.1$.

quantum Stirling cycle, we will analyze the heat and work for the first two spins only. In order to assess the effect of the auxiliary system A, we need to find out how these first two spins evolve during the process. Therefore, we trace out the third spin partially from the joint density matrix of the three spins.

$$\begin{aligned}\rho_S = &\mathrm{Tr}_3(\rho_{tot}) = \rho_{11}\left|11\right\rangle\left\langle 11\right| + \rho_{22}\left|10\right\rangle\left\langle 10\right| + \rho_{23}\left|10\right\rangle\left\langle 01\right| \\ &+ \rho_{32}\left|01\right\rangle\left\langle 10\right| + \rho_{33}\left|01\right\rangle\left\langle 01\right| + \rho_{44}\left|00\right\rangle\left\langle 00\right| \ ,\end{aligned} \tag{2.28}$$

where the density matrix elements ρ_{11}, ρ_{22}, ρ_{23}, ρ_{32}, ρ_{33}, and ρ_{44} depend on the parameters J_1, J_2, B and T. This reduced density matrix ρ_S describes the behaviour of the subsystem (S) (i.e., first two spins coupled by the interaction J_1). Finally, the generalized form of the density matrix of the system S based on the first two spins can thus be written as

$$\rho_S = \sum_n P_n^S \left|\psi_n\right\rangle\left\langle\psi_n\right| \ , \tag{2.29}$$

where P_n^S is the occupation probability of the energy eigenstates $|\psi_n\rangle$ [see **Eq. 2.2**] of the subsystem S.

We consider that the three-spin system maintains a thermal equilibrium. But when we focus on the first two spins (as a part of a bigger system), they would not

necessarily maintain the equilibrium (with the heat baths) at different stages of the cycle. If the coupling J_2 is not zero, then the local temperature of this subsystem S will not be equal to the bath temperature and will change with a change in the local magnetic field at a finite coupling constant. Thus the stages A→ B and C→ D will not remain isothermal for the two-spin subsystem S. In such a case, the heat exchanged by the subsystem S with the baths at temperatures T_H and T_L, respectively, during those two stages can be calculated as [210]

$$\begin{aligned} Q_S^{AB} &= \int_{B_H}^{B_L} \mathrm{Tr}\left\{\left(\frac{\partial \rho_S^{AB}}{\partial B}\right) H_S\left(B\right)\right\} dB \ , \\ Q_S^{CD} &= \int_{B_L}^{B_H} \mathrm{Tr}\left\{\left(\frac{\partial \rho_S^{CD}}{\partial B}\right) H_S\left(B\right)\right\} dB \ , \end{aligned} \tag{2.30}$$

where ρ_S^{AB} and ρ_S^{CD} are the reduced density matrices of the subsystem S that evolve with the changing magnetic fields during the stages A→ B and C→ D, respectively. Here H_S is the part of the Hamiltonian H, relevant to the subsystem S, as given by

$$\frac{B}{2}(\sigma_1^z + \sigma_2^z) + J_1(\sigma_1^+\sigma_2^- + \sigma_1^-\sigma_2^+) \ . \tag{2.31}$$

The heat transfer of the subsystem S when all the three spins undergo an isochoric stage (B→ C and D→ A), are given by

$$Q_S^{BC} = U_S^C - U_S^B, \text{ and } Q_S^{DA} = U_S^A - U_S^D \ , \tag{2.32}$$

where $U_S^\mu = Tr(\rho_S^\mu H_S^\mu)$, $\mu \in$ A,B,C,D are the internal energies of the subsystem S at the points μ of the cycle, respectively. So, the work done by the subsystem in a complete cycle is given by

$$W_S = Q_S^{AB} + Q_S^{BC} + Q_S^{CD} + Q_S^{DA} \ . \tag{2.33}$$

The expressions of the efficiency (for heat engine) and the COP (for refrigerator) thus can be written as

$$\eta_S = \frac{W_S}{Q_S^{AB} + Q_S^{DA}}, \text{ and } \epsilon_S = \frac{Q_S^{BC} + Q_S^{CD}}{|W_S|} \ , \tag{2.34}$$

where the denominator in the expression of the efficiency represents the total heat input to the subsystem S and the numerator in the expression of the COP refers to the total heat released by S.

Now to find the effect of the auxiliary system on the performance of the cycle

performed by the subsystem we choose that the cycle is working at the QCP (i.e., $B_L = J_1$ for the heat engine operation and $B_H = J_1$ for the refrigerator operation). The interaction of the working system with an auxiliary system A affects the heat exchange of the working system with the heat baths.

We plot the efficiency as a function of J_2 in the **Fig. 2.13** when the subsystem works as a heat engine. Here, all the quantities are calculated numerically as their analytic expressions are too large to write down here. The efficiency of the thermal machine is reduced as the coupling constant J_2 with the third spin increases. Similarly, when the subsystem works as a refrigerator, we can also see that its performance degrades as J_2 increases. A similar result was reported by one of us [179] in the case of an ion-based Otto engine operating at QCP. Interestingly, we find that the efficiency at the QCP in a three-spin heat engine is more robust against the change in the coupling J_2 than that in a two-spin heat engine (see **Fig. 2.13**). This means that the coupling with an external spin affects substantially the performance of the thermal machines, when the two spins are not in thermal equilibrium.

2.6 Summary

In this work, we have investigated the performance of a quantum Stirling cycle based on two coupled spins as a working system, near QCP. Quantum phase transition in the system has been studied in terms of entanglement and correlation. One can implement a heat engine cycle or a refrigerator cycle by a suitable choice of the cycle parameters B_L, B_H, J, T_H, and T_L, at very low temperatures and over a large range of the magnetic field. Near the critical point $B_L = J$, the Stirling heat engine cycle reaches the Carnot efficiency for $B_H \gg J$. Similarly, the refrigerator cycle attains the Carnot limit of coefficient of performance for $B_L \ll B_H$ near the critical point $B_H = J$. However, for larger temperatures $\sim J$, the maximum values of these performance markers deviate substantially from their respective Carnot limits. Moreover, the maximum achievable work output also does not get associated with the maximum efficiency.

We have also analysed the behaviour of three spins as a thermal machine. We have found that as the coupling to a third spin increases, the performance of the quantum machine near the quantum critical point gets degraded. If we view the system of three spins as a combination of two spins and one additional spin, the performance of the two-spin thermal machine gets degraded. This can be attributed to the fact that the machine does not undergo ideal Stirling stages. For example, the machine cannot maintain its equilibrium temperature and thus does not have an isothermal stage, when coupled to the auxiliary spin.

Chapter 3

Effect of anisotropy on the performance of a quantum Otto machine

In the previous chapter, we discussed the quasistatic operation of quantum Starling machines. In this chapter, we will focus on the finite-time operation of QTM, specifically, we will show the implementation of a quantum Otto engine, and discuss the role of anisotropy and the finite-time effect on its performance.

3.1 Motivation

Finite power is required in various practical applications of quantum technologies. Operating a quantum heat engine (QHE) quasistatically leads to null power generation, which may not be useful in practice. Furthermore, the finite-time operation of the QTMs may exploit genuine non-classical properties in their performances [147, 215]. In fact, various QHE models have been studied for finite times. It has been shown that the non-Markovian character of dynamics can speed up the control of a quantum system and improve the power output of a thermal machine [216, 217]. In other studies, it is found that quantum coherence can be harnessed to increase the power of QHEs [121, 218, 96, 81, 219] and the efficiency at maximum power (EMP) [122], as well. Furthermore, the role of quantum internal friction on the work extraction and performance of the QHEs has been investigated [75, 76, 77, 78, 79, 215].

Coupled spin systems play an important role as a working system for QTMs [116, 220, 212, 221, 213, 222, 76, 214, 223, 224, 147, 225]. The coupling strength between the spin can serve as an additional control parameter for the cycle [226]. The anisotropy in the coupling between the spins adds further flexibility. The effect of such anisotropy on entanglement [200, 227, 228, 229, 230], teleportation [231, 232, 233] and the tripartite uncertainty bound [234] has been studied. Recently, the role of anisotropy in quantum batteries has been studied [235, 236, 237]. It was shown

that the maximum power output of this battery can be enhanced by maintaining the anisotropy at low values.

In this chapter, we study the performance of a QOE with a two-spin working system coupled to each other via Heisenberg's anisotropic XY interaction. Our investigation focuses on different time limits of the cycle: firstly, the quasistatic operation; then, the nonadiabatic unitary processes; and finally, the incomplete thermalization in the hot isochoric process. Due to the anisotropy in the interaction between the spin, the Hamiltonian does not commute at two times and due to this non-commutation, a genuine quantum feature appears in the finite time operation of the cycle [238]. We will investigate how the anisotropy affects the engine's performance both for the quasistatic and finite-time operation of the engine.

Then we will consider one of the two spins, as the working system. The heat engine performance of this single spin (the 'local' spin) in the presence of the other will be analyzed. Primarily, we aim to investigate how it differs from a single-spin QHE which does not couple to any other spin. We ask the following question: Can we get any thermodynamic advantage in such a local scenario? We want to explore how the anisotropic interaction (and, therefore, the non-commuting nature of the Hamiltonian affects the performance of a local spin QHE.

In this chapter, we present our QHE model and implementation of the cycle. We discuss the various limiting cases of the duration of the QHE operation. Further, we explore the QHE operation of the 'local' spin. Then, we discuss potential experimental implementations of our QHE model.

3.2 Implementation of the quantum Otto cycle

3.2.1 System model

Let's consider a system of two-spin coupled by an anisotropic XY interaction (with anisotropy parameter $0 \leq \gamma \leq 1$) of Heisenberg type in a transverse time-dependent magnetic field $B(t)$. The Hamiltonian that describes this system can be written as (in the unit of $\hbar = 1$ and considering multiplication factor as 1) [147, 145]

$$\hat{H}(t) = \hat{H}_0(t) + \hat{H}_I, \tag{3.1}$$

where,

$$\begin{aligned} \hat{H}_0(t) &= B(t)\left(\hat{\sigma}_1^z + \hat{\sigma}_2^z\right) \\ \hat{H}_I &= J\left[(1+\gamma)\hat{\sigma}_1^x\hat{\sigma}_2^x + (1-\gamma)\hat{\sigma}_1^y\hat{\sigma}_2^y\right]. \end{aligned}$$

Here $\hat{H}_0$ represents the free part, and $\hat{H}_I$ represents the interaction between two-spin with the coupling strength J. Various spin systems are represented by the Pauli spin operators $\hat{\sigma}_i^{x,y,z}$ with the subscript $i \in (1,2)$. In the limiting case of γ, we obtain the isotropic XX interaction Hamiltonian when $\gamma = 0$ and the Ising spin Hamiltonian when $\gamma = 1$. The fact is that $[\hat{H}_0, \hat{H}_I] \neq 0$ when $\gamma \neq 0$, which results in $[\hat{H}(t_1), \hat{H}(t_2)] \neq 0$, brings in a true quantum feature in the operation of the finite-time QHE [238, 147].

The eigenvalues and the corresponding eigenvectors of the total Hamiltonian (**Eq. 4.1**) are given by

$$\begin{aligned} |\psi_0\rangle &= \tfrac{1}{\sqrt{2}}(a\,|11\rangle + b\,|00\rangle), & E_0 &= -2K \\ |\psi_1\rangle &= \tfrac{1}{\sqrt{2}}(-\,|10\rangle + |01\rangle), & E_1 &= -2J \\ |\psi_2\rangle &= \tfrac{1}{\sqrt{2}}(|10\rangle + |01\rangle), & E_2 &= 2J \\ |\psi_3\rangle &= \tfrac{1}{\sqrt{2}}(c\,|11\rangle + d\,|00\rangle), & E_4 &= 2K, \end{aligned} \tag{3.2}$$

where $k = \sqrt{B^2 + \gamma^2 J^2}$, $a = \frac{B-K}{\sqrt{K^2-BK}}$, $b = \frac{\gamma J}{\sqrt{K^2-BK}}$, $c = \frac{B+K}{\sqrt{K^2+BK}}$ and $d = \frac{\gamma J}{\sqrt{K^2+BK}}$.

The energy eigenstates (see **Eq. 3.2**) of the Hamiltonian can be divided into two categories. The states that are dependent on the system parameters $B(t)$ and J, namely, $|\psi_0\rangle$ and $|\psi_3\rangle$, evolve with time. The other ones which are independent of the system parameters, namely $|\psi_1\rangle$ and $|\psi_2\rangle$ are the standard Bell states that remain unchanged with time.

3.2.2 Quantum Otto Cycle and thermodynamic quantities

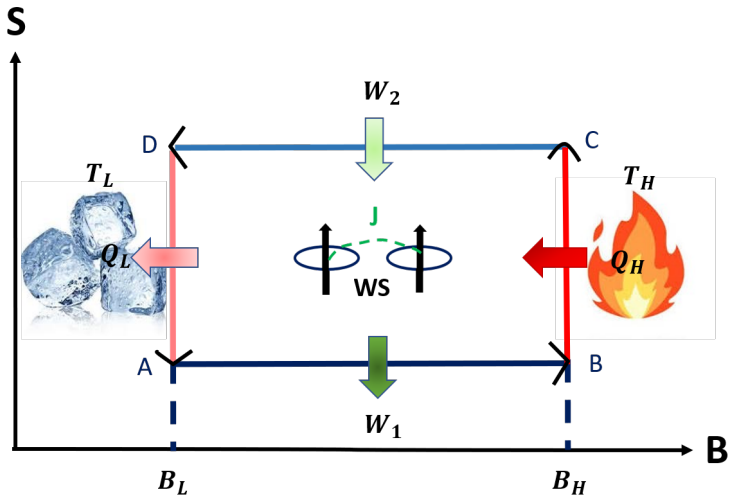

Figure 3.1: Schematic diagram of the quantum Otto cycle on the entropy (S) Vs magnetic field (B) plane when it functions as a heat engine. In other types of thermal machines, the direction of heat flows and work differ.

In the following, we will discuss the implementation of the four strokes of the quantum Otto cycle. The schematic diagram of the cycle is shown in **Fig. 3.1**.

Unitary expansion ($A \rightarrow B$) : We assume that the cycle begins with the working system in thermal equilibrium with the cold bath at temperature $T_L = 1/\beta_L\,(k_B = 1)$ at point A. The corresponding thermal state of the system is $\hat{\rho}_A = e^{-\beta_L \hat{H}_1}/Z_1$, with $\hat{H}_1 = \hat{H}(0)$ and $Z_1 = \mathrm{Tr}(e^{-\beta_L \hat{H}_1^{exp}})$. In this stroke, the working medium is disconnected from the cold heat bath, and the external magnetic field is changed from B_L to B_H ($B_L < B_H$) following the protocol $B(t) = B_L + (B_H - B_L)(t/\tau)$, where $0 \leq t \leq \tau$ and τ is the timescale of changing the magnetic field from B_L to B_H or vice versa. So at point B, the state of the system can be obtained as $\hat{\rho}_B = \hat{U}(\tau)\hat{\rho}_A\hat{U}^\dagger(\tau)$, where $\hat{U}(\tau) = \mathcal{T}e^{-i\int_0^\tau dt\hat{H}^{exp}(t)}$ is the time evolution operator, $\mathcal{T}$ indicates the time-ordering. The amount of work done by the system in this process is given by $W_1 = \langle E_B\rangle - \langle E_A\rangle$, where $\langle E_A\rangle = \mathrm{Tr}(\hat{\rho}_A\hat{H}_1)$ and $\langle E_B\rangle = \mathrm{Tr}(\hat{\rho}_B\hat{H}_2)$, represent the internal energies of the system at A and B, and $\hat{H}_2 = \hat{H}(\tau)$ represents the Hamiltonian of the system at B.

Isochoric heating ($B \rightarrow C$): In this stroke, the working medium is connected with a heat bath at temperature T_H ($T_H > T_L$), and the external magnetic field remains fixed at a value B_H, so the Hamiltonian of the system remains fixed. Therefore, there is no work exchange in this stroke. Also, if the process is carried out for a time t_h and the relaxation time of the system is t_{relax}, then the case $t_h >> t_{relax}$ represents the system is completely thermalized, otherwise, the system is incompletely thermalized in this process. At the end of this process, the state of the system, in the case of complete thermalization, can be represented by $\hat{\rho}_C = e^{-\beta_H \hat{H}_2}/Z_2$ at temperature $T_H = 1/\beta_H\,(k_B = 1)$, with $\hat{H}_2 = \hat{H}(\tau)$ and $Z_2 = \mathrm{Tr}(e^{-\beta_H \hat{H}_2})$. In the case of incomplete thermalization, the state of the system can be obtained by solving **Eq. 4.30**. The system absorbs some amount of heat in this process which can be calculated as, $Q_H = \langle E_C\rangle - \langle E_B\rangle$, where $\langle E_C\rangle = \mathrm{Tr}(\hat{\rho}_C\hat{H}_2)$ is the internal energy of the system at C.

Unitary compression ($C \rightarrow D$): In this stroke, again the working system is disconnected from the hot heat bath and the external magnetic field is changed from B_H to B_L following the protocol $B(\tau - t)$, where $0 \leq t \leq \tau$. In this process, the state of the working system changes to $\hat{\rho}_D = \hat{V}(\tau)\hat{\rho}_C\hat{V}^\dagger(\tau)$, where $\hat{V}(\tau) = \mathcal{T}e^{-i\int_0^\tau dt\hat{H}^{com}(t)}$ is the time evolution operator with $\hat{H}^{com}(t) = \hat{H}^{exp}(\tau - 1)$. The amount of work done on the system in this process can be obtained as $W_2 = \langle E_D\rangle - \langle E_C\rangle$, where $\langle E_D\rangle = \mathrm{Tr}(\hat{\rho}_D\hat{H}_1)$, represent the internal energy of the system at D.

Isochoric cooling ($D \rightarrow A$): In this stroke, the working system is connected with a cold heat bath at temperature T_L, and the external magnetic field remains

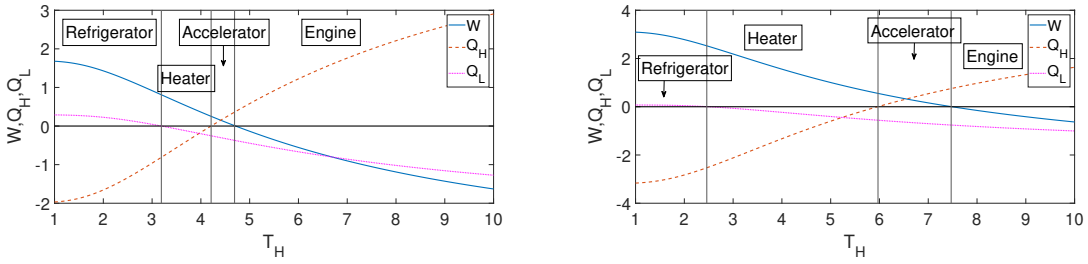

((a)) ((b))

Figure 3.2: Variation of the thermodynamic quantities W, Q_H and Q_L as a function of temperature (T_H) of the hot bath for different values of the anisotropy parameter (a) $\gamma = 1$, and (b) $\gamma = 0$. The other parameters are $B_L = 1, B_H = 4, J = 1, T_L = 1$.

fixed at B_L. If the process is carried out for a time t_c, then the case $t_c >> t_{relax}$ represents that the system reaches thermal equilibrium with the heat bath at the end of this process. The state of the system comes back to the initial state ρ_A, and the system releases some amount of heat in this process, which can be obtained as, $Q_L = \langle E_A \rangle - \langle E_D \rangle$.

3.2.3 Operation of the quantum Otto cycle as different thermal machines

In this part, we will study the parameter regimes of different thermal machines' operation of the cycle [239, 8]. To do that, we have studied the thermodynamic quantities of the cycle, which are shown in **Fig. 3.2**. We observed that with the different choices of the parameters, specifically T_H and γ, the cycle can act in a QHE, a refrigerator, an accelerator, or a heater cycle.

The cycle acts as an engine when the system absorbs some amount of heat from the hot bath ($Q_H > 0$) and releases a portion of it to the cold bath ($Q_L > 0$), while the remaining portion is converted to work ($W < 0$) in a complete cycle. It acts as a refrigerator when heat flows in the opposite direction, i.e., $Q_L > 0$ and $Q_H < 0$, with the help of a certain amount of work done on the system ($W > 0$). It acts as a thermal accelerator when heat flows in the natural direction, i.e., $Q_H > 0$ and $Q_L < 0$, as work is done on the system ($W > 0$). It operates as a heater when the system releases heat to the hot and cold heat baths, i.e., $Q_H < 0$ and $Q_L < 0$, with the assistance of work done on the system ($W > 0$). From **Fig. 3.2**, we can see that the operation regime of different thermal machines varies with the anisotropy parameter γ.

In our work, we will mainly focus on the heat engine operation. The thermodynamic quantities of the QHE are as follows. Total work in a complete

cycle can be obtained as $W = W_1 + W_2 = -(Q_H + Q_L)$. So, the efficiency of the heat engine is defined as

$$\eta = -\frac{W_1 + W_2}{Q_H} = \frac{Q_H + Q_L}{Q_H}$$

.

3.3 Operation of the heat engine in different time limits

In this section, we will focus on the various limiting cases of duration over which the QHE can be operated.

3.3.1 Quasi-static operation

We first consider that two unitary processes (expansion and compression) in the cycle are carried out over a long time such that these processes are adiabatic, i.e., there is no transition between two energy eigenstates. Furthermore, two isochoric processes are carried out for long times, so the system is fully thermalized at the end of these processes. For such long-duration stages, the cycle becomes quasi-static. The analytical expressions of the internal energies of the working system at A, B, C, and D for a quasistatic cycle are given below.

At A:

The Hamiltonian at point A of the cycle can be expressed as

$$H_A = H_1 = \sum_{n=0}^{3} E_n^{(1)} |\psi_n^{(1)}\rangle\langle\psi_n^{(1)}|,$$

where $\{|\psi_n^{(1)}\rangle\}$ are the eigenstates of the Hamiltonian H_1. As we consider that the system at A is in thermal equilibrium with the heat bath, the thermal density matrix is given by

$$\rho_A = \frac{e^{-\beta H_1}}{Z} = \sum_{n=0}^{3} P_n^L |\psi_n^{(1)}\rangle\langle\psi_n^{(1)}| \tag{3.3}$$

where $P_n^L = e^{-\beta_L E_n^{(1)}}/Z_1$ is the thermal occupation probability of the nth eigenstate, $Z_1 = 2[\cosh(2K_L\beta_L) + \cosh(2J\beta_L)]$ is the relevant partition function and $\beta_L = 1/T_L$ is the inverse temperature of the cold bath. So, the average internal energy at point

A is given by

$$\begin{aligned}\langle E_A\rangle &= \mathrm{Tr}(H_1\rho_A) = \sum_{n=0}^{3} P_n E_n^{(1)} \\ &= -4K_L\frac{\sinh 2K_L\beta_L}{Z_1} - 2J\frac{\sinh 2J\beta_L}{Z_1},\end{aligned} \tag{3.4}$$

where $K_L = \sqrt{B_L^2 + \gamma^2 J^2}$.

At B:

The Hamiltonian at point B of the cycle can be expressed as

$$H_B = H_2 = \sum_{n=0}^{3} E_i^{(2)} |\psi_n^{(2)}\rangle\langle\psi_n^{(2)}|,$$

where $\{|\psi_n^{(2)}\rangle\}$ are the eigenstates of the Hamiltonian H_2. We consider that the unitary time evolution process $A \to B$ is carried out adiabatically i.e. the system follows the instantaneous energy eigenstates. Thus, the state of the system at B can be written as

$$\rho_B = \sum_{n=0}^{3} P_n^{\mathrm{L}} |\psi_n^{(2)}\rangle\langle\psi_n^{(2)}|. \tag{3.5}$$

The average internal energy at the point B can be obtained as

$$\begin{aligned}\langle E_B\rangle &= \mathrm{Tr}(H_2\rho_B) = \sum_{n=0}^{3} P_n^L E_n^{(2)} \\ &= -4K_H\frac{\sinh 2K_L\beta_L}{Z_1} - 4J\frac{\sinh 2J\beta_L}{Z_1}\ ,\end{aligned} \tag{3.6}$$

where $K_H = \sqrt{B_H^2 + \gamma^2 J^2}$.

At C:

As in the isochoric heating process $C \to D$, the system reaches thermal equilibrium with the bath, so the thermal density matrix at C is given by

$$\rho_C = \frac{e^{-\beta H_2}}{Z_2} = \sum_{n=0}^{3} P_n^H |\psi_n^{(2)}\rangle\langle\psi_n^{(2)}|, \tag{3.7}$$

where $P_n^H = e^{-\beta_H E_n^{(2)}}/Z_2$ is the thermal occupation probability of the nth eigenstate, and $Z_2 = 2[\cosh(2K_H\beta_H) + \cosh(2J\beta_H)]$ is the relevant partition function and $\beta_H = 1/T_H$ is the inverse temperature of the hot bath.

Similarly, to point A, we can derive the expression of average energy at C which

is given by

$$\langle E_C\rangle = \mathrm{Tr}(H_2\rho_c) = -4K_H\frac{\sinh 2K_H\beta_H}{Z_2} - 4J\frac{\sinh 2J\beta_H}{Z_2}, \tag{3.8}$$

At D:

Similarly, to the unitary time evolution process $A \to B$, we consider that the unitary time evolution process $C \to D$ is also carried out adiabatically. Therefore, the density matrix at the point D can be written as

$$\rho_D = \sum_{n=0}^{3} P_n^{\mathrm{H}} \left|\psi_n^{(1)}\right\rangle \left\langle\psi_n^{(1)}\right|. \tag{3.9}$$

Similarly, to point B, we can derive the average internal energy at point D which is given by

$$\langle E_D\rangle = \mathrm{Tr}(H_1\rho_D) = -4K_L\frac{\sinh 2K_H\beta_H}{Z_2} - 4J\frac{\sinh 2J\beta_H}{Z_2}\ , \tag{3.10}$$

Thermodynamic quantities in a complete cycle for the quasistatic operation:

The thermodynamic quantities of the cycle can be obtained using the expression of the internal energies at A, B, C and D [**Eq. 3.4**, **Eq. 3.6**, **Eq. 3.8**, **Eq. 3.10**]. The work in a complete cycle is given by

$$W = W_1 + W_2 = 4(K_L - K_H)\left[\frac{\sinh 2K_L\beta_L}{Z_1} - \frac{\sinh 2K_H\beta_H}{Z_2}\right]. \tag{3.11}$$

Also, the heat absorbed by the system during the isochoric heating process is given by

$$Q_H = 4K_H\left[-\frac{\sinh 2K_H\beta_H}{Z_2} - \frac{\sinh 2K_L\beta_L}{Z_1}\right] + 4J\left[-\frac{\sinh 2J\beta_H}{Z_2} + \frac{\sinh 2J\beta_L}{Z_1}\right] \tag{3.12}$$

Therefore, the efficiency becomes

$$\begin{aligned}\eta &= \frac{-W}{Q_H}\\ &= 1 - \frac{K_L[\sinh(2K_L\beta_L) - \sinh(2K_H\beta_H)] + J[\sinh(2J\beta_L) - \sinh(2J\beta_H)]}{K_H[\sinh(2K_L\beta_L) - \sinh(2K_H\beta_H)] + J[\sinh(2J\beta_L) - \sinh(2J\beta_H)]},\end{aligned} \tag{3.13}$$

From the above equation, we clearly observe that the efficiency depends on the temperatures of both hot and cold baths, T_H and T_L, and also on the magnetic fields B_L and B_H and the anisotropy parameter γ. Also, two intermediate energy levels $|\psi_{1,2}\rangle$ (**Eq. 3.2**) participate in the engine operation. To compare with the measurement-based QOE in a coupled two-spin system [147], the quasistatic

efficiency does not depend on the temperature of the cold bath, and also $|\psi_{1,2}\rangle$ do not participate in the engine operation.

Now, from **Fig. 3.3a**, we can observe that the quasistatic efficiency increases gradually and reaches a steady value at higher values of T_H. In the rest of this Chapter, we consider $T_H = 10$. Further, from the plot of the efficiency as a function of work (**Fig. 3.3b**), we find that both the work and the efficiency increase with the anisotropy parameter γ, which is contrary to the measurement-based QOE where the quasistatic efficiency decreases with the increase of γ [147]. So, we can adjust the parameters of the cycle to achieve a higher efficiency performance of the engine.

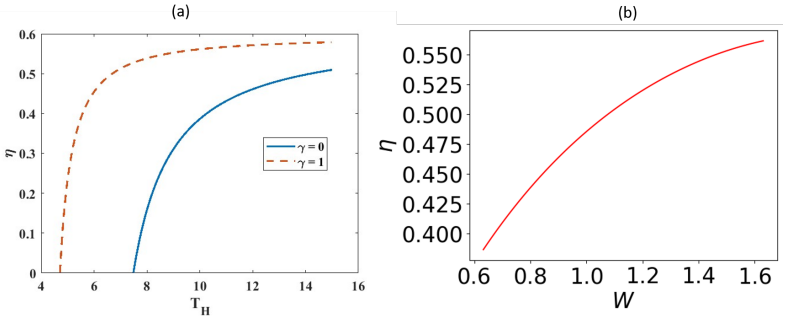

Figure 3.3: (a) Variation of efficiency (η) as a function of the temperature (T_H) of the hot bath. (b) The parametric plot of the variable anisotropy (γ) on the work-efficiency plane when $T_H = 10$. γ varies from 0 to 1, the left side of the graph represents $\gamma = 0$ and the right side represents $\gamma = 1$. The other parameters are $B_L = 1, B_H = 4, J = 1, T_L = 1$. The normalization parameter is $J = 1$ throughout this work; therefore, all the quantities are in units of J.

3.3.2 Unitary time evolution for finite times

We next consider that the cycle's unitary stages (expansion and compression) are run for finite times. For a larger duration, these stages become adiabatic, while for a shorter duration, the non-adiabatic features start to appear. We further assume that during each of the two isochoric stages, the system attains a thermal equilibrium with the baths.

We next obtain the expressions of the internal energies of the system at B and D of the cycle. The expressions of the internal energies at A and C will be the same as written in **Sec. 3.3.1**.

At B:

The density matrix at point B after the unitary process $A \to B$ can be obtained as

$$\rho_B = U(\tau)\rho_A U^\dagger(\tau) = \sum_{i=0}^{3} P_i U(\tau)|\psi_i^{(1)}\rangle\langle\psi_i^{(1)}|U^\dagger(\tau)\ . \tag{3.14}$$

The average internal energy at the point B can be obtained as

$$\begin{aligned}\langle E_B\rangle = \mathrm{Tr}(H_2\rho_B) &= \sum_{i,j=0,3} P_i E_j^{(2)} \langle\psi_j^{(2)}|U(\tau)|\psi_i^{(1)}\rangle\langle\psi_i^{(1)}|U^\dagger(\tau)|\psi_j^{(2)}\rangle + P_1E_1^{(2)} + P_2E_2^{(2)} \\ &= P_0E_0^{(2)}(1-\xi_\tau) + P_3E_0^{(2)}\xi_\tau + P_1E_1^{(2)} + P_2E_2^{(2)} + P_0E_3^{(2)}\xi_\tau + P_3E_3^{(2)}(1-\xi_\tau) \\ &= -4K_H(1-2\xi_\tau)\frac{\sinh 2K_L\beta}{Z_1} - 4J\frac{\sinh 2J\beta}{Z_1},\end{aligned} \tag{3.15}$$

where we have used the microreversibility condition $|\langle\psi_i^{(2)}|U(\tau)|\psi_j^{(1)}\rangle|^2 = \xi_\tau$ for $i \neq j$ and $|\langle\psi_i^{(2)}|U(\tau)|\psi_i^{(1)}\rangle|^2 = 1-\xi_\tau$.

Proof of the relation $|\langle\psi_3^{(2)}|U(\tau)|\psi_0^{(1)}\rangle|^2 = |\langle\psi_0^{(2)}|U(\tau)|\psi_3^{(1)}\rangle|^2$*:*

$$\begin{aligned}&|\langle\psi_3^{(2)}|U(\tau)|\psi_0^{(1)}\rangle|^2 = \langle\psi_3^{(2)}|U(\tau)|\psi_0^{(1)}\rangle\langle\psi_0^{(1)}|U^\dagger(\tau)|\psi_3^{(2)}\rangle \\ &= \langle\psi_3^{(2)}|U(\tau)(\mathbb{I} - |\psi_1^{(1)}\rangle\langle\psi_1^{(1)}| - |\psi_2^{(1)}\rangle\langle\psi_2^{(1)}| - |\psi_3^{(1)}\rangle\langle\psi_3^{(1)}|)U^\dagger(\tau)|\psi_3^{(2)}\rangle\,,\end{aligned}$$

where we have used the completeness relation $\sum_{i=0}^{3}|\psi_i^{(1)}\rangle\langle\psi_i^{(1)}| = \mathbb{I}$. The above relation can then be rewritten as

$$\begin{aligned}&\langle\psi_3^{(2)}|U(\tau)U^\dagger(\tau)|\psi_3^{(2)}\rangle - |\langle\psi_3^{(2)}|U(\tau)|\psi_3^{(1)}\rangle|^2 \\ &= 1 - \left(1 - |\langle\psi_0^{(2)}|U(\tau)|\psi_3^{(1)}\rangle|^2\right) = |\langle\psi_0^{(2)}|U(\tau)|\psi_3^{(1)}\rangle|^2\,.\end{aligned}$$

where in the last line we have used the conservation of probability

$$|\langle\psi_0^{(2)}|U(\tau)|\psi_3^{(1)}\rangle|^2 + |\langle\psi_3^{(2)}|U(\tau)|\psi_3^{(1)}\rangle|^2 = 1.$$

□

In unitary stages for a short time interval τ, nonadiabatic transitions occur between energy eigenstates that are coupled [240]. In the present case, such transitions will be induced between the levels $|\psi_0\rangle$ and $|\psi_3\rangle$. So, the terms like $\langle\psi_i^{(2)}|U(\tau)|\psi_j^{(1)}\rangle = 0$ for $i \neq j$ and i,j take values from any of the group $(0,1,2)$ or $(1,2,3)$.

At D: The density matrix at point D after the unitary process $C \to D$ is given by

$$\rho_D = V(\tau)\rho_C V^\dagger(\tau)\,. \tag{3.16}$$

As done at point B, we can derive the average internal energy at point D as

$$\langle E_D\rangle = \mathrm{Tr}(H_1\rho_D) = -4K_L(1-2\xi_\tau)\frac{\sinh 2K_H\beta_H}{Z_2} - 4J\frac{\sinh 2J\beta_H}{Z_2}\,, \tag{3.17}$$

where we have used the microreversibility condition $|\langle\psi_i^{(2)}|V(\tau)|\psi_j^{(1)}\rangle|^2 = \xi_\tau$ for $i \neq j$ and $|\langle\psi_i^{(2)}|V(\tau)|\psi_i^{(1)}\rangle|^2 = 1 - \xi_\tau$. Here $\xi_\tau = |\langle\psi_i^{(2)}|\hat{U}(\tau)|\psi_j^{(1)}\rangle|^2 = |\langle\psi_i^{(1)}|\hat{V}(\tau)|\psi_j^{(2)}\rangle|^2$ represents the transition probability between the energy levels. The relation $|\langle\psi_3^{(1)}|V(\tau)|\psi_0^{(2)}\rangle|^2 = |\langle\psi_0^{(1)}|V(\tau)|\psi_3^{(2)}\rangle|^2$ can be proven in the same way, as was done for the previous microreversibility relation after **Eq. 3.15**.

From the definitions of the unitary time evolution operators (see **Sec. 4.2.1**) for the expansion and compression stages [241, 240], we have

$$\begin{aligned} U(\tau) &= \mathcal{T}\exp\left[-i\int_0^\tau H^{exp}(t)dt\right] \\ &= \mathcal{T}\exp\left[-i\int_\tau^0 H^{exp}(\tau-t')d(\tau-t')\right] \\ &= \mathcal{T}\exp\left[-i\int_0^\tau H^{exp}(\tau-t)dt\right] \\ &= \mathcal{T}\exp\left[-i\int_0^\tau H^{com}(t)dt\right] \\ &= V(\tau). \end{aligned}$$

Clearly, the two-time evolution operators $U(\tau)$ and $V(\tau)$, in the unitary compression and expansion stages, respectively, are equivalent.

Thermodynamic quantities in a complete cycle in terms of transition probability:

Thermodynamic quantities of the cycle can be calculated using the expressions of the internal energies at A, B, C and D following **Sec. 4.2.1**. If the system remains decoupled from the heat bath in a unitary driving process (work extraction process), the work done in that process is given by

$$\langle W\rangle = \int_0^\tau dt\,\mathrm{Tr}\left[\rho(t)\frac{dH(\lambda(t))}{dt}\right] = \mathrm{Tr}(H_\tau\rho_\tau) - \mathrm{Tr}(H_0\rho_0) = \langle E\rangle_\tau - \langle E\rangle_0,$$

which is essentially the difference between the internal energies of the system before and after the process. The associated heat in this process can be calculated as

$$\langle Q\rangle = \int_0^\tau dt\,\mathrm{Tr}\left[\frac{d\rho(t)}{dt}H(\lambda(t))\right] = 0.$$

because, the diagonal elements of the density matrix remain constant during these adiabatic (isentropic) stages.

Therefore, the work in the unitary expansion and the compression processes are

given by

$$W_1 = -4K_H(1-2\xi_\tau)\frac{\sinh 2K_L\beta_L}{Z_1} + 4K_L\frac{\sinh 2K_L\beta_L}{Z_1},$$
$$W_2 = -4K_L(1-2\xi_\tau)\frac{\sinh 2K_H\beta_H}{Z_2} + 4K_H\frac{\sinh 2K_H\beta_H}{Z_2}.$$

So, the work in a complete cycle is given by

$$\begin{aligned} W =& 4K_L\left[\frac{\sinh 2K_L\beta_L}{Z_1} - (1-2\xi_\tau)\frac{\sinh 2K_H\beta_H}{Z_2}\right] \\ &+ 4K_H\left[-(1-2\xi_\tau)\frac{\sinh 2K_L\beta_L}{Z_1} + \frac{\sinh 2K_H\beta_H}{Z_2}\right]. \end{aligned} \tag{3.18}$$

Also, the heat absorption during the isochoric heating can be written as

$$Q_H = 4K_H\left[-\frac{\sinh 2K_H\beta_H}{Z_2} - (1-2\xi_\tau)\frac{\sinh 2K_L\beta_L}{Z_1}\right] + 4J\left[-\frac{\sinh 2J\beta_H}{Z_2} + \frac{\sinh 2J\beta_L}{Z_1}\right]. \tag{3.19}$$

Therefore, the expression of efficiency is given by

$$\eta_\tau = -W/Q_H = 1 - \frac{K_L\left[\sinh(2K_L\beta_L) - (1-2\xi_\tau)\sinh(2K_H\beta_H)\right] + J\left[\sinh(2J\beta_L) - \sinh(2J\beta_H)\right]}{K_H\left[(1-2\xi_\tau)\sinh(2K_L\beta_L) - \sinh(2K_H\beta_H)\right] + J\left[\sinh(2J\beta_L) - \sinh(2J\beta_H)\right]}. \tag{3.20}$$

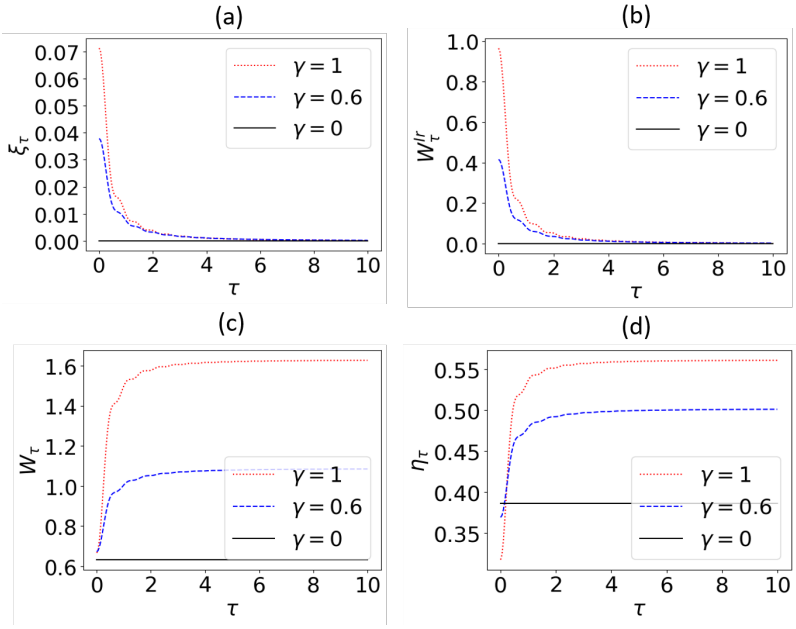

Figure 3.4: Variation of (a) transition probability (ξ_τ) between two instantaneous energy eigenstates (b) irreversible work W_τ^{Ir} (a) work (W_τ) in a complete cycle and (c) efficiency η_τ with respect to the duration τ of the unitary processes, for different values of γ. The other parameters are the same as in **Fig. 3.3**.

The plots of the transition probability ξ_τ efficiency η_τ (**Eq. 3.20** are displayed

in **Fig. 3.4(a)**) and **Fig. 3.4(d)**, respectively. In **Fig. 3.4 (b)**, we have shown how the work in a complete cycle, W_τ, varies with τ for different values of γ. These plots are produced using QuTip [242] package. The plots indicate that the engine's work output and efficiency strongly depend on τ. The work and the efficiency both degrade for a very small τ and then gradually increase with increasing values of τ before eventually reaching the adiabatic (quasistatic) value.

As the Hamiltonian does not commute at different times, the system cannot follow the instantaneous energy eigenstates. This induces a nonadiabatic transition between the instantaneous eigenstates of the Hamiltonian when the system is driven by an external control parameter [here, $B(t)$], for a finite time. Therefore, the relevant unitary dynamics becomes nonadiabatic. In this case, the work extractable in a complete cycle gets reduced. An extra amount of work needs to be performed in order to derive the system in finite time, which can be defined by irreversible work, given by

$$W_\tau^{Ir} = W_{\tau\to\infty} - W_\tau, \tag{3.21}$$

where $W_{\tau\to\infty}$ is the work as given by **Eq. 3.11**. Once the driving process is completed and the system is coupled with the cold bath, the system dumps more amount of heat into the cold bath. This degrades the overall performance of the engine in finite-time unitary processes which can be seen in **Fig. 3.4(c), 3.4(d)**. This is referred to as the quantum internal friction [75, 76, 77, 78, 79] and is quantified by W_τ^{Ir}. The irreversible work (W_τ^{Ir}) is also linked with entropy production in the system in the finite-time driving process.

The plot of W_τ^{Ir} with respect to τ is shown in **Fig. 3.4(b)**. The plot indicates that in the short time limit (nonadiabatic regime), the more the anisotropy (γ) is, the more the irreversible work. Therefore, we can say that irreversibility increases with the increase of anisotropy (γ). For $\gamma = 1$, the system becomes an Ising spin model, which gives rise to maximum irreversibility in finite time operation, and for $\gamma = 0$, the system becomes a Heisenberg XX model which gives rise to reversible operation of the cycle irrespective of the time duration of the unitary processes.

In the adiabatic limit, i.e., $\tau \to \infty$, there is no transition between the instantaneous energy eigenstates. Therefore, in the limit $\tau \to \infty$, we can write $\xi_\tau = |\langle\psi_0^{(2)}|\hat{U}(\tau)|\psi_3^{(1)}\rangle|^2 \overset{\tau\to\infty}{=} 0$, which gives rise to $W_\tau = W$, $W_\tau^{Ir} = 0$, and $\eta_\tau = \eta$. Therefore, the expression of the quasistatic efficiency (**Eq. 3.13**) is recovered by putting $\xi_\tau = 0$ in the expression of the finite time efficiency (**Eq. 3.20**).

3.3.3 Isochoric heating for finite duration

We now consider that the hot isochoric stage is performed for a finite duration [215, 241]. This leads us to different thermalization scenarios of the working system depending on the time scale chosen. In the case $t_h \gg t_{relax}$, the system is completely thermalized; otherwise, the system is partially thermalized. We will investigate how the different time scales, particularly for incomplete thermalization, affect the performance of the QHE. We also consider that the time for the unitary processes is long enough so that these processes are adiabatic in nature.

With the above-mentioned conditions, the states of the working system at points A and B can be represented by the states as given in **Eq. 3.3** and **Eq. 3.5** respectively. But, to determine the state at point C, we need to solve the master equation (**Eq. 4.30**), and after that, to determine the state at D, we need to solve the von Neumann equation, which is similar to the situation when there is no dissipative part in **Eq. 4.30**.

To understand the thermalization of the working system, the trace distance between two states, the reference state represented by **Eq. 3.7** and the time-evolved state obtained by solving **Eq. 4.30**, can be a suitable marker. This is defined as $D(\rho, \sigma) = \frac{1}{2} \operatorname{Tr} |\rho - \sigma|$ [241]. The plot of the trace distance D with respect to the duration of the isochoric process t_h is shown in **Fig. 3.5(c)**. We found that the thermalization time increases with the increase in the anisotropy γ [147].

The plots of the heat absorption (Q_{Ht}) of the working system from the hot bath and the work done in a complete cycle as a function of t_h are displayed in **Fig. 3.5(a), 3.5(b)**. These plots show that the Q_{Ht} increases with the increase of t_h and then reaches a steady value when the system is completely thermalized. Also, with the increase in Q_{Ht}, the system receives more amount of energy to perform work in a complete cycle. Therefore the work done increases with t_h, and reaches a steady state at long times.

The plot of the efficiency (η_t) with respect to t_h is shown in **Fig. 3.5(d)**. For the lower value of γ, with the time t_h, work (W_t) increases slowly than the significant increase of heat absorption (Q_{Ht}), which gives rise to a slow increase in η_t. With increasing γ, for very short values of t_h, W_t increases significantly rather than the Q_{Ht}, which gives rise to a sudden increase in efficiency. In the larger value of t_h, both Q_{Ht} and W_t become steady, η_t becomes steady for all values of γ, which is the quasistatic value of the efficiency (see **Sec. 3.3.1**).

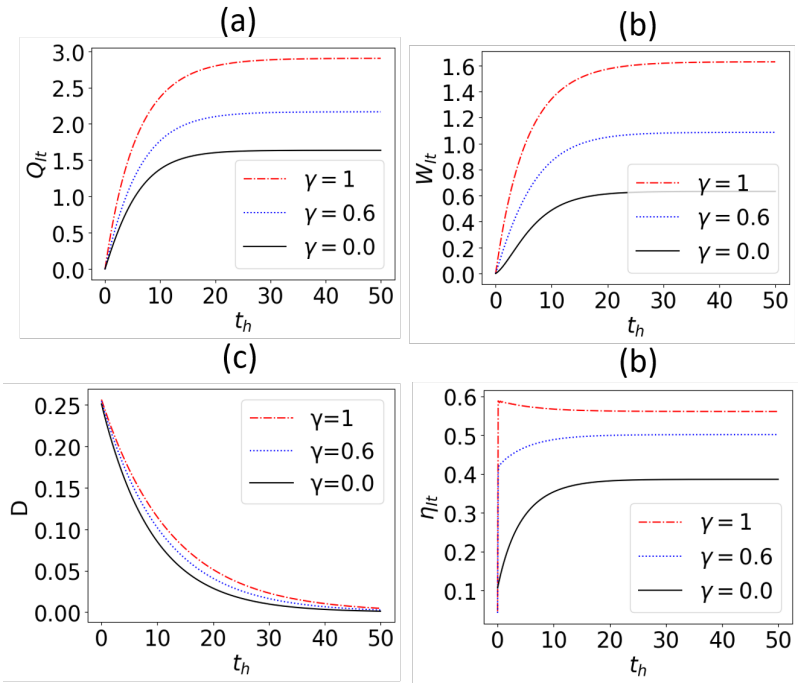

Figure 3.5: Variation of (a) heat absorption of the system (Q_{Ht}) (b) work in a complete cycle (c) trace distance (D) between two states, one is for incomplete thermalization and another is the thermal state at C (d) efficiency of the QHE as a function time of the isochoric heating process (t_h) for different values of anisotropy parameter (γ). For $\gamma = 0$, D is around 75, whereas, for $\gamma = 1$, D is around 100, in the unit of J, if the accuracy in the trace distance is considered of the order 10^{-5}. Other parameters are the same with **Fig. 3.3** and $\Gamma = 0.1$.

3.3.4 Effect of different cycle forms

So far, we considered only the conventional form of the Otto cycle, in which the magnetic field is changed only during the times between two isochoric stages, corresponding to the so-called reciprocating cycle. An alternative approach could be a continuous (say, sinusoidal) variation of the magnetic field, even during the isochoric stages. We will next investigate the effect of a hybrid temporal profile of the magnetic field, which is a mix of both these types [243].

We consider the magnetic field modulation $B(k,t)$ of the working system, parameterized by a variable k, called a smoothness parameter. So, by changing k the cycle's form can be changed. In [244], the amplitude modulation of the coupling to the baths has also been used - however, this is beyond the scope of this thesis.

We have used the following protocol for the cycle form: In the $A \to B$ stage,

$$B(t) = [B_L + (B_H - B_L)(t/\tau)]\exp(-1/k) + \omega_{con}(t)\exp(-k) \quad \text{for } 0 \le t \le \tau. \quad (3.22)$$

In the $B \to C$ stage,

$$B(t) = B_H \exp(-1/k) + \omega_{con}(\tau + t)\exp(-k) \quad \text{for } 0 \leq t \leq t_{iso}. \tag{3.23}$$

In the $C \to D$ stage,

$$B(t) = [B_H + (B_L - B_H)(t/\tau)]\exp(-1/k) + \omega_{con}(\tau + t_{iso} + t)\exp(-k) \quad \text{for } 0 \leq t \leq \tau. \tag{3.24}$$

In the $D \to A$ stage,

$$B(t) = B_L \exp(-1/k) + \omega_{con}(2\tau + t_{iso} + t)\exp(-k) \quad \text{for } 0 \leq t \leq t_{iso}. \tag{3.25}$$

where $\omega_{con}(t) = \lambda\Delta_m \sin(\Delta_m t)$ is a continuous periodic modulation of the magnetic field. The component of $B(t)$ with the coefficient $\exp(-1/k)$ is the one used in a standard Otto cycle, in which we have used a linear ramp for variation of the magnetic field from $B_L \to B_H$ or vice versa. We consider $\Delta_m t_{iso} = n\pi$ (n is even) to make the field the same at B and C, and $\Delta_m(2\tau + 2t_{iso}) = l\pi$ (l is an integer) to make the field the same at D and A. Also, t_{iso} should be large enough to completely thermalize the system in the isochoric processes.

Based on the above protocol, we studied the performance of the heat engine for various cycle forms depending on the smoothness parameter k. In this regard, the plot of the efficiency as a function of anisotropy (γ) is shown in **Fig. 3.6**. From the

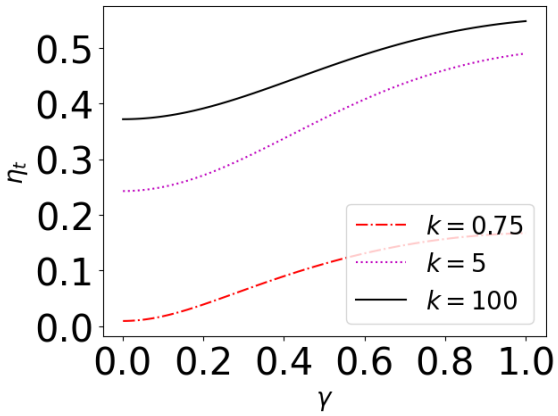

Figure 3.6: Efficiency of the heat engines for various cycles depending on the smoothness parameter k values as a function of anisotropy parameter γ. We have chosen $\Delta_m = 0.1$, $B_L = 1$, $B_4 = 4$, $\tau = 10\pi$, $t_{iso} = 400\pi$, $\lambda = 1$.

plot, it can be seen that for larger k, the efficiency varies with γ in the same way, as it does without periodic modulation $\omega_{con}(t)$. For other values of k, the performance of the heat engine degrades. This means that the standard Otto cycle form is the optimum to get maximum efficiency for a system with a fixed anisotropy. In any

case, for a fixed value of k, the engine performs better for larger anisotropy.

3.4 Heat engine operation with a local spin

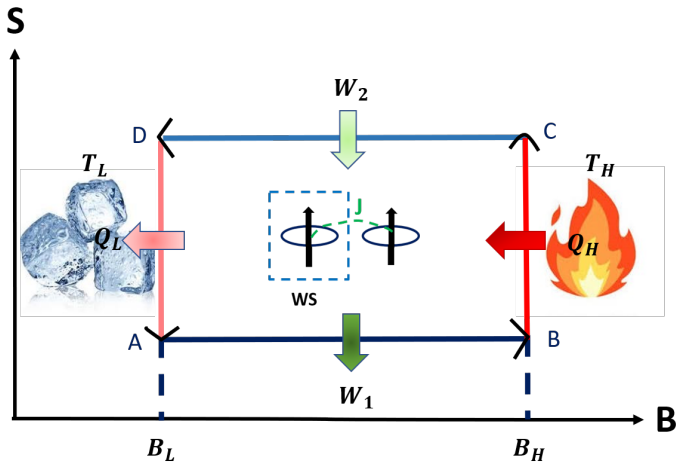

Figure 3.7: Schematic diagram of the quantum Otto cycle on the entropy (S) vs magnetic field (B) plane when it functions as a heat engine. We consider a single local spin as a working system when the coupled two-spin global system is operated in the Otto cycle.

In the previous section, we have considered that the coupled two-spin, let's say a global system, operated in the quantum Otto cycle as illustrated in **Sec. 4.2.1**. In this section, we will consider a single spin which is a part of the global system, let's call it a local system, as a working system. We will study the QOE operation with such a local spin under the effect of another spin. The primary aim is to investigate how the QHE operation in a local spin differs from an engine operating with a single-spin working system which is not under the effect of another spin. We want to illustrate the thermodynamic benefits of a local approach in the QHE operation.

Quantum heat engines and refrigerators that function with local systems have received significant attention in recent studies [116, 212, 213, 214, 245, 246, 247, 248, 249]. These studies primarily focused on analyzing the quasistatic operation of the cycle and also employed the Hamiltonian that commutes at different times. In contrast, our Hamiltonian does not commute at different times (see **Eq. 4.1**) which may give rise to some unique characteristics [147] in the finite time behaviour of the QHE operating with a local spin working system. The primary objective is to explore how the non-commuting nature of the Hamiltonian impacts the performance of a local spin QHE.

Now to study the thermodynamics of a local spin, we will trace out one spin from the states of the global two-spin system at A, B, C, and D of the cycle (see

Sec. 4.2.1), which will give us the states of the local spin. If the states of the global two-spin system are represented by ρ_j, where $j \in A, B, C, D$ (see **Sec. 3.3.1**, **Sec. 3.3.2**), then the reduced density matrices for the first local spin are given by

$$\rho_{jL} = \langle 0_2|\rho_j|0_2\rangle + \langle 1_2|\rho_j|1_2\rangle,$$

where subscript 2 represents tracing out the second spin (any spin can be traced out). Therefore, the internal energies of the local spin can be obtained as $\langle E_j\rangle_L = \mathrm{tr}(H_{jL}\rho_{jL})$, where $H_{1L} = B_L\sigma_z$ for $j \in A, D$, and $H_{2L} = B_H\sigma_z$ for $j \in B, C$ represent the Hamiltonian of the local spin.

Thermodynamic quantities of a local spin can be defined in a similar way as that of the global system (see **Sec. 4.2.1**). Heat absorption in the isochoric heating process is given by $Q_{HL} = \langle E_C\rangle_L - \langle E_B\rangle_L$, work in the unitary expansion is defined as $W_{1L} = \langle E_B\rangle_L - \langle E_A\rangle_L$, and that in the unitary compression is defined as $W_{2L} = \langle E_D\rangle_L - \langle E_C\rangle_L$, so the work in a complete cycle is $W_L = W_{1L} + W_{2L}$.

3.4.1 Quasistatic operation of the cycle -

Let's consider that the cycle (see **Sec. 4.2.1**) for the global system is carried out quasistatically, therefore, two unitary processes are adiabatic, and the system is completely thermalized in two isochoric processes. So, the expressions of the internal energies for the local spin can be derived as follows.

At A:

The density matrix of the local spin at A is given by

$$\begin{aligned}\rho_{AL} &= \langle 0_2|\rho_A|0_2\rangle + \langle 1_2|\rho_A|1_2\rangle \\ &= \frac{1}{2}[p_0^{\mathrm{L}}(b_L^2\,|0\rangle\langle 0| + a_L^2\,|1\rangle\langle 1|) + p_1^{\mathrm{L}}(|1\rangle\langle 1| + |0\rangle\langle 0|) \\ &+ p_2^{\mathrm{L}}(|1\rangle\langle 1| + |0\rangle\langle 0|) + p_3^{\mathrm{L}}(d_L^2\,|0\rangle\langle 0| + c_L^2\,|1\rangle\langle 1|)]\ ,\end{aligned} \tag{3.26}$$

where $P_0^L = \frac{\exp(2K_L/T_L)}{Z_L}$, $P_3^L = \frac{\exp(-2K_L/T_L)}{Z_L}$ are the thermal probabilities of the 0th and 3rd energy levels at A. The average internal energy at point A can be obtained as

$$\begin{aligned}\langle E_A\rangle &= \mathrm{Tr}(H_{L1}\rho_{AL}) \\ &= \sum_{j=0,1}\langle j|(-B_L\,|0\rangle\langle 0| + B_L\,|1\rangle\langle 1|)\rho_{LA}|j\rangle \\ &= \frac{B_L}{2}\left[P_0^L(a_L^2 - b_L^2) + P_3^L(c_L^2 - d_L^2)\right] \\ &= B_L\left[(P_3^L - P_0^L)(1 - a_L^2)\right]\ ,\end{aligned} \tag{3.27}$$

where we have used $a_L^2 = d_L^2$, $b_L^2 = c_L^2$, and $a_L^2 + b_L^2 = 2$.

At B:

The density matrix of the local spin at B is given by

$$\begin{aligned}\rho_{BL} =&\langle 0_2|\rho_A|0_2\rangle + \langle 1_2|\rho_A|1_2\rangle \\ =&\frac{1}{2}[p_0^{\mathrm{L}}(b_H^2\,|0\rangle\langle 0| + a_H^2\,|1\rangle\langle 1|) + p_1^{\mathrm{L}}(|1\rangle\langle 1| + |0\rangle\langle 0|) \\ &+ p_2^{\mathrm{L}}(|1\rangle\langle 1| + |0\rangle\langle 0|) + p_3^{\mathrm{L}}(d_H^2\,|0\rangle\langle 0| + c_H^2\,|1\rangle\langle 1|)]\,.\end{aligned} \tag{3.28}$$

The average internal energy at point B can be obtained as

$$\begin{aligned}\langle E_B\rangle_L &= \mathrm{Tr}(H_{L2}\rho_{BL}) \\ &= \sum_{j=0,1}\langle j|(-B_H\,|0\rangle\langle 0| + B_H\,|1\rangle\langle 1|)\rho_{LB}|j\rangle \\ &= \frac{B_H}{2}\left[P_0^L(a_H^2 - b_H^2) + P_3^L(c_H^2 - d_H^2)\right] \\ &= B_H\left[(P_3^L - P_0^L)(1 - a_H^2)\right]\,,\end{aligned} \tag{3.29}$$

where we have used $a_H^2 = d_H^2$, $b_H^2 = c_H^2$, and $a_H^2 + b_H^2 = 2$.

At C:

Similarly to point A, we can derive the average internal energy at point C given by

$$\begin{aligned}\langle E_C\rangle_L =&\,\mathrm{Tr}(H_{L2}\rho_{CL}) \\ =&\frac{B_H}{2}\left[P_0^H(a_H^2 - b_H^2) + P_3^H(c_H^2 - d_H^2)\right] \\ =&B_H\left[(P_3^H - P_0^H)(1 - a_H^2)\right]\,,\end{aligned} \tag{3.30}$$

where $P_0^H = \frac{\exp(2K_H/T_H)}{Z_H}, P_3^H = \frac{\exp(-2K_H/T_H)}{Z_H}$ are the thermal probabilities 0th and 3rd energy levels at C.

At D:

Similarly, to point B, we can derive the average internal energy given by

$$\begin{aligned}\langle E_D\rangle_L =&\,\mathrm{Tr}(H_{L1}\rho_{DL}) \\ =&\frac{B_L}{2}\left[P_0^H(a_L^2 - b_L^2) + P_3^H(c_L^2 - d_L^2)\right] \\ =&B_L\left[(P_3^H - P_0^H)(1 - a_L^2)\right]\,.\end{aligned} \tag{3.31}$$

Thermodynamic quantities of the local spin are given by

$$\begin{aligned} W_{Lq} =& 2\left[B_L(1-a_L^2) - B_H(1-a_H^2)\right]\left(\frac{\sinh 2K_L\beta_L}{Z_1} - \frac{\sinh 2K_H\beta_H}{Z_2}\right) \\ Q_{LHq} =& 2B_H(1-a_H^2)\left(\frac{\sinh 2K_L\beta_L}{Z_1} - \frac{\sinh 2K_H\beta_H}{Z_2}\right). \end{aligned} \tag{3.32}$$

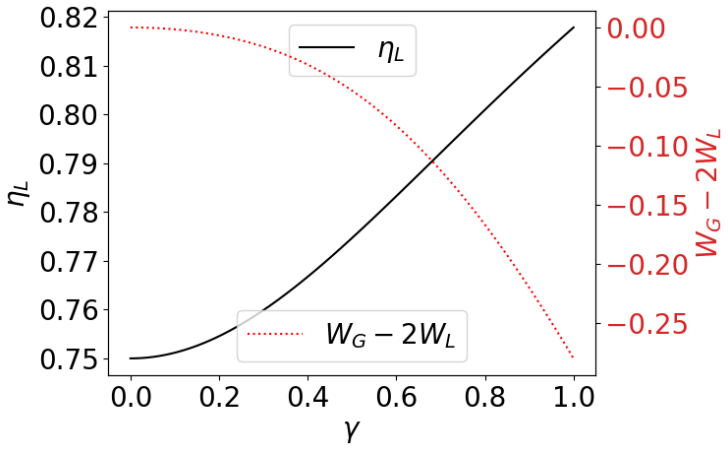

Figure 3.8: Variation of the work difference $W_G - 2W_L$ as a function of anisotropy parameter γ. The figure in the inset represents the variation of efficiency for a local system as a function of the anisotropy parameter (γ). The efficiency of a single spin QOE is 0.75 for $B_L = 1, B_H = 4$. The other parameters are the same as in **Fig. 3.3**.

Comparison between global and local work extraction:

Now to find the potential figure of merit of the local approach, we will compare the local work extraction with the global work extraction for the two-spin system. To do that, we will study the quantity $W_G - 2W_L$, where W_G (**Eq. 3.11**) represents the work for the global two-spin system and W_L (**Eq. 3.32**) represents the work for a local spin and the multiplication factor 2 comes to consider the contribution from the two local spins. The quantity $W_G - 2W_L$ can be calculated as

$$\begin{aligned} W_G - 2W_L =& 4\left[(K_H - B_H) - (K_L - B_L) + (B_H a_H^2 - B_L a_L^2)\right] \\ &\times \left(\frac{\sinh 2K_L\beta_L}{Z_1} - \frac{\sinh 2K_H\beta_H}{Z_2}\right). \end{aligned} \tag{3.33}$$

The variation of $W_G - 2W_L$ with respect to γ is shown in **Fig. 3.8**. The plot shows that $W_G < 2W_L$ if the two-spin is coupled by anisotropic interaction. For the isotropic interaction, i.e. in the limit of $\gamma \to 0$, $K_H \to B_H$, $K_L \to B_L$, $a_H^2 \to 0$, and also $a_L^2 \to 0$, so $W_G - 2W_L = 0$. The case $\gamma > 0$ gives rise to $(K_H - B_H) < (K_L - B_L)$ and also $a_H^2 < a_L^2$, so $W_G - 2W_L < 0$ i.e., the sum of the local work from each local spin surpasses the global work from the global system. Therefore, we can say that extracting work locally is better than globally in the OOE operation with a two-spin

system coupled by anisotropic interaction.

Comparison between the efficiencies of a local spin and a single QOE:

The efficiency of the QOE cycle followed by the local spin is given by

$$\eta_{Lq} = -\frac{W_L}{Q_{HL}} = 1 - \frac{B_L\,(1-a_L^2)}{B_H\,(1-a_H^2)}. \tag{3.34}$$

The expression of the efficiency of the local spin shows that it depends on γ through $a_{L,H}$.

If a QOE operates with a single spin working system under the same physical conditions of B_L and B_H (or the same compression ratio B_L/B_H), then the expression of the efficiency of a single spin working system QOE is given by [8, 97]

$$\eta_S = 1 - \frac{B_L}{B_H}. \tag{3.35}$$

We can see that $\gamma \geq 0$ makes the quantity $(1-a_L^2)/(1-a_H^2) \leq 1$, which gives rise to $\eta_{Lq} \geq \eta_S$. Therefore, as γ increases the quantity $(1-a_L^2)/(1-a_H^2)$ becomes more and more less than 1, which makes η_L (**Eq. 3.34**) is more and more larger than η_S (**Eq. 3.35**), and for $\gamma = 0$, we get $\eta_{Lq} = \eta_S$. All of these can be seen in the plot of efficiency (**Fig. 3.8**) of the local spin QOE as a function of γ. The local spin system QOE outperforms the single spin system QOE for $\gamma > 0$. Therefore, we can say that the efficiency of the QOE operating with a local spin working system in conjunction with another spin with an anisotropic interaction between the spin can surpass the standard quantum Otto limit.

It can be emphasized that a single spin, in the presence of a second spin, performs better than a single isolated spin. For N non-interacting spins, each independently interacting with the bath, the thermodynamic quantities in a complete cycle can be represented by $Q_H^{(N)} = NQ_H^{(1)}$, $Q_L^{(N)} = NQ_L^{(1)}$ and $W^{(N)} = NW^{(1)}$. Then the efficiency becomes $\eta = 1 - \frac{B_L}{B_H}$, which is the same as the efficiency of a single-spin QOE (**Eq. 3.35**). The interacting spins, on the other hand, exhibit larger efficiency (for nonzero γ), as can be seen from **Eq. 3.34** and the **Fig. 3.8**.

3.4.2 Finite time operation: unitary processes are time dependent

In this section, we consider that two unitary processes in the cycle (see **Sec. 4.2.1**) for the global two-spin system are carried out in a finite time τ i.e., they are nonadiabatic in nature. However, the thermalization of the working system in the

hot isochoric process is complete. The expressions of the internal energies of the local spin at B and D in terms of transition probabilities are given below. The internal energies at A and C will be the same with **Sec. 3.4.1**.

At B:

The density matrix at B is given by

$$\begin{aligned}\rho_{BLt} =&\langle 0_2|\rho_A|0_2\rangle + \langle 1_2|\rho_A|1_2\rangle \\ =&\frac{1}{2}[p_1^{\mathrm{L}}(|1\rangle\langle 1| + |0\rangle\langle 0|) + p_2^{\mathrm{L}}(|1\rangle\langle 1| + |0\rangle\langle 0|)] \\ &+ P_0^L\langle 0_2|U(\tau)|\psi_0^{(1)}\rangle\langle\psi_0^{(1)}|U^\dagger(\tau)|0_2\rangle + P_3^L\langle 0_2|U(\tau)|\psi_3^{(1)}\rangle\langle\psi_3^{(1)}|U^\dagger(\tau)|0_2\rangle \\ &+ P_0^L\langle 1_2|U(\tau)|\psi_0^{(1)}\rangle\langle\psi_0^{(1)}|U^\dagger(\tau)|1_2\rangle \ + \ P_3^L\langle 1_2|U(\tau)|\psi_3^{(1)}\rangle\langle\psi_3^{(1)}|U^\dagger(\tau)|1_2\rangle \ .\end{aligned} \tag{3.36}$$

The average internal energy is given by

$$\begin{aligned}\langle E_B\rangle_{L\tau} =& \mathrm{Tr}(H_{L2}\rho_{BLt}) \\ =& \sum_{j=0,1}\langle j|(-B_H|0\rangle\langle 0| + B_H|1\rangle\langle 1|)\rho_{LB}|j\rangle \\ =& - P_0^H B_H|\langle 00|U(\tau)|\psi_0^{(1)}\rangle|^2 - P_3^H B_H|\langle 00|U(\tau)|\psi_3^{(1)}\rangle|^2 \\ &+ P_0^H B_H|\langle 11|U(\tau)|\psi_0^{(1)}\rangle|^2 + P_3^H B_H|\langle 11|U(\tau)|\psi_3^{(1)}\rangle|^2 \\ =& B_H(P_3^L - P_0^L)(1-2\lambda_\tau) \ ,\end{aligned} \tag{3.37}$$

where we have used the microreversibility conditions $|\langle 00|U(\tau)|\psi_0^{(1)}\rangle|^2 = 1-\lambda_\tau$, $|\langle 00|U(\tau)|\psi_3^{(1)}\rangle|^2 = \lambda_\tau$, $|\langle 11|U(\tau)|\psi_0^{(1)}\rangle|^2 = \lambda_\tau$, $|\langle 11|U(\tau)|\psi_3^{(1)}\rangle|^2 = 1-\lambda_\tau$.

Proof of the relation $|\langle 00|U(\tau)|\psi_3^{(1)}\rangle|^2 = |\langle 11|U(\tau)|\psi_0^{(1)}\rangle|^2$:

$$\begin{aligned}&|\langle 00|U(\tau)|\psi_3^{(1)}\rangle|^2 = \langle 00|U(\tau)|\psi_3^{(1)}\rangle\langle\psi_3^{(1)}|U^\dagger(\tau)|00\rangle \\ &= \langle 00|U(\tau)(\mathbb{I} - |\psi_0^{(1)}\rangle\langle\psi_0^{(1)}| \ - \ |\psi_1^{(1)}\rangle\langle\psi_1^{(1)}| \ - \ |\psi_2^{(1)}\rangle\langle\psi_2^{(1)}|)U^\dagger(\tau)|00\rangle \ ,\end{aligned}$$

where we have used the completeness relation $\sum_{i=0}^{3}|\psi_i^{(1)}\rangle\langle\psi_i^{(1)}| = \mathbb{I}$. The above relation can then be rewritten as

$$\begin{aligned}&\langle 00|U(\tau)U^\dagger(\tau)|00\rangle - |\langle 00|U(\tau)|\psi_0^{(1)}\rangle|^2 \\ &= 1 - \left(1 - |\langle 11|U(\tau)|\psi_0^{(1)}\rangle|^2\right) \\ &= |\langle 11|U(\tau)|\psi_0^{(1)}\rangle|^2 \ .\end{aligned}$$

In the last line, we have used the conservation of probability

$$|\langle 00|U(\tau)|\psi_0^{(1)}\rangle|^2 + |\langle 11|U(\tau)|\psi_0^{(1)}\rangle|^2 = 1,$$

whereas other two terms $|\langle 01|U(\tau)|\psi_0^{(1)}\rangle|^2 = 0$, and $|\langle 10|U(\tau)|\psi_0^{(1)}\rangle|^2 = 0$.

At D:

Similarly, to point B, we can derive the expression of the average internal energy at D given by

$$\langle E_D\rangle_{L\tau} = \mathrm{Tr}(H_{L1}\rho_{DL\tau}) = B_L(P_3^H - P_0^H)(1-2\delta_\tau)\ , \tag{3.38}$$

where we need to use the microreversibility conditions $|\langle 00|V(\tau)|\psi_0^{(2)}\rangle|^2 = 1-\delta_\tau$, $|\langle 00|V(\tau)|\psi_3^{(2)}\rangle|^2 = \delta_\tau$, $|\langle 11|V(\tau)|\psi_0^{(2)}\rangle|^2 = \delta_\tau$, and $|\langle 11|V(\tau)|\psi_3^{(2)}\rangle|^2 = 1-\delta_\tau$.

Proof of the relation $|\langle 00|V(\tau)|\psi_3^{(2)}\rangle|^2 = |\langle 11|V(\tau)|\psi_0^{(2)}\rangle|^2$:

Similarly to the above microreversibility condition, we can prove that $|\langle 00|V(\tau)|\psi_3^{(2)}\rangle|^2 = |\langle 11|V(\tau)|\psi_0^{(2)}\rangle|^2$, where we need to use the conservation of probability

$$|\langle 00|V(\tau)|\psi_0^{(2)}\rangle|^2 + |\langle 11|V(\tau)|\psi_0^{(2)}\rangle|^2 = 1.$$

Here $\lambda_\tau = |\langle 00|\hat{U}(\tau)|\psi_3^{(1)}\rangle|^2 = |\langle 11|\hat{U}(\tau)|\psi_0^{(1)}\rangle|^2$, and $\delta_\tau = |\langle 11|\hat{V}(\tau)|\psi_0^{(2)}\rangle|^2 = |\langle 00|\hat{V}(\tau)|\psi_3^{(2)}\rangle|^2$ represent the non-zero overlap between the basis states of a two-spin system and the instantaneous energy eigenstates. In the adiabatic limit i.e. $\tau\to\infty$, λ_τ and δ_τ become $\lambda_{\tau\to\infty} = a_H^2/2$ and $\delta_{\tau\to\infty} = a_L^2/2$ respectively, illustrating that finite time average internal energies approach quasistatic average internal energies (see **Sec. 3.4.1**).

Thermodynamic quantities in a complete cycle for the finite time operation of a local spin QOE:

Thermodynamic quantities of the local spin are given by

$$\begin{aligned} W_{L\tau} =& -2[\frac{\sinh 2K_L\beta_L}{Z_1}\left[B_H(1-2\lambda_\tau]) - B_L(1-2\delta_{\tau\to\infty})\right] \\ &+ \frac{\sinh 2K_H\beta_H}{Z_2}\left[B_L(1-2\delta) - B_H(1-2\lambda_{\tau\to\infty})\right]], \\ Q_{LH\tau} =& -2B_H\left[\frac{\sinh 2K_H\beta_H}{Z_2}(1-2\lambda_{\tau\to\infty}) - \frac{\sinh 2K_L\beta_L}{Z_1}(1-2\lambda_\tau)\right]. \end{aligned}$$

So, the efficiency of the heat engine cycle experienced by the local spin is given by

$$\eta = -\frac{W_L}{Q_{LH}} = 1 - \frac{B_L\left[\sinh(2K_H\beta_H)(1-2\delta) - \sinh(2K_L\beta_L)\left(1-2\delta_{\tau\to\infty}\right)\right]}{B_H\left[\sinh(2K_H\beta_H)\left(1-2\lambda_{\tau\to\infty}\right) - \sinh(2K_L\beta_L)(1-2\lambda)\right]} \tag{3.39}$$

It can be seen that the finite-time local efficiency depends on the temperatures of the heat baths as the coefficients u_1, u_2 depend on the temperatures, whereas the quasistatic local efficiency does not depend on the temperatures of the heat baths.

Plots of the transition probabilities $(\lambda_\tau, \delta_\tau)$ with respect to τ are shown in

Fig. 3.9. If we put the value of λ_τ and δ_τ in the expression of efficiency (**Eq. 3.39**), we get the plot of efficiency with respect to τ which is shown in **Fig. 3.9**. This plot shows an oscillatory dependence of efficiency on τ for $\gamma \neq 0$. Depending on the exact value of τ in the short time duration, a local spin system QHE can either underperform or outperform the counterpart which operates in the adiabatic limit. Thus, by adjusting the time of the unitary processes, the efficiency of a local spin system QOE can be enhanced beyond its quasistatic limit. In a long time duration i.e. in the adiabatic limit ($\tau \to \infty$), efficiency gradually approaches the adiabatic (quasistatic) value (see **Sec. 3.4.1**). In that case, the local spin system efficiency which is represented by **Eq. 3.39** will be reduced to **Eq. 3.34**.

In the sudden quench limit i.e. $\tau \to 0$, the external magnetic field is changed B_L to B_H or vice-versa suddenly, in this case, both the δ_τ and λ_τ attain their sudden value which can be obtained as $\lambda_{\tau\to 0} = |\langle 00|\psi_3^{(1)}\rangle|^2 = |\langle 11|\psi_3^{(1)}\rangle|^2$, and $\delta_{\tau\to 0} = |\langle 11|\psi_3^{(2)}\rangle|^2 = |\langle 00|\psi_3^{(2)}\rangle|^2$, as in this case $\hat{U}(\tau), \hat{V}(\tau) \to \mathbb{1}$. The engine's performance degraded in this case (see **Fig. 3.9**). Also, in the adiabatic limit i.e. $\tau \to \infty$, both λ_τ and δ_τ reach their adiabatic value $\lambda_{\tau\to\infty}$ and $\delta_{\tau\to\infty}$. In between these two limiting cases of time, there is an oscillation in $\delta_\tau, \lambda_\tau$ with respect to τ. The oscillation in the efficiency is mainly because of the oscillation in the transition probabilities $\delta_\tau, \lambda_\tau$ in finite times of the unitary processes, which can be attributed to the interference-like phenomena that happen between two probability amplitudes, which can be seen if we rewrite the $\lambda_\tau, \delta_\tau$ in the form given in **Eq. 3.40**.

$$\begin{aligned}
\delta_\tau &= \left| \frac{\sqrt{2}a_L}{a_L d_L - b_L c_L} \langle \psi_3^{(2)}|\hat{V}(\tau)|\psi_3^{(1)}\rangle - \frac{\sqrt{2}c_L}{a_L d_L - b_L c_L} \langle \psi_0^{(2)}|\hat{V}(\tau)|\psi_3^{(1)}\rangle \right|^2, \\
\lambda_\tau &= \left| \frac{\sqrt{2}a_H}{a_H d_H - b_H c_H} \langle \psi_3^{(2)}|\hat{U}(\tau)|\psi_3^{(1)}\rangle - \frac{\sqrt{2}c_H}{a_H d_H - b_H c_H} \langle \psi_0^{(2)}|\hat{U}(\tau)|\psi_3^{(1)}\rangle \right|^2,
\end{aligned} \tag{3.40}$$

where $a_H = \frac{B_H - k_H}{\sqrt{k_H^2 - B_H k_H}}$, $b_H = \frac{\gamma J}{\sqrt{k_H^2 - B_H k_H}}$, $c_H = \frac{B_H + k_H}{\sqrt{k_H^2 + B_H k_H}}$, $d_H = \frac{\gamma J}{\sqrt{k_H^2 + B_H k_H}}$, and for a_L, b_L, c_L, d_L we need to replace the subscript H by L. Although the oscillation in δ_τ is less prominent here compare to λ_τ in the parameter value we are using for the engine operation (see **Fig. 3.9**), in other regions of the parameter, particularly B_H, the oscillation in δ_τ can be found significant. From **Fig. 3.9** we can see that when λ_τ goes below the $\lambda_{\tau\to\infty}$, the finite time QHE outperforms the counterparts operating in the adiabatic limit ($\tau \to \infty$). Also, it can be shown that for $\gamma = 0$ efficiency does not change with τ, which is because there is no interference-like effect in this case [147].

The plot of the efficiency of the local spin QHE with respect to the anisotropy

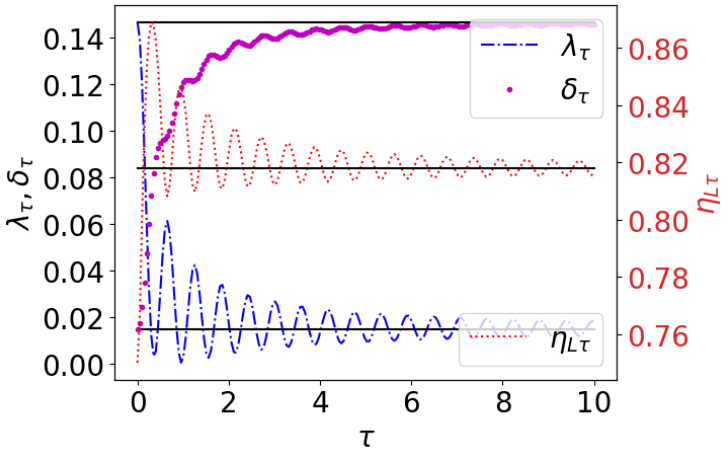

Figure 3.9: Variation of the transition probability λ_τ and δ_τ on the left axis, and efficiency of a local spin on the right axis as a function of time of the unitary processes. The solid line on the top represents the quasistatic value of δ_τ, at the bottom represents the quasistatic value of λ_τ, and in the middle represents the quasistatic value of the local efficiency respectively. Other parameters $\gamma = 1$, remaining are the same with **Fig. 3.3**.

parameter γ is shown in **Fig. 3.10**. It shows that the outperformance increases with the increase of anisotropy (γ) for the finite time operation of the engine, which is similar to the measurement-based QOE [147].

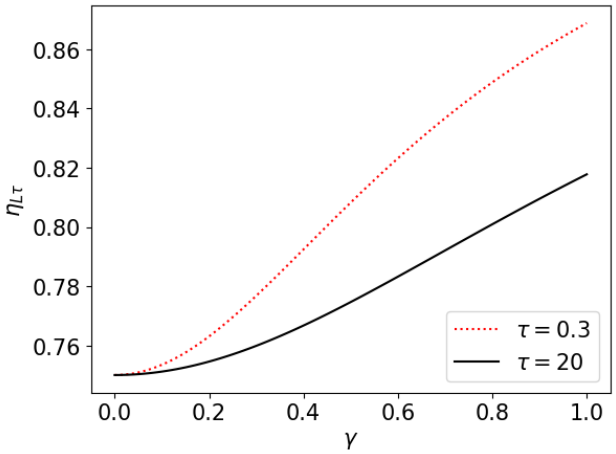

Figure 3.10: Variation of efficiency of the local spin heat engine as a function of anisotropy parameter (γ) for different values of the unitary process time (τ). $\tau = 20$ represents the adiabatic and $\tau = 0.3$ represents the non-adiabatic cases of the unitary time evolution. The other parameters are the same with **Fig. 3.3**.

Power Analysis:

As we are studying the finite-time performance of the engine, it is imperative to explore the power of the engine and its relation to efficiency in this type of local

spin QHE. The power of the local spin QHE can be defined as

$$P_L = \frac{|W_L|}{t_h + t_c + 2\tau}, \tag{3.41}$$

where it is assumed that two isochoric processes are carried out over a long time, but not infinite time so that the states of the working system reach very close to the reference thermal states in two isochoric processes. The 3D plot of efficiency as a function of power and the time of the unitary processes is shown in **Fig. 3.11**. From this plot, it can be seen that we can have improved efficiency even at maximum power.

The power can also be boosted if one considers collective dissipation of N (an even number) non-interacting spins. In terms of the collective spin operators $J_\alpha = \frac{1}{2}\sum_{i=1}^{N}\sigma_\alpha^{(i)}, \quad \alpha = x, y, z$, we can write the Hamiltonian of such system as $H(t) = -\lambda(t)\omega J_z$. The collective dissipation, described in terms of the relevant ladder operators $J_\pm = J_x \pm iJ_y$, is governed via the following master equation:

$$\dot{\rho} = i\lambda(t)\omega\left[J_z, \rho\right] + \gamma\left(1 + n_b\right)\mathcal{D}\left[J_+\right]\rho + \gamma n_b \mathcal{D}\left[J_-\right]\rho.$$

The collective dissipation significantly speeds up the thermalization process and so can boost the power output compared to the case when the spins dissipate independently [250, 251]. This cooperative boost in power represents a close analog of the Dicke superradiance (i.e., the collective enhancement of coherent spontaneous emission from a dense ensemble of atoms).

3.4.3 Experimental Implementation

Heisenberg's anisotropic XY interaction between two-spin can be constructed using state-of-the-art technologies [193], particularly in NMR systems or trapped ion systems. In a typical trapped ion system, the coupling constant J can range from a few hundred Hz to one kHz [252, 253]. Also, the external magnetic field can be of the order of a few kHz[253, 254, 255]. Therefore, depending on the value of J, the time for the unitary processes τ can range from 2μs to a few ms. Also, the working system needs to be cooled at $T_L = 50$ nK and $T_H = 500$ nK.

3.5 Operation of the cycle as a Refrigerator

A similar type of analysis can be done for the refrigerator operation of the cycle. In contrast to the heat engine operation, it can be shown that the COP of the refrigerator degrades as the anisotropy (γ) increases for the quasistatic operation of

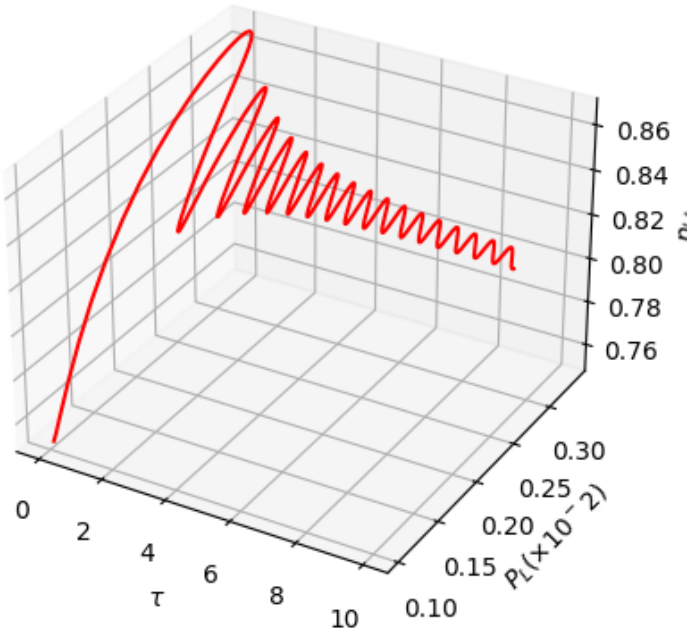

Figure 3.11: Variation of efficiency ($\eta_{L\tau}$ on the z-axis) of the local spin heat engine as a function of power and the time of the unitary processes (τ) for $\gamma = 1$. Parameters for the isochoric processes are $t_h = 100, t_c = 220$, $\Gamma = 0.1$. Other parameters are the same with **Fig. 3.3**.

the cycle. The COP also declines when the refrigerator is operated for a finite time, which is similar to an engine.

Also, using the local analysis as that of the heat engine mentioned above, we can show that the COP of a local spin refrigerator can be enhanced in finite-time unitary processes, which is similar to the local spin HE operation.

3.6 Summary

We have studied the quantum Otto cycle with a two-spin working system coupled by anisotropic interaction. The cycle can be operated in different thermal machine cycles, including a heat engine, refrigerator, accelerator and heater depending on different temperatures of the hot bath, for a fixed value of the coupling constant and the cold bath temperature. Among all thermal machines, the quantum Otto engine (QOE) is studied in different time frames. The role of anisotropy on engine performance has been investigated. We found that the engine's efficiency increases with the increase of the anisotropy parameter (γ) for the quasistatic operation of the cycle. But, efficiency decreases for finite-time engine operation due to quantum internal friction. We found that the decrease in efficiency increases with the increase

of γ, which signifies irreversibility in engine operation which increases with the increase of γ. In the isochoric heating process, the case of incomplete thermalization of the working system on the thermodynamic quantities is also discussed. We observed that heat absorption and work in a complete cycle both increase with the increase in the time of the process and reach a steady value after a long time.

Further, we studied the QOE performance with a local spin working system, which is obtained by tracing out one spin from the global two-spin system. We found that the combined local work extraction from all the spin is larger than the global work extraction in the two-spin system and the difference between these two types of work extraction increases with γ. Also, for anisotropic interaction between two-spin ($\gamma > 0$), a local spin QOE outperforms, in terms of efficiency, a single spin QOE when both function quasistatically with the same cycle parameters. We found that the efficiency of the local spin heat engine oscillates for the finite time unitary processes of the global two-spin system. Therefore, a local spin OQE can outperform the same operating in a long time limit and this outperformance in efficiency is also associated with the maximum power output by the engine. We have shown that the oscillation in efficiency of the local spin QOE comes due to the same origin of an interference-like effect between two probability amplitudes as that of a non-selective measurement-based QOE.

Chapter 4

Effect of anisotropy on a measurement-based quantum Otto engine at finite times

In the previous chapter, we discussed the finite-time operation of a standard QOE, where the engine operates between two heat baths. In this chapter, we want to explore how a measurement based-QOE operates in finite time and how it differs from the finite-time operation of a standard QOE. Also, we will discuss the role of anisotropy in its performance.

4.1 Motivation

From the time of Maxwell, it was known that work could be extracted from a single-temperature heat bath using information gained from measurements. This type of engine is known as Szilard's engine, in which results of selective measurement are used to provide feedback on engine operation [14, 256, 257]. Recently, it was also shown that projective measurement of the ground state can be used to mimic the release of heat from a system to a cold bath during an isochoric process [215, 223, 258] in an ion-based QHE. In later works, quantum measurement has been used to fuel the working system in a QHE, in which the isochoric heating stage in a standard quantum Otto engine (QOE) is replaced by a non-selective quantum measurement [214, 257, 259, 260]. Therefore, the engine works with a single heat bath as a heat shrink and non-selective quantum measurement as a heat source.

A finite-time analysis is also an important aspect of studying QHE, as for practical applications we need a finite amount of power. Moreover, a QHE in finite time may show true quantum nature in its performance which may not be possible to observe in the quasistatic performance.

While the measurement processes and finite-time operation can individually have substantial effects on the performance of the QHEs, there have been very

few studies when both protocols are used together. It has recently shown that it is possible to improve the performance of a single-qubit QHE by suitably choosing the measurement basis such that the degradation effect due to coherence production in a standard QOE can be overcome [261]. In this chapter, we will investigate the finite-time performance of a two-spin QOE by using a non-selective quantum measurement to fuel the engine.

In this chapter, we will investigate the finite-time performance of a two-spin QOE by using non-selective quantum measurements to fuel the engine. We aim to investigate if a measurement-based engine operating in finite time performs better than when operated quasistatically. We will also discuss the case that if the spins remain coupled with a heat bath throughout the cycle (including the stages, when the magnetic fields are varied), how it will affect the engine's performance.

In this chapter, we introduce the two-spin model of the working system. We describe different stages of the quantum Otto cycle and the relevant thermodynamic quantities. Next, we describe the finite-time performance of the cycle. We provide a theoretical analysis of the thermodynamic quantities in terms of the transition probabilities. We also compare them with the quasistatic and the sudden limit of work and efficiency. Also, we study the case when the thermal bath continuously interacts with the spins, even when the magnetic field is changed.

The role of non-selective measurements:

The heating of a system can be generally understood to be associated with an increase in its entropy. Usually, a system is heated using a heat bath. This can be alternatively achieved by applying non-selective quantum measurements on the working system. In order to ensure that the energy supplied by this measurement is nonzero, the measurement operator $\hat{M}$ should not commute with the Hamiltonian, i.e. $[\hat{H}(B_2), \hat{M}] \neq 0$. If $\hat{\rho}$ is the state before the measurement, the post-measurement state is usually written as $\sum_\alpha \hat{M}_\alpha \hat{\rho} \hat{M}_\alpha$, where $\hat{M}_\alpha = |M_\alpha\rangle\langle M_\alpha|$ is the projection operator associated to the non-degenerate eigenvalues of the observable M with eigenstates $|M_\alpha\rangle$, satisfying $\hat{M}_\alpha^\dagger = \hat{M}_\alpha$ and $\sum_\alpha \hat{M}_\alpha^2 = \mathbb{1}$. The entropy of the system increases due to its interaction with the measurement apparatus and this increase can be considered equivalent to heating. Therefore, the engine works with a single heat bath as a heat shrink and non-selective quantum measurements as a heat source.

4.2 System model

We consider a system of two spins coupled by Heisenberg anisotropic XY interaction in a transverse time-dependent magnetic field $B(t) \geq 0$. The Hamiltonian is represented by (see **Eq. 4.1**)

$$\hat{H}(t) = B(t)\,(\hat{\sigma}_1^z + \hat{\sigma}_2^z) + J\,[(1+\gamma)\hat{\sigma}_1^x\hat{\sigma}_2^x + (1-\gamma)\hat{\sigma}_1^y\hat{\sigma}_2^y]\,, \tag{4.1}$$

the Hamiltonian is the same as the previous chapter.

The energy eigenstates (see **Eq. 3.2**) of the Hamiltonian can be divided into two categories. The states that are dependent on the system parameters $B(t)$ and J, namely, $|\psi_0\rangle$ and $|\psi_3\rangle$, evolve with time. The other ones which are independent of the system parameters, namely $|\psi_1\rangle$ and $|\psi_2\rangle$ are the standard Bell states that remain unchanged with time. We will show in this work that the former ones play a fundamental role in the behaviour of the measurement-based cycle. Note that in the limit of $\gamma = 0$, the eigenstates $|\psi_{0,3}\rangle$ take the form of product (i.e., disentangled) states, with the respective eigenvalues $\mp 2B$.

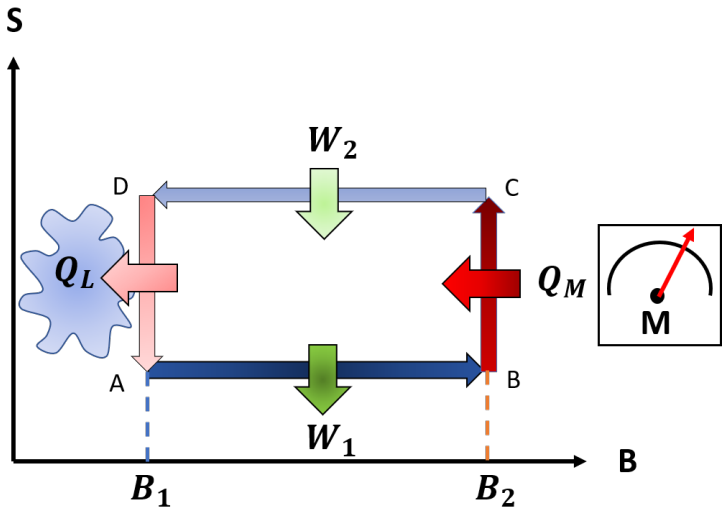

Figure 4.1: Schematic diagram of the Otto cycle with quantum measurements

4.2.1 Quantum Otto cycle and thermodynamic quantities

We consider that the working system undergoes an Otto cycle. The schematic diagram of the cycle is shown in the **Fig. 4.1**. The strokes of the cycle are described below.

Unitary expansion (A to B): The working system is initially prepared in a thermal state $\hat{\rho}_A = e^{-\beta\hat{H}_1}/Z$ at inverse temperature $\beta = 1/T(k_B = 1)$, with

$\hat{H}_1 = \hat{H}(0)$ and $Z = \mathrm{Tr}(e^{-\beta\hat{H}_1})$. During this stage of the cycle, the system is decoupled from the heat bath and the external magnetic field is changed from B_1 to B_2 during a finite time-interval τ. We choose a linear ramp for this change: $B(t) = B_1 + (B_2 - B_1)(t/\tau)$, where $0 \leqslant t \leqslant \tau$. The state of the working system at the end of this stage changes to $\hat{\rho}_B = \hat{U}(\tau)\hat{\rho}_A\hat{U}^\dagger(\tau)$, where $\hat{U}(\tau) = \mathcal{T}\exp\left[-\iota\int_0^\tau dt\hat{H}(t)\right]$ is the relevant time evolution operator, with $\mathcal{T}$ indicating the time-ordering. Also, a certain amount of work, W_1 is done by the system, which can be calculated as $W_1 = \langle E_B\rangle - \langle E_A\rangle$, where $\langle E_A\rangle = \mathrm{Tr}(\hat{\rho}_A\hat{H}_1)$ and $\langle E_B\rangle = \mathrm{Tr}(\hat{\rho}_B\hat{H}_2)$ indicate the expectation values of the internal energies of the system at the start and the end of this stage. Note that $\hat{H}_2 = \hat{H}(\tau)$.

Isochoric heating (B to C): In this stroke, we perform global measurements of the state of the system [259], in the Bell basis $\{|\psi_\pm\rangle = \frac{1}{\sqrt{2}}(|00\rangle \pm |11\rangle)$, $|\phi_\pm\rangle = \frac{1}{\sqrt{2}}(|01\rangle \pm |10\rangle)\}$. The leads to a post-measurement state given by $\hat{\rho}_C = \sum_{\alpha=1}^{4}\hat{M}_\alpha\hat{\rho}_B\hat{M}_\alpha$. where $\hat{M}_\alpha$ describes the relevant projection operators as follows: $\hat{M}_{1,2} = |\psi_\pm\rangle\langle\psi_\pm|$ and $\hat{M}_{3,4} = |\phi_\pm\rangle\langle\phi_\pm|$. The heat absorption in this process can be calculated as $Q_M = \langle E_C\rangle - \langle E_B\rangle$, where the internal energy $\langle E_C\rangle = \mathrm{Tr}(\hat{\rho}_C\hat{H}_2)$.

Unitary compression (C to D): The working system remains decoupled from the heat bath in this stage. The magnetic field is driven from B_2 to B_1 in a finite time τ using the protocol $B(\tau - t)$. The state of the working system at the end of this stage becomes $\hat{\rho}_D = \hat{V}(\tau)\hat{\rho}_C\hat{V}^\dagger(\tau)$, where $\hat{V}(\tau) = \mathcal{T}\exp\left[-\iota\int_0^\tau dt\hat{H}(\tau - t)\right]$ is the time evolution operator. A certain amount of work, W_2, is done on the system, which can be calculated as $W_2 = \langle E_D\rangle - \langle E_C\rangle$, where the internal energy $\langle E_D\rangle = \mathrm{Tr}(\hat{\rho}_D\hat{H}_1)$.

Isochoric cooling (D to A): During this final stage of the cycle, the system is now coupled with a heat bath at the temperature T, whereas the magnetic field remains fixed at B_1. The system releases some amount of heat Q_L to the bath, which can be calculated as $Q_L = \langle E_A\rangle - \langle E_D\rangle$. We assume that this process is carried out over a long time so that the system reaches thermal equilibrium with the bath.

Total work done in a complete cycle can be calculated as $W = (W_1 + W_2) = -(Q_M + Q_L)$. If $W < 0$, then the total work in a complete cycle is done by the working system. Also, the working system absorbs some amount of heat in the measurement process, if $Q_M > 0$. Then, the working system in a complete cycle works as a heat engine. So, the efficiency of the engine is given by $\eta = |W|/Q_M$.

4.3 Finite time operation of the engine

Usually, quantum heat engines are studied quasistatically. If we allow different stages of the engine cycle only for finite times, the performance of the engine is expected to deviate substantially from the steady state. We show in **Fig. 4.2**, how the efficiency varies with respect to the duration of the unitary stages. We assume that each of these stages (unitary expansion and compression) occurs for the same duration τ. All simulations are done using QuTip [242] software package.

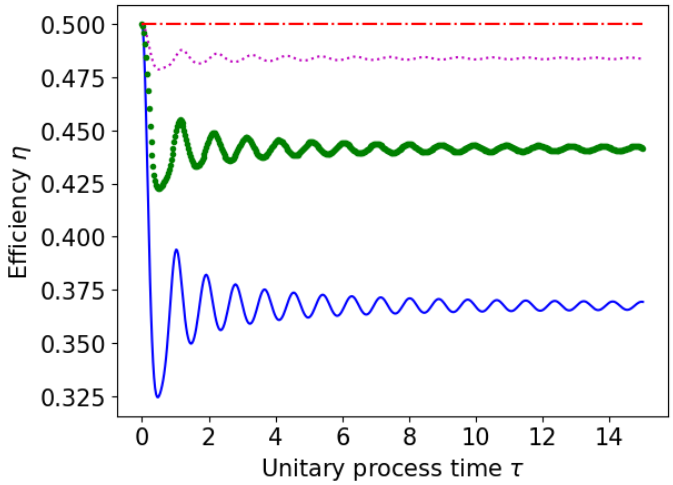

Figure 4.2: Efficiency as a function of duration τ of the unitary stages, for different values of the anisotropy parameter $\gamma = 0$ (dash-dotted red line), $\gamma = 0.3$ (point-marked magenta line), $\gamma = 0.6$ (dotted green line), $\gamma = 1$ (solid blue line). The other parameters are $B_1 = 1$, $B_2 = 2$, $T = 1$. All the quantities are dimensionless with respect to J and also we have used $k_B = \hbar = 1$.

As seen in the **Fig. 4.2**, the efficiency oscillates at the transient time-scale for $\gamma \neq 0$. This means that if the unitary stages are executed for a very short time $\tau \gtrsim 0$, the efficiency can be larger or smaller than that obtained for a large value of τ. If the unitary processes are prolonged, the oscillation in efficiency disappears. Thus, a finite-time measurement-based engine can perform better than the same engine operating for a longer duration, for a suitable selection of the duration τ for unitary processes.

Note that, if one would use a local measurement, instead of global ones, similar oscillatory behaviour in the efficiency of the engine could be seen, for finite-time operation [214, 262]. Also in these cases, the engine performs better than its quasistatic counterpart at finite times for specific choices of the local basis.

4.3.1 Thermodynamic quantities in terms of transition probabilities

The results as mentioned above can further be analyzed in terms of the transition probabilities between the instantaneous eigenstates of the Hamiltonian.

The internal energies of the system at four vertices of the QHE diagram in **Fig. 4.1**, are derived below.

At A:

The Hamiltonian at point A of the cycle can be expressed as

$$H_A = H_1 = \sum_{i=0}^{3} E_i^1 |\psi_i^{(1)}\rangle\langle\psi_i^{(1)}|$$

where $\{|\psi_i^{(1)}\rangle\}$ are the eigenstates of the Hamiltonian H_1. As we consider that the system at A is in thermal equilibrium with the heat bath, the thermal density matrix is given by

$$\rho_A = \frac{e^{-\beta H_1}}{Z} = \sum_{i=0}^{3} P_i |\psi_i^{(1)}\rangle\langle\psi_i^{(1)}| \tag{4.2}$$

where $P_i = \frac{e^{-\beta E_i^1}}{Z}$ is the thermal occupation probability of the ith eigenstate. So, the average internal energy at point A is given by

$$\langle E_A\rangle = \mathrm{Tr}(H_1\rho_A) = \sum_{i=0}^{3} P_i E_i^1 = -2K_1 \frac{2\sinh 2K_1\beta}{Z} - 2J\frac{\sinh 2J\beta}{Z}. \tag{4.3}$$

At B:

The Hamiltonian at the point B of the cycle can be expressed as

$$H_B = H_2 = \sum_{i=0}^{3} E_i^2 |\psi_i^{(2)}\rangle\langle\psi_i^{(2)}|$$

where $\{|\psi_i^{(2)}\rangle\}$ are the eigenstates of the Hamiltonian H_2. The density matrix at point B after the unitary processes AB can be obtained as

$$\begin{aligned}\rho_B = U(\tau)\rho_A U^\dagger(\tau) = \sum_{i=0}^{3} P_i U(\tau)|\psi_i^{(1)}\rangle\langle\psi_i^{(1)}|U^\dagger(\tau) = P_0 U(\tau)|\psi_0^{(1)}\rangle\langle\psi_0^{(1)}|U(\tau)^\dagger \\ + \; P_1|\psi_1^{(1)}\rangle\langle\psi_1^{(1)}| \; + \; P_2|\psi_2^{(1)}\rangle\langle\psi_2^{(1)}| \; + \; P_3 U(\tau)|\psi_3^{(1)}\rangle\langle\psi_3^{(1)}|U^\dagger(\tau)\end{aligned} \tag{4.4}$$

where we have used $U(\tau)|\psi_i^{(1)}\rangle = |\psi_i^{(1)}\rangle$ and $\langle\psi_i^{(1)}|U^\dagger(\tau) = \langle\psi_i^{(1)}|$ for $i \in (1, 2)$, as

these two energy eigenstates remain unchanged with respect to time. The average internal energy at the point B can be obtained as

$$\begin{aligned}\langle E_B\rangle =& \mathrm{Tr}(H_2\rho_B)\\ =& \sum_{i,j=0,3} P_i E_j^2\ \langle\psi_j^{(2)}|U(\tau)|\psi_i^{(1)}\rangle\langle\psi_i^{(1)}|U(\tau)^\dagger|\psi_j^{(2)}\rangle\ +\ E_1^2P_1\ +\ E_2^2P_2\\ =& P_0E_0^2|\langle\psi_0^{(2)}|U(\tau)|\psi_0^{(2)}\rangle|^2\ +\ P_3E_0^2|\langle\psi_0^{(2)}|U(\tau)|\psi_3^{(1)}\rangle|^2\ +\ E_1^2P_1\ +\ E_2^2P_2\\ &+\ P_0E_3^2|\langle\psi_3^{(2)}|U(\tau)|\psi_0^{(1)}\rangle|^2\ +\ P_3E_3^2|\langle\psi_3^{(2)}|U(\tau)|\psi_3^{(1)}\rangle|^2\\ =& P_0E_0^2(1-\xi)\ +\ P_3E_0^2\xi\ +\ P_1E_1^2\ +\ P_2E_2^2\ +\ P_0E_3^2\xi\ +\ P_3E_3^2(1-\xi)\\ =& -2K_2(1-2\xi)\frac{2\sinh 2K_1\beta}{Z} - 2J\frac{2\sinh 2J\beta}{Z},\end{aligned} \tag{4.5}$$

where we have used the microreversibility condition $|\langle\psi_i^{(2)}|U(\tau)|\psi_j^{(j)}\rangle|^2 = \xi$ for $i \neq j$ (proof is given below) and $|\langle\psi_i^{(2)}|U(\tau)|\psi_i^{(1)}\rangle|^2 = 1-\xi$. During execution a unitary stroke in a short interval τ led to a nonadiabatic transition between energy eigenstates that are coupled [240]. In the present case, such transitions will be induced between the levels $|\psi_0\rangle$ and $|\psi_3\rangle$. So, the terms like $\langle\psi_i^{(2)}|U(\tau)|\psi_j^{(1)}\rangle = 0$ for $i \neq j$ and i, j take values from any of the group $(0, 1, 2)$ or $(1, 2, 3)$.

Proof of the condition $|\langle\psi_0^{(2)}|U(\tau)|\psi_3^{(1)}\rangle|^2 = |\langle\psi_3^{(2)}|U(\tau)|\psi_0^{(1)}\rangle|^2$:

$$\begin{aligned}|\langle\psi_3^{(2)}|U(\tau)|\psi_0\rangle_1|^2 &= \langle\psi_3^{(2)}|U(\tau)|\psi_0^{(1)}\rangle\langle\psi_0^{(1)}|U^\dagger(\tau)|\psi_3^{(2)}\rangle\\ &= \langle\psi_3^{(2)}|U(\tau)(\mathbb{I} - |\psi_1^{(1)}\rangle\langle\psi_1^{(1)}|\ -\ |\psi_2^{(1)}\rangle\langle\psi_2^{(1)}|\ -\ |\psi_3^{(1)}\rangle\langle\psi_3^{(1)}|)U^\dagger(\tau)|\psi_3^{(2)}\rangle\\ &= \langle\psi_3^{(2)}|U(\tau)U^\dagger(\tau)|\psi_3^{(2)}\rangle - |\langle\psi_3|U(\tau)|\psi_3^{(1)}\rangle|^2\\ &= 1 - (1 - |\langle\psi_0^{(2)}|U(\tau)|\psi_3^{(1)}\rangle|^2) = |\langle\psi_0^{(2)}|U(\tau)|\psi_3^{(1)}\rangle|^2,\end{aligned} \tag{4.6}$$

where the identity matrix is given by

$$\begin{aligned}&\mathbb{I} = |\psi_0^{(1)}\rangle\langle\psi_0^{(1)}|\ +\ |\psi_1^{(1)}\rangle\langle\psi_1^{(1)}|\ +\ |\psi_2^{(1)}\rangle\langle\psi_2^{(1)}|\ +\ |\psi_3^{(1)}\rangle\langle\psi_3^{(1)}|\\ &\Rightarrow |\psi_0^{(1)}\rangle\langle\psi_0^{(1)}| = \mathbb{I} - |\psi_1^{(1)}\rangle\langle\psi_1^{(1)}|\ -\ |\psi_2^{(1)}\rangle\langle\psi_2^{(1)}|\ -\ |\psi_3^{(1)}\rangle\langle\psi_3^{(1)}|,\end{aligned} \tag{4.7}$$

and also, we have used the conservation of probability

$$|\langle\psi_0^{(2)}|U(\tau)|\psi_3^{(1)}\rangle|^2\ +\ |\langle\psi_3^{(2)}|U(\tau)|\psi_3^{(1)}\rangle|^2 = 1.$$

At C:

Again, the density matrix after the measurement stage can be written as

$$\begin{aligned}\rho_C =&\sum_{k=1}^{4} M_k\rho_B M_k\\ =&\sum_{i=(0,3),j=(+,-)} P_i|\langle\psi_j|U(\tau)|\psi_i^{(1)}\rangle|^2|\psi_+\rangle\langle\psi_j| \ + \ P_1|\psi_1^{(1)}\rangle\langle\psi_1^{(1)}| \ + \ P_2|\psi_2^{(1)}\rangle\langle\psi_2^{(1)}|\\ =&P_0\delta|\psi_+\rangle\langle\psi_+| \ + \ P_0(1-\delta)|\psi_-\rangle\langle\psi_-| \ + \ P_1|\psi_1^{(1)}\rangle\langle\psi_1^{(1)}| \ + \ P_2|\psi_2^{(1)}\rangle\langle\psi_2^{(1)}|\\ &+ \ P_3(1-\delta)|\psi_+\rangle\langle\psi_+| \ + \ P_3\delta|\psi_-\rangle\langle\psi_-|,\end{aligned} \tag{4.8}$$

where $M_k^\dagger = M_k$ and we have used the microreversibility condition $|\langle\psi_+|U(\tau)|\psi_0^{(1)}\rangle|^2 = |\langle\psi_-|U(\tau)|\psi_3^{(1)}\rangle|^2 = \delta$ (proof is given below) and $|\langle\psi_-|U(\tau)|\psi_0^{(1)}\rangle|^2 = |\langle\psi_+|U(\tau)|\psi_3^{(1)}\rangle|^2 = 1-\delta$.

Proof of the condition $|\langle\psi_+|U(\tau)|\psi_0^{(1)}\rangle|^2 = |\langle\psi_-|U(\tau)|\psi_3^{(1)}\rangle|^2$:

$$\begin{aligned}&|\langle\psi_+|U(\tau)|\psi_0^{(1)}\rangle|^2 = \langle\psi_+|U(\tau)|\psi_0^{(1)}\rangle\langle\psi_0^{(1)}|U^\dagger(\tau)|\psi_+\rangle\\ &= \langle\psi_+|U(\tau)(\mathbb{I} - |\psi_1^{(1)}\rangle\langle\psi_1^{(1)}| \ - \ |\psi_2^{(1)}\rangle\langle\psi_2^{(1)}| \ - \ |\psi_3^{(1)}\rangle\langle\psi_3^{(1)}|)U^\dagger(\tau)|\psi_+\rangle\\ &= \langle\psi_+|U(\tau)U^\dagger(\tau)|\psi_+\rangle - |\langle\psi_+|U(\tau)|\psi_3^{(1)}\rangle|^2\\ &= 1-(1-|\langle\psi_-|U_\tau|\psi_3^{(1)}\rangle|^2) = |\langle\psi_-|U_\tau|\psi_3^{(1)}\rangle|^2,\end{aligned} \tag{4.9}$$

where we used the conservation of probability

$$|\langle\psi_+|U_\tau|\psi_3\rangle_1|^2 \ + \ |\langle\psi_-|U_\tau|\psi_3\rangle_1|^2 = 1.$$

The average internal energy at the point C can be obtained as

$$\begin{aligned}&\langle E_C\rangle = \mathrm{Tr}(H_2\rho_C)\\ &= E_0^2P_0\delta|\langle\psi_0^{(2)}|\psi_+\rangle|^2 \ + \ E_0^2P_0(1-\delta)\langle\psi_0^{(2)}|\psi_-\rangle|^2 \ + \ E_0^2P_3(1-\delta)|\langle\psi_0^{(2)}|\psi_+\rangle|^2\\ &+ \ E_0^2P_3\delta|\langle\psi_0^{(2)}|\psi_-\rangle|^2 \ + \ E_1^2P_1 \ + \ E_2^2P_2 \ + \ E_3^2P_0\delta|\langle\psi_3^{(2)}|\psi_+\rangle|^2\\ &+ \ E_3^2P_3(1-\delta)|\langle\psi_3^{(2)}|\psi_-\rangle|^2 \ + \ E_3^2P_3(1-\delta)|\langle\psi_3^{(2)}|\psi_+\rangle|^2 \ + \ E_3^2P_3\delta\langle\psi_3^{(2)}|\psi_-\rangle|^2\\ &= E_0^2P_0\delta\chi \ + \ E_0^2P_0(1-\delta)(1-\chi) \ + \ E_0^2P_3(1-\delta)\chi \ + \ E_0^2P_3\delta(1-\chi) \ + \ E_1^2P_1\\ &+ \ E_2^2P_2 \ + \ E_3^2P_0\delta(1-\chi) \ + \ E_3^2P_3(1-\delta)\chi \ + \ E_3^2P_3(1-\delta)(1-\chi) \ + \ E_3^2P_3\delta\chi\\ &= -2K_2(1-2\delta)(1-2\chi)\frac{2\sinh 2K_1\beta}{Z} - 2J\frac{2\sinh 2J\beta}{Z},\end{aligned} \tag{4.10}$$

where we have used the condition $|\langle\psi_0^{(2)}|\psi_+\rangle|^2 = |\langle\psi_3^{(2)}|\psi_-\rangle|^2 = \chi$ (proof is given below) and $|\langle\psi_0^{(2)}|\psi_-\rangle|^2 = |\langle\psi_3^{(2)}|\psi_+\rangle|^2 = 1-\chi$.

Proof of the condition $|\langle\psi_0^{(2)}|\psi_+\rangle|^2 = |\langle\psi_3^{(2)}|\psi_-\rangle|^2$:

$$
\begin{aligned}
|\langle\psi_0^{(2)}|\psi_+\rangle|^2 =& \langle\psi_0^{(2)}|\psi_+\rangle\langle\psi_+|\psi_0^{(2)}\rangle \\
=& \langle\psi_0^{(2)}|(\mathbb{I} - |\psi_-\rangle\langle\psi_-| - |\phi_+\rangle\langle\phi_+| - |\phi_-\rangle\langle\phi_-|)|\psi_0^{(2)}\rangle \\
=& 1 - \langle\psi_0^{(2)}|\psi_-\rangle\langle\psi_-|\psi_0^{(2)}\rangle = 1 - |\langle\psi_0^{(2)}|\psi_-\rangle|^2 = |\langle\psi_3^{(2)}|\psi_-\rangle|^2,
\end{aligned} \tag{4.11}
$$

where we have used the conservation of probability

$$
|\langle\psi_0^{(2)}|\psi_-\rangle|^2 + |\langle\psi_3^{(2)}|\psi_-\rangle|^2 = 1.
$$

At D:

Density matrix at point D after the unitary process $C \to D$ is given by

$$
\begin{aligned}
&\rho_D = V(\tau)\rho_C V^\dagger(\tau) \\
&= P_0\delta V(\tau)|\psi_+\rangle\langle\psi_+|V^\dagger(\tau) + P_0(1-\delta)V(\tau)|\psi_-\rangle\langle\psi_-|V^\dagger(\tau) + P_1|\psi_1^{(1)}\rangle\langle\psi_1^{(1)}| \\
&+ P_2|\psi_2^{(1)}\rangle\langle\psi_2^{(1)}| + P_3(1-\delta)V(\tau)|\psi_+\rangle\langle\psi_+|V^\dagger(\tau) + P_3\delta V(\tau)|\psi_-\rangle\langle\psi_-|V^\dagger(\tau)
\end{aligned} \tag{4.12}
$$

The average internal energy at the point D can be obtained as

$$
\begin{aligned}
&\langle E_D\rangle = \mathrm{Tr}(H_1\rho_D) \\
&= \sum_{i=0}^{3}\langle\psi_i^{(1)}| \{P_0\delta E_0^1|\psi_0^{(1)}\rangle\langle\psi_0^{(1)}|V(\tau)|\psi_+\rangle\langle\psi_+|V^\dagger(\tau) \\
&+ P_0(1-\delta)E_0^1|\psi_0^{(1)}\rangle\langle\psi_0^{(1)}|V(\tau)|\psi_-\rangle\langle\psi_-|V^\dagger(\tau) \\
&+ P_3(1-\delta)E_0^1|\psi_0^{(1)}\rangle\langle\psi_0^{(1)}|V(\tau)|\psi_+\rangle\langle\psi_+|V^\dagger(\tau) \\
&+ P_3\delta E_0^1|\psi_0^{(1)}\rangle\langle\psi_0^{(1)}|V(\tau)|\psi_-\rangle\langle\psi_-|V^\dagger(\tau) + E_1^1P_1 \\
&+ E_2^1P_2 + P_0\delta E_3^1|\psi_3^{(1)}\rangle\langle\psi_3^{(1)}|V(\tau)|\psi_+\rangle\langle\psi_+|V^\dagger(\tau) \\
&+ P_0(1-\delta)E_3^1|\psi_3^{(1)}\rangle\langle\psi_3^{(1)}|V(\tau)|\psi_-\rangle\langle\psi_-|V^\dagger(\tau) \\
&+ P_3(1-\delta)E_3^1|\psi_3^{(1)}\rangle\langle\psi_3^{(1)}|V(\tau)|\psi_+\rangle\langle\psi_+|V^\dagger(\tau) \\
&+ P_3\delta E_3^1|\psi_3^{(1)}\rangle\langle\psi_3^{(1)}|V(\tau)|\psi_-\rangle\langle\psi_-|V^\dagger(\tau)\ \}|\psi_i^{(2)}\rangle \\
&= P_0\delta E_0^1|\langle\psi_0^{(1)}|V(\tau)|\psi_+\rangle|^2 + P_0(1-\delta)E_0^1|\langle\psi_0^{(1)}|V(\tau)|\psi_-\rangle|^2 \\
&+ P_3(1-\delta)E_0^1|\langle\psi_0^{(1)}|V(\tau)|\psi_+\rangle|^2 + P_3\delta E_0^1|\langle\psi_0^{(1)}|V(\tau)|\psi_-\rangle|^2 + E_1^1P_1 \\
&+ E_2^1P_2 + P_0\delta E_3^1|\langle\psi_3^{(1)}|V(\tau)|\psi_+\rangle|^2 + P_0(1-\delta)E_3^1|\langle\psi_3^{(1)}|V(\tau)|\psi_-\rangle|^2 \\
&+ P_3(1-\delta)E_3^1|\langle\psi_3^{(1)}|V(\tau)|\psi_+\rangle|^2 + P_3\delta E_3^1|\langle\psi_3^{(1)}|V(\tau)|\psi_-\rangle|^2 \\
&= P_0E_0^1\delta\lambda + P_0E_0^1(1-\delta)(1-\lambda) + P_3E_0^1(1-\delta)\lambda + P_3E_0^1\delta(1-\lambda) + E_1^1P_1 \\
&+ E_2^1P_2 + P_0E_3^1\delta(1-\lambda) + P_0E_3^1(1-\delta)\lambda + P_3E_3^1(1-\delta)(1-\lambda) + P_3E_3^1\delta\lambda \\
&= -2K_1(1-2\delta)(1-2\lambda)\frac{2\sinh 2K_1\beta}{Z} - 2J\frac{2\sinh 2J\beta}{Z},
\end{aligned} \tag{4.13}
$$

where we have used the microreversibility condition $|\langle\psi_0^{(1)}|V(\tau)|\psi_+\rangle|^2 =$

$|\langle\psi_3^{(1)}|V(\tau)|\psi_-\rangle|^2 = \lambda$ and $\langle\psi_3^{(1)}|V(\tau)|\psi_+\rangle|^2 = |\langle\psi_0^{(1)}|V(\tau)|\psi_-\rangle|^2 = 1-\lambda$.

Proof of the condition $|\langle\psi_0^{(1)}|V(\tau)|\psi_+\rangle|^2 = |\langle\psi_3^{(1)}|V(\tau)|\psi_-\rangle|^2$**:**

$$\begin{aligned}
&|\langle\psi_0^{(1)}|V(\tau)|\psi_+\rangle|^2 = \langle\psi_0^{(1)}|V(\tau)|\psi_+\rangle\langle\psi_+|V(\tau)|\psi_0^{(1)}\rangle \\
&= \langle\psi_0^{(1)}|V(\tau)(\mathbb{I} - |\psi_-\rangle\langle\psi_-| - |\phi_+\rangle\langle\phi_+| - |\phi_-\rangle\langle\phi_-|)V^\dagger(\tau)|\psi_0^{(1)}\rangle \\
&= \langle\psi_0^{(1)}|V(\tau)V^\dagger(\tau)|\psi_0\rangle - |\langle\psi_0^{(1)}|V(\tau)|\psi_-\rangle|^2 = |\langle\psi_3|V(\tau)|\psi_-\rangle|^2,
\end{aligned} \tag{4.14}$$

where the identity matrix is given by

$$\begin{aligned}
&\sum_{k=1}^{4} M_k^2 = \mathbb{I} \\
&\Rightarrow \mathbb{I} = |\psi_+\rangle\langle\psi_+| + |\psi_-\rangle\langle\psi_-| + |\phi_+\rangle\langle\phi_+| + |\phi_-\rangle\langle\phi_-| \\
&\Rightarrow |\psi_+\rangle\langle\psi_+| = \mathbb{I} - |\psi_-\rangle\langle\psi_-| - |\phi_+\rangle\langle\phi_+| - |\phi_-\rangle\langle\phi_-|,
\end{aligned} \tag{4.15}$$

and we have used the conservation of the probability

$$|\langle\psi_0^{(1)}|V(\tau)|\psi_-\rangle|^2 + |\langle\psi_3^{(1)}|V(\tau)|\psi_-\rangle|^2 = 1.$$

Here $Z = 2\cosh(2K_1\beta) + 2\cosh(2J\beta)$ is the partition function, $K_1 = \sqrt{B_1^2+\gamma^2J^2}$, $K_2 = \sqrt{B_2^2+\gamma^2J^2}$, $\xi = |\langle\psi_0^{(2)}|\hat{U}(\tau)|\psi_3^{(1)}\rangle|^2$, $\delta = |\langle\psi_+|\hat{U}(\tau)|\psi_0^{(1)}\rangle|^2$, $\chi = |\langle\psi_0^{(2)}|\psi_+\rangle|^2$, and $\lambda = |\langle\psi_3^{(1)}|\hat{V}(\tau)|\psi_-\rangle|^2$. Clearly, ξ accounts for the transition probability between two different eigenstates $|\psi_3\rangle$ and $|\psi_0\rangle$ during the unitary expansion. Also, because the instantaneous energy eigenstates $|\psi_{0,3}\rangle$ do not truly coincide with the measurement basis states $|\psi_\pm\rangle$, their nonzero overlap gives rise to certain transition between them during measurement and unitary compression stages of the cycle. This can be seen by rewriting the states $|\psi_\pm\rangle$ in terms of the instantaneous energy eigenstates, as

$$\begin{aligned}
|\psi_+\rangle &= -\frac{c_2-d_2}{a_2d_2-b_2c_2}|\psi_0^{(2)}\rangle + \frac{a_2-b_2}{a_2d_2-b_2c_2}|\psi_3^{(2)}\rangle \\
|\psi_-\rangle &= -\frac{c_2+d_2}{a_2d_2-b_2c_2}|\psi_0^{(2)}\rangle + \frac{a_2+b_2}{a_2d_2-b_2c_2}|\psi_3^{(2)}\rangle,
\end{aligned} \tag{4.16}$$

where

$$a_2 = \frac{B_2-K_2}{\sqrt{K_2^2-B_2K_2}}, b_2 = \frac{\gamma J}{\sqrt{K_2^2-B_2K_2}}, c_2 = \frac{B_2+K_2}{\sqrt{K_2^2+B_2K_2}}, d_2 = \frac{\gamma J}{\sqrt{K_2^2+B_2K_2}} \tag{4.17}$$

Then the relevant transition probabilities can be written as

$$\begin{aligned}\delta &= \left| -\frac{c_2 - d_2}{a_2 d_2 - b_2 c_2} \langle \psi_0^{(2)} | U(\tau) | \psi_0^{(1)} \rangle + \frac{a_2 - b_2}{a_2 d_2 - b_2 c_2} \langle \psi_3^{(2)} | U(\tau) | \psi_0^{(1)} \rangle \right|^2 , \\ \lambda &= \left| -\frac{c_2 + d_2}{a_2 d_2 - b_2 c_2} \langle \psi_3^{(1)} | V(\tau) | \psi_0^{(2)} \rangle + \frac{a_2 + b_2}{a_2 d_2 - b_2 c_2} \langle \psi_3^{(1)} | V(\tau) | \psi_3^{(2)} \rangle \right|^2 ,\end{aligned} \tag{4.18}$$

and

$$\chi = \left| \frac{c_2 - d_2}{a_2 d_2 - b_2 c_2} \right|^2 . \tag{4.19}$$

The expressions of the work can be obtained using the expression of the internal energies as

$$W_1 = 4[K_1 - K_2(1 - 2\xi)] \frac{\sinh 2K_1\beta}{Z}, \text{ and}$$
$$W_2 = 4(K_2 - K_1)(1 - 2\delta)(1 - 2\lambda) \frac{\sinh 2K_1\beta}{Z}$$

Thus, the total work in a complete cycle is given by

$$W = W_1 + W_2 = -4[K_2\{(1-2\xi) - (1-2\delta)(1-2\chi)\} - K_1\{1 - (1-2\delta)(1-2\lambda)\}] \frac{\sinh 2K_1\beta}{Z}. \tag{4.20}$$

Also, the heat absorption in the measurement stroke is given by

$$Q_M = 4K_2[(1 - 2\xi) - (1 - 2\delta)(1 - 2\chi)] \frac{\sinh 2K_1\beta}{Z}. \tag{4.21}$$

The efficiency of the heat engine cycle is therefore given by

$$\eta = \frac{|W|}{Q_M} = 1 - \frac{K_1[1 - (1 - 2\delta)(1 - 2\lambda)]}{K_2[(1 - 2\xi) - (1 - 2\delta)(1 - 2\chi)]} . \tag{4.22}$$

The plot of the transition probabilities ξ, δ, χ, and λ with respect to the duration τ of the individual unitary processes are shown in the **Fig. 4.3**. Note that δ and λ exhibit oscillatory dependence on τ, χ remains constant, while ξ displays a monotonic decay, as τ increases. Though the transition probabilities δ and λ are the same, for our choice of the measurement basis and the eigenstates of the Hamiltonian, it is, generally speaking, not a universal feature [261].

The oscillation in the finite time efficiency is primarily due to the oscillation in the transition probabilities δ and λ. The oscillation in the transition probabilities δ can be attributed to the interference between the probability amplitudes for the transitions $|\psi_0^{(1)}\rangle \to |\psi_0^{(2)}\rangle$ and $|\psi_0^{(1)}\rangle \to |\psi_3^{(2)}\rangle$ (see **Eq. 4.18**). Similarly, oscillation in λ is due to the transition $|\psi_-\rangle \to |\psi_3^{(1)}\rangle$. The other transition probability ξ, also known as quantum internal friction [263, 79], is negligible with respect to the δ, χ

and λ in a measurement-based QHE. As the unitary stages are prolonged, oscillation in the finite time efficiency disappears and the efficiency approaches the quasistatic limit (see **Sec. 4.3.2**).

Note that the two energy eigenstates $|\psi_1\rangle$ and $|\psi_2\rangle$ are the same as two Bell states $|\phi_\pm\rangle$. As these states have been used in measurement basis, their occupation probabilities do not change in the measurement process, and therefore, these states do not contribute to the calculation of heat [see Eq. (4.18), (4.19), and (4.21)]. Moreover, the eigenvalues of these eigenstates are independent of the external control parameter $B(t)$, and thus the contribution of these states to work is also zero [see Eq. (4.20)]. The only contribution to the engine performance arises from the two other eigenstates $|\psi_0\rangle$ and $|\psi_3\rangle$.

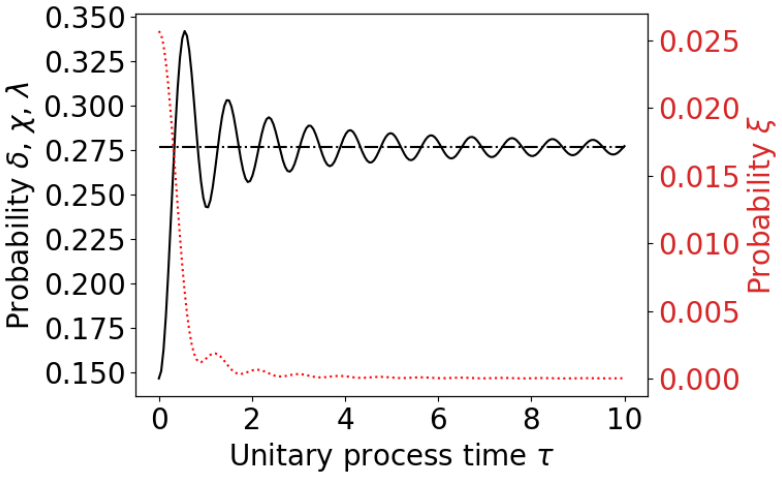

Figure 4.3: Transition probabilities as a function of the duration τ of each unitary stage. We have used the left y-axis for transition probabilities δ and λ (solid black line), and χ (dash-dotted black line) and the right y-axis for transition probability ξ (point-marked red line). The other parameters are $B_1 = 1$, $B_2 = 2$, $\gamma = 1$.

4.3.2 Quasistatic (adiabatic) limit of the thermodynamic quantities

In order to calculate the quasistatic value of the efficiency, we consider that the unitary processes are performed quasistatically, i.e., for an infinite time interval. Therefore, there are no nonadiabatic transitions between two instantaneous energy eigenstates, and the unitary processes become adiabatic. So, in such limit, we can write, $\xi = |\langle\psi_0^{(2)}|\hat{U}(\tau)|\psi_3^{(1)}\rangle|^2 \overset{\tau\to\infty}{=} 0$ (**Fig. 4.3**). Also, the transition probabilities between the instantaneous energy eigenstates and the basis states of measurement take the following forms for very large τ:

$$\delta \overset{\tau\to\infty}{=} |\frac{c_2 - d_2}{a_2 d_2 - b_2 c_2}|^2 \quad , \quad \lambda \overset{\tau\to\infty}{=} |\frac{a_2 + b_2}{a_2 d_2 - b_2 c_2}|^2.$$

Using the expressions of a_2, b_2, c_2, d_2 (see **Eq. 4.17**) we can indeed find that $\delta = \chi = \lambda = \frac{1}{2} - \gamma J/2K_2$, at the quasistatic limit (see also **Fig. 4.3**).

Thus, the expressions of the work and heat absorption of the cycle can be obtained as

$$\begin{aligned} W_q &= -16(K_2 - K_1)\chi(1-\chi)\frac{\sinh 2K_1\beta}{Z}, \\ Q_{Mq} &= 16K_2\chi(1-\chi)\frac{\sinh 2K_1\beta}{Z}\ , \end{aligned} \tag{4.23}$$

and the quasistatic value of the efficiency is given by

$$\eta_q = |W_q|/Q_{Mq} = 1 - \frac{K_1}{K_2}\ . \tag{4.24}$$

Clearly, the expression of this efficiency is independent of the temperature of the heat bath used in the cold isochoric process. This indicates that the performance of the engine does not depend upon the temperature of the heat bath in the case of global measurement, which we have used in the isochoric heating stage. We emphasize that this is unlike the case for a local measurement where the performance of an engine depends upon the temperature of the heat bath [214]. Also, it can be seen from the **Eq. 4.24** that for nonzero γ, the expression of the efficiency is very much similar to the efficiency of a single-spin QHE with two heat baths [71] or a single heat bath and a non-selective quantum measurement at the isochoric heating stage [264]. This similarity arises as only two intermediate energy levels ($|\psi_{0,3}\rangle$, as mentioned in **Sec. 4.2**) contribute to the engine performance, due to our specific choice of the measurement basis. Therefore, a measurement-based heat engine with a coupled two-spin working system for global measurement acts like a two-level (single-spin) heat engine, which is evident in the expression of the efficiency (**Eq. 4.24**). Interestingly, even a two-stroke QHE made up of two different working systems with two different frequencies can lead to the same form of efficiency [265]. However, the expression of efficiency will differ if one uses a coupled two-spin working system along with two heat baths or with a single bath plus local measurement instead of global measurement.

4.3.3 Sudden quench limit of the thermodynamic quantities

In order to calculate the sudden limit of the thermodynamic quantities, we consider that the external magnetic field is changed suddenly ($\tau \to 0$) from B_1 to B_2 or vice versa. In this case $\hat{U}(\tau), \hat{V}(\tau) \to \mathbb{1}$, therefore the state of the system does not change over unitary processes. So, in this limit, the transition probabilities can be

written as

$$\begin{aligned}
\delta &\overset{\tau\to 0}{=} \left| -\frac{c_2-d_2}{a_2d_2-b_2c_2}\ \langle\psi_0^{(2)}|\psi_0^{(1)}\rangle + \frac{a_2-b_2}{a_2d_2-b_2c_2}\ \langle\psi_3^{(2)}|\psi_0^{(1)}\rangle \right|^2 \\
&= \left| -\frac{c_2+d_2}{a_2d_2-b_2c_2}(a_2c_1+b_2d_1) + \frac{a_2+b_2}{a_2d_2-b_2c_2}(c_1c_2+b_1b_2) \right|^2 \\
&= -\frac{(B_1-K_1+\gamma J)^2}{4K_1(B_1-K_1)}, \\
\lambda &\overset{\tau\to 0}{=} \left| -\frac{c_2+d_2}{a_2d_2-b_2c_2}\ \langle\psi_3^{(1)}|\psi_0^{(2)}\rangle + \frac{a_2+b_2}{a_2d_2-b_2c_2}\ \langle\psi_3^{(1)}|\psi_3^{(2)}\rangle \right|^2 \\
&= \left| -\frac{c_2+d_2}{a_2d_2-b_2c_2}(a_2c_1+b_2d_1) + \frac{a_2+b_2}{a_2d_2-b_2c_2}(c_1c_2+b_1b_2) \right|^2 \\
&= \frac{(B_1+K_1-\gamma J)^2}{4K_1(B_1+K_1)}, \\
\xi &\overset{\tau\to 0}{=} |\langle\psi_0^{(2)}|\psi_3^{(1)}\rangle|^2 \\
&= \left| \frac{1}{2}(a_2c_1+b_2d_1) \right|^2 = -\frac{\gamma^2J^2+(B_1+K_1)(B_2-K_2)}{4K_1K_2(B_2-B_1)(B_1+K_1)}\ .
\end{aligned} \tag{4.25}$$

Also from the **Eq. 4.19**, we get

$$\chi = \frac{(B_2-K_2)(B_2+K_2-\gamma J)^2}{4\gamma J^2K_2}\ . \tag{4.26}$$

Using (4.25) and (4.26) in the expressions of work (**Eq. 4.20**) and heat absorption (**Eq. 4.21**), we obtain the sudden limits of work and heat absorption which are given by

$$\begin{aligned}
W_s &= -4\frac{B_1(B_2-B_1)}{K_1}\frac{\sinh 2K_1\beta}{Z}, \\
Q_{Ms} &= 4\frac{B_1B_2}{K_1}\frac{\sinh 2K_1\beta}{Z}\ .
\end{aligned} \tag{4.27}$$

Therefore, the efficiency at this limit is given by

$$\eta_s = \frac{|W_s|}{Q_{Ms}} = 1-\frac{B_1}{B_2}. \tag{4.28}$$

Interestingly, the efficiency does not depend on the anisotropy parameter in the sudden limit. This means that the QOE has the same efficiency for all γ when $\tau \to 0$. This can be seen in the **Fig. 4.2** that for our choices of $B_1 = 1$ and $B_2 = 2$, this is equal to 0.5, irrespective of the values of γ, whereas for large τ, the efficiency saturates to a lower value. Therefore, with two spins coupled by anisotropic interaction as the working system, a measurement-based QHE operating in the sudden limit performs better than an engine operating in the adiabatic limit.

4.3.4 Analysis of the heat engine performance

For the quasistatic operation of the cycle, we show the variation of the efficiency as a function of work in the **Fig. 4.5**. It is clear from this plot that the engine performance degrades with the increase of the anisotropy parameter γ. This is because, as γ increases, the heat absorption in the measurement process increases and the work output decreases after a slow increase in the lower range of γ. We also observed that there exists a certain value of $\gamma \sim 0.46$, for which the work output gets maximized.

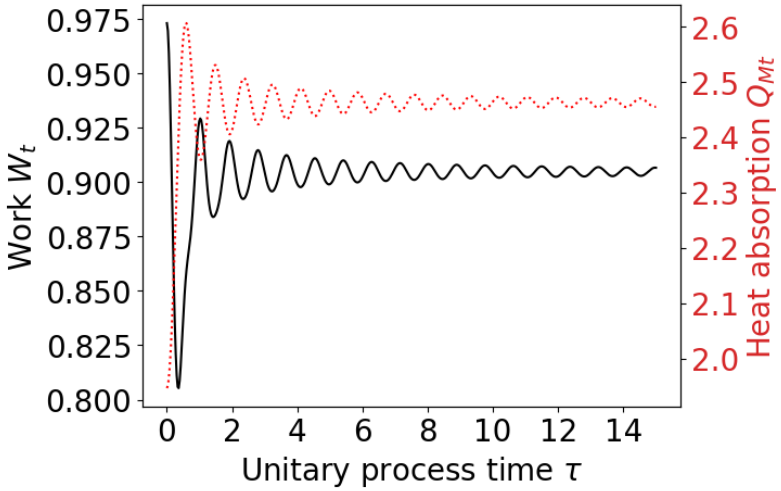

Figure 4.4: Variation of the absolute value of the work done W_t (solid black line, labelled on the left y-axis) and heat absorbed Q_{Mt} (point-marked red line, labelled on the right y-axis) as a function of duration τ of the unitary stage. The other parameters are $B_1 = 1$, $B_2 = 2$, $T = 1$, and $\gamma = 1$.

The variation of the work and heat absorption with respect to the duration τ of the unitary processes are shown in the **Fig. 4.4**. Also, the plots of the efficiency with respect to work are shown in the **Fig. 4.5**. From these plots, we can see that a finite-time engine can deliver more work than the same engine operating in the quasistatic limit with a proper choice of the time interval τ of the unitary processes. In addition to that, the finite-time engine absorbs less amount of heat in the measurement process than the same engine operating in the quasistatic limit. Consequently, when operated for finite times, the engine requires less energy resource, and still can perform better than its quasistatic counterpart.

Interestingly, this outperforming is further improved for larger anisotropy parameter γ. When $\gamma = 0$, no transition takes place between two instantaneous energy eigenstates, and the unitary stages remain adiabatic, irrespective of their duration. Also, there is no interference-like effect between two transition probability amplitudes as for the anisotropic case, which can be seen below.

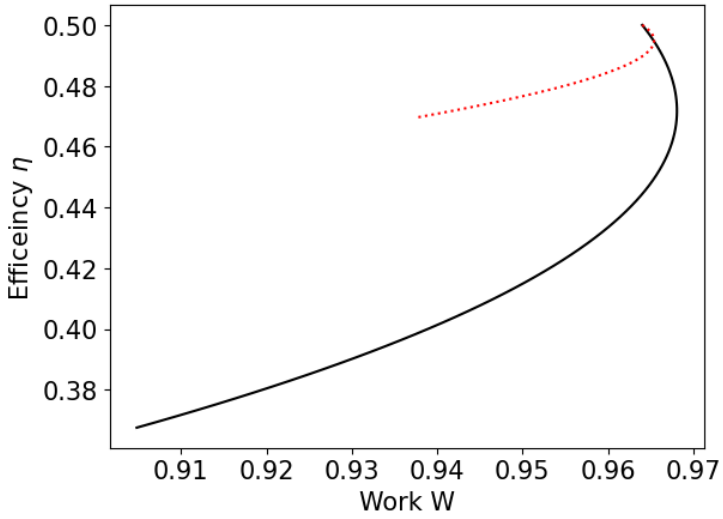

Figure 4.5: The parametric plot of the variable γ on the work-efficiency plane. We have taken the absolute value of the work. Here the point-marked red line represents the finite-time value (for $\tau = 0.1$) and the solid black line represents the quasistatic value. The anisotropy parameter γ varies from 0 to 1. The point 0.5 on the solid black line corresponds to $\gamma = 0$, while the left end of the plot corresponds to $\gamma = 1$. The other parameters are $B_1 = 1$, $B_2 = 2$, and $T = 1$.

In the limit of $\gamma \to 0$, the eigenstates and corresponding eigenvectors of the Hamiltonian $\hat{H}(t)$ take the following forms:

$$\begin{aligned} |\psi_0\rangle &= |00\rangle\,, & E_0 &= -2B \\ |\psi_1\rangle &= \tfrac{1}{\sqrt{2}}(-|10\rangle + |01\rangle), & E_1 &= -2J \\ |\psi_2\rangle &= \tfrac{1}{\sqrt{2}}(|10\rangle + |01\rangle), & E_2 &= 2J \\ |\psi_3\rangle &= |11\rangle\,, & E_3 &= 2B. \end{aligned} \tag{4.29}$$

Clearly, the states $|\psi_{0,3}\rangle$ are no longer entangled, though they differ from the Bell states $|\psi_\pm\rangle$. Also in this limit, it can be shown using the above eigenstates, that the transition probabilities as mentioned in the **Sec. 4.3.1**, are reduced to $\delta = \lambda = \chi = 1/2$ and $\xi = 0$, where we used: $\langle\psi_0^{(2)}|\hat{U}(\tau)|\psi_3^{(1)}\rangle = \langle\psi_3^{(2)}|\hat{U}(\tau)|\psi_0^{(1)}\rangle = \langle\psi_0^{(1)}|\hat{V}(\tau)|\psi_3^{(2)}\rangle = \langle\psi_3^{(1)}|\hat{V}(\tau)|\psi_0^{(2)}\rangle = 0$, and $\langle\psi_0^{(2)}|\hat{U}(\tau)|\psi_0^{(1)}\rangle = \langle\psi_3^{(1)}|\hat{V}(\tau)|\psi_3^{(2)}\rangle = 1$. Therefore, for the isotropic case, the efficiency becomes $\eta = 1 - B_1/B_2$, which does not depend on τ. Thus, the efficiency does not change with respect to τ, as displayed in the **Fig. 4.2**. Therefore, operating the engine even for a finite time would lead to the same efficiency as for the case when operated quasistatically.

4.4 Always-on coupling to the heat bath

It may not always be possible to decouple a quantum system from its bath, which acts as a heat bath for the HE operation, depending upon the architecture of the working system and the bath. Also, there is a cost associated with coupling and decoupling the working system from a heat bath [55, 266]. In the previous section, we assumed that the working system is completely isolated from its bath during the work-delivering stages, so that the stages AB and CD remain unitary. We consider here that the HE operation is implemented in a type of realistic architecture in which the working system cannot be decoupled from its bath [266]. It is therefore necessary to take into account the dissipation of energy from the working system to the bath during the stages AB and CD. The schematic diagram of the Otto cycle for always-on bath interaction is shown in **Fig. 4.6**. This requires solving the master equation, which is given below, with a time-dependent Hamiltonian under a dissipative bath. Here, we assume that the remaining two isochoric stages of the cycle are identical to those mentioned in the **Sec. 4.2.1**. Furthermore, since the measurement process is assumed to be instantaneous, the bath will not have any effect on the system during measurement.

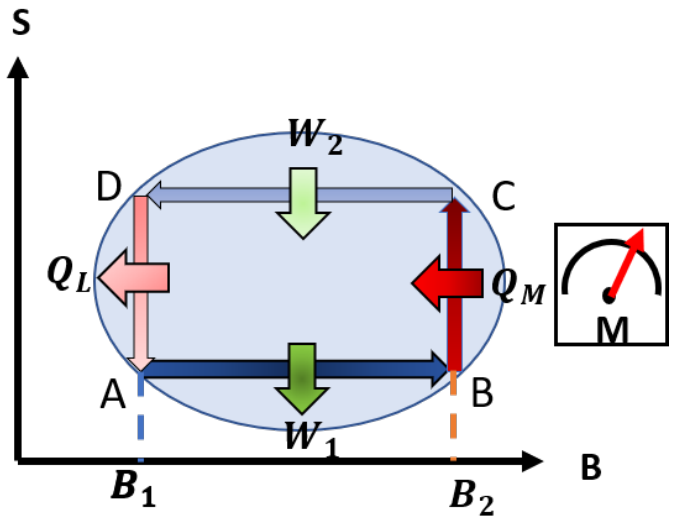

Figure 4.6: Schematic diagram of a quantum Otto cycle with quantum measurements for always-on bath interaction case.

We consider that the temperature of the heat bath is T and a single spin decays to the bath. Then the master equation in the interaction picture for two spins can

therefore be written as [82]

$$\begin{aligned}\frac{\partial\hat{\rho}}{\partial t} =&\iota[\hat{\rho},\hat{H}]+\sum_{i=1,2}[\Gamma_i(t)\{n(\omega_i(t))+1\}(\hat{X}_i\hat{\rho}\hat{X}_i^\dagger-\frac{1}{2}\hat{X}_i^\dagger\hat{X}_i\hat{\rho}-\frac{1}{2}\hat{\rho}\hat{X}_i^\dagger\hat{X}_i).\\ &.+\ \Gamma_i(t)n(\omega_i(t))(\hat{X}_i^\dagger\hat{\rho}\hat{X}_i-\frac{1}{2}\hat{X}_i\hat{X}_i^\dagger\hat{\rho}-\frac{1}{2}\hat{\rho}\hat{X}_i\hat{X}_i^\dagger)]\ ,\end{aligned} \tag{4.30}$$

where $\Gamma_i(t) = 0.1\omega_i^\alpha(t)e^{-\omega_i(t)/\omega_c}$ is a time-dependent dissipation rate at $T = 0$, $n(\omega_i(t)) = [\exp\left(\frac{\hbar\omega_i(t)}{kT}\right) - 1]^{-1}$ is the average number of photons in the bath at the transition frequencies $\omega_i(t)$, and ω_c is the cut-off frequency of the bath spectral density. Here $\alpha = 1$ corresponds to the Ohmic bath spectrum. We have chosen $\alpha = 0.5$ (< 1) for the sub-Ohmic spectrum and $\alpha = 2$ (> 1) for the super-Ohmic spectrum [267, 268], These rates are time-dependent because of the time-dependence of the Hamiltonian $\hat{H}(t)$ [267, 269]. Note that we are assuming that the **Eq. 4.30** remains valid for the time scales involved with the system and the bath dynamics. This is possible if the bath time scale $1/\omega_c$ is much smaller than the system timescale $1/\min_j(E_j)$ [where E_j is given by **Eq. 4.1**] and the duration τ during which the magnetic field is changed [267].

The jump operators are given in **Sec. 1.3.5**. Note that K and $|\psi_{0,3}\rangle$ are functions of $B(t)$, and are therefore time-dependent, which also gives rise to the time dependence of the jump operators in **Eq. 1.35**. Such a time dependence of the jump operators and the bath spectrum makes the evolution of the system non-Markovian. The heat and work in an open quantum system in the presence of an external drive are defined by **Eq. 1.15** [266]. The total change in the average energy of the system in a process is given by $\Delta E(t) = E(t) - E(0)$, where $E(t) = \mathrm{Tr}[\hat{\rho}(t)\hat{H}(t)]$ is the average energy at a time t. As the bath is connected with the system during the driving stage, the change in energy of the system contains both the heat and the work:

$$\Delta E(t) = W(t) + Q(t). \tag{4.31}$$

During the stages $A \to B$ and $C \to D$, the working system remains coupled with the heat bath, therefore, the work during these stages can be calculated as

$$\begin{aligned}W_1(\tau) &= \int_0^\tau \mathrm{Tr}[\hat{\rho}_{A\to B}(t')\dot{\hat{H}}_{A\to B}(t')]dt'\\ W_2(\tau) &= \int_0^\tau \mathrm{Tr}[\hat{\rho}_{C\to D}(t')\dot{\hat{H}}_{C\to D}(t')]dt'.\end{aligned} \tag{4.32}$$

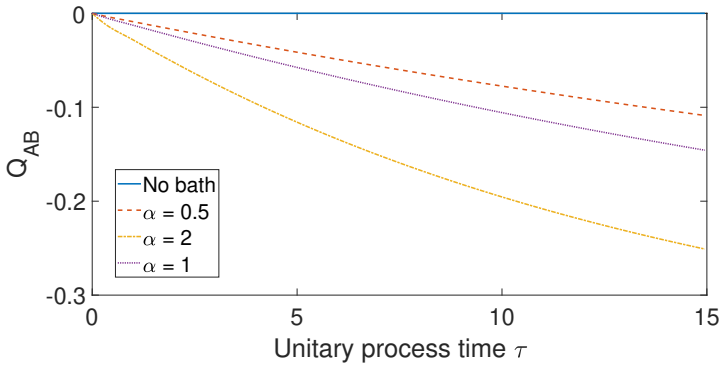

Figure 4.7: Heat transfer (Q_{AB}) as a function of duration τ of the unitary stages for $\Gamma_i(t) = 0$ (for the isolated system: solid blue line) $\alpha = 0.5$ (sub-Ohmic: dashed maroon line), $\alpha = 1$ (Ohmic: dotted purple line), and $\alpha = 2$ (super-Ohmic: dash - dotted yellow line). . The other parameters are $B_1 = 1$, $B_2 = 2$, $T = 1$, $\omega_c = 1000$, and $\gamma = 1$.

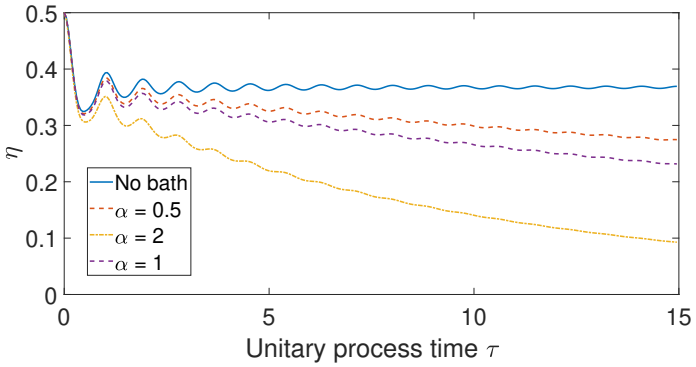

Figure 4.8: Efficiency (η) as a function of duration τ of the unitary stages for $\Gamma_i(t) = 0$ (for the isolated system: solid blue line), $\alpha = 0.5$ (sub-Ohmic: dashed maroon line), $\alpha = 1$ (Ohmic: dotted purple line), and $\alpha = 2$ (super-Ohmic: dash - dotted yellow line). The other parameters are $B_1 = 1$, $B_2 = 2$, $T = 1$, $\omega_c = 1000$, and $\gamma = 1$.

Similarly, the heat transferred can be calculated as

$$\begin{aligned} Q_{AB}(\tau) &= \int_0^\tau \mathrm{Tr}\left[\dot{\hat{\rho}}_{A\to B}\left(t'\right)\hat{H}_{A\to B}\left(t'\right)\right]dt' \\ Q_{CD}(\tau) &= \int_0^\tau \mathrm{Tr}\left[\dot{\hat{\rho}}_{C\to D}\left(t'\right)\hat{H}_{C\to D}\left(t'\right)\right]dt'. \end{aligned} \tag{4.33}$$

Also, we can calculate the heat in the driving process by using $Q(t) = \Delta E(t) - W(t)$ (**Eq. 4.31**) if we know the change in internal energy $\Delta E(t)$ and work $W(t)$ in these processes. The heat transfer in the driving process $A \to B$ is shown in **Fig. 4.7**. Also, the heat transfer Q_{CD} in the driving process $C \to D$ can be calculated in a similar way.

So, the total work is given by $W = W_1 + W_2$. We calculated the heat transfer

between the system and the heat bath using the **Eq. 4.31**. The numerical solution of the master equation has been done using the 4th-order adaptive Runge-Kutta method and the numerical integration to calculate the work is done using the Trapezoidal rule. The heat absorption in the measurement process is calculated as discussed in the **Sec. 4.2.1**.

We show in the **Fig. 4.8** how the efficiency varies with the duration τ of the unitary stages, for different values of α. It is clear from this plot that the presence of the bath has a negligible effect on its performance in a very short time. We can, therefore, employ such a measurement-based heat engine model whenever one requires a finite amount of power. One does not have to decouple the working system ever to obtain a finite amount of power, if the engine runs for a finite duration. However, the longer the duration τ, the engine efficiency decreases, due to the dominant effects of the bath over the external control parameter. The dissipative part of the master equation dominates over the unitary part and therefore, the system releases more energy to the bath as heat than it releases as the work. Also, the spins absorb more energy during the measurement stage as τ increases. We must emphasize that if both the spins are considered to individually interact with the heat bath [270, 271], the main results will remain the same. Further the efficiency deteriorates as α increases. This is because, with larger α, the spins decay faster, and delivers less work in finite τ.

In this section, we have considered the QOE with an always-on single bath along with a measurement protocol. On the other hand, it is possible for a QOE that operates with two heat baths to maintain such an always-on coupling, while still achieving a reciprocating cycle by periodically changing the interaction strength with the baths. However, as the performance of these QOEs deteriorates in a short time, such an always-on interaction cannot give us operational advantages over a measurement-based engine.

4.4.1 Power analysis of the engine

The isochoric cooling process of the system with a thermal bath is not an instantaneous process, and ideally takes infinite time. To make a power analysis, we assume that the state of the system becomes very close to a thermal state ρ_A at a finite time t_c. In order to make an estimate of this closeness we have calculated the trace distance between two states $\hat{\rho}$ and $\hat{\rho}_A$, defined as $D(\hat{\rho}, \hat{\rho}_A) = \frac{1}{2}\,\mathrm{Tr}\,|\hat{\rho} - \hat{\rho}_A|$ [74], where the state $\hat{\rho}$ is obtained by solving by the master equation (**Eq. 4.30**), with time-independent dissipation rate coefficients, as the magnetic field is kept constant at $B = B_1$ during this cooling process. Also, as defined in **Sec. 4.2.1**, ρ_A represents

the thermal state at a temperature T (that of the cold bath) when the magnetic field is maintained at $B = B_1$ (also see **Fig. 4.1**). We estimated t_c, as a time when the trace distance $D(\hat{\rho}, \hat{\rho_A})$ becomes $\sim 10^{-2}$. Such a finite-time analysis of the cooling process helps us in defining the power of the engine as $P = W/(2\tau + t_c)$, where τ is the duration of each unitary stage, and we have assumed that the measurement is an instantaneous process. The plot of the power as a function of the anisotropy is shown in **Fig. 4.9**.

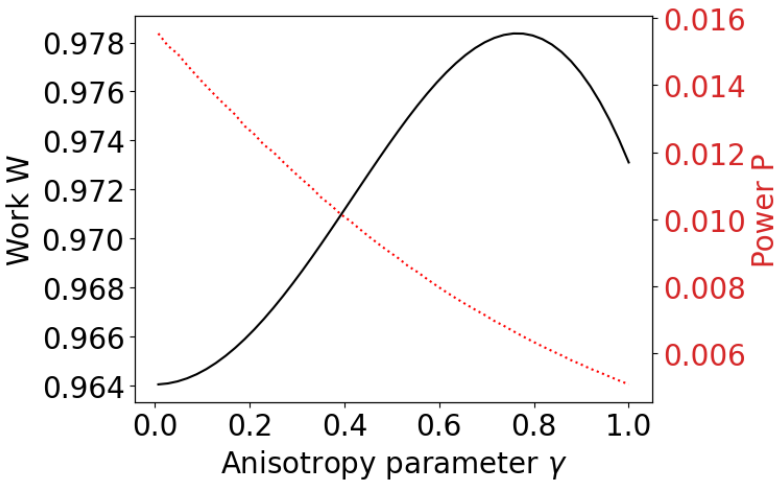

Figure 4.9: Variation of the absolute value of work (black solid line, labelled on the left y-axis) and power (point-marked red line, labelled on the right y-axis) as a function of anisotropy parameter γ in the limit of $\tau \to 0$. A moderate thermalization time ranges from 61 to 191 for anisotropy $0 \leq \gamma \leq 1$ when the trace distance $D(\hat{\rho}, \hat{\rho}_A) \sim 10^{-2}$. The other parameters are $B_1 = 1$, $B_2 = 2$, $T = 1$.

We found that in the limit of $\tau \to 0$, the work does not change substantially with respect to γ, as compared to the quasistatic limit, which is discussed in the **Sec. 4.3.4**. However, the thermalization time increases with the increase in anisotropy, leading to a reduction of power. Further, if we consider that both spins interact with the bath, thermalization of the system during the isochoric cooling process can be achieved at a much faster pace, and hence more power would be generated by the engine.

4.5 Similarity between a measurement-based QOE and a local spin QOE

In Chapter 2, we have seen that the transition probability $\xi_\tau = |\langle\psi_0^{(2)}|\hat{U}(\tau)|\psi_3^{(1)}\rangle|^2 = |\langle\psi_3^{(2)}|\hat{U}(\tau)|\psi_0^{(1)}\rangle|^2 = |\langle\psi_3^{(1)}|\hat{V}(\tau)|\psi_0^{(2)}\rangle|^2 = |\langle\psi_0^{(1)}|\hat{V}(\tau)|\psi_3^{(2)}\rangle|^2$ between the energy eigenstates is non-zero in finite time, therefore responsible for the decrease in performance of a heat engine.

In Chapters 2 and 3, we have seen the transition probabilities or non-zero overlap $\lambda_\tau = |\langle 00|\hat{U}(\tau)|\psi_3^{(1)}\rangle|^2 = |\langle 11|\hat{U}(\tau)|\psi_0^{(1)}\rangle|^2$, and $\delta_\tau = |\langle 11|\hat{V}(\tau)|\psi_0^{(2)}\rangle|^2 = |\langle 00|\hat{V}(\tau)|\psi_3^{(2)}\rangle|^2$ between the instantaneous energy eigenstates and the bare basis states of the system, and the transition probability or non-zero overlap $\delta = |\langle\psi_+|\hat{U}(\tau)|\psi_0^{(1)}\rangle|^2$, $\lambda = |\langle\psi_3^{(1)}|\hat{V}(\tau)|\psi_-\rangle|^2$ between the energy eigenstates and measurement basis states oscillate with respect to time, therefore can give better performance in finite times.

It will be worth mentioning if we are able to construct a QHE model with a transition probability between the energy eigenstates and bare basis states of the working system, then we may see an oscillation in the transition probability in finite times. This oscillation allows us to improve the performance of QHEs in finite times than the quasistatic limit. Also, this will be independent of the type of QHE model. The prescribed type of transition probabilities here are obtained from the perspective of non-selective measurements protocol and also from a heat engine with a local working system. Therefore, we can say that the QOE with a local working system can function like a measurement-based engine for the finite-time operation of both of them.

4.6 Summary

We have studied the performance of a measurement-based QOE in a two-spin working system coupled by the Heisenberg anisotropic XY interaction. A non-selective quantum measurement is used to fuel the engine. The non-commuting nature of the Hamiltonian at two different times initiates transitions between the instantaneous energy eigenstates at finite time unitary processes. Furthermore, the instantaneous energy eigenstates do not coincide with the measurement basis states which causes some transition between them. The relevant thermodynamic quantities are calculated in terms of these transition probabilities. We found that the efficiency oscillates largely at short times when the two-spin system is coupled by an anisotropic interaction, while for isotropic interaction there is no oscillation. This oscillation in efficiency is explained in terms of interference between different transition probabilities at finite times. It is observed that the oscillation in efficiency dies out as the unitary processes extend for a longer time and eventually the efficiency approaches the quasistatic limit. Thus, proper control of the duration of unitary processes during transient times can lead to higher work output and less heat absorption. As a result, a finite-time engine can be more efficient than a quasi-static engine. The efficiency further increases with increasing anisotropy while in the quasistatic limit, it is observed that the performance deteriorates with

an increase in anisotropy.

Also, we studied the performance of the HE under the condition of always-on coupling to the heat bath. We found that the presence of the bath has a negligible effect on its performance in a very short time limit. However, for a longer duration of the stages AB and CD, its performance degrades. This is primarily due to the dominance of the bath interaction over external control during these stages.

Chapter 5

Discussions - Conclusions and Future directions

In conclusion, we explored the behaviour of QTMs, particularly the heat engines and refrigerators, in coupled spin systems. We have primarily studied thermal machines based on Stirling and Otto cycles. We have shown that by suitably choosing the system and cycle parameters, one can make the cycle work as a heat engine or a refrigerator. We have shown that the quantum Stirling heat engine and the refrigerator can function at the Carnot limit of efficiency and COP, respectively, at the quantum critical point at low temperatures of the baths.

The role of anisotropy in the interaction between the spins is investigated. We found that the quasistatic efficiency increases with the anisotropy for the operation of the quantum Otto engine (QOE) with two heat baths. However, for a measurement-based model, it decreases. For the finite-time operation of the engines, on the other hand, the efficiencies of a local-spin Otto engine and a measurement-based one oscillate with respect to the duration of the unitary stages. Therefore, by selecting this duration suitably, the performance of the engine can be enhanced more than that of an engine operating in the quasistatic limit. This behaviour is contrary to the standard Otto engine, which operates between two heat baths, where efficiency decreases with the duration of the unitary stages. We demonstrated that the oscillation originates from the interference effect between two probability amplitudes. We also find that in the case of always-on bath interaction, the bath has a negligible effect on the performance of a measurement-based QOE in finite-time operation, which gives it an operational advantage over a standard QOE which operates between two heat baths.

Our studies show that the coupling between the spin can play various important roles in the operation and the performance of QTMs. These are summarized as follows: A quantum thermodynamic cycle can be operated in various QTMs (heat engine or refrigerator) depending on the value of the coupling constant. A coupling between the spins leads to a quantum phase transition which in turn causes a better performance of QTMs. A single-spin QOE can break the standard quantum

Otto limit of efficiency when the spin is coupled with another auxiliary spin by an anisotropic interaction. Also, the anisotropic nature of the coupling between the spin played an important role in the finite-time performance of QTMs. An oscillation in the efficiency was found due to the anisotropic nature of the coupling which can also provide better efficiency at finite times. In our studies, we found how and in what parameter regimes we can get better performance from QTMs. The effect of anisotropic interaction, measurement-based heating protocols, and the quantum phase transitions, are the key issues that are addressed in this thesis.

Future directions: In recent years, quantum stochastic thermodynamics has gained interest, where the quantum version of work statistics, fluctuation theorems etc. are being studied [32]. Thermodynamic variables become random (stochastic) at the microscopic level owing to the presence of non-negligible thermal fluctuations and additional quantum fluctuations at low enough temperatures. A central question is then to determine their probability distributions (statistics) to assess their stochastic properties.

In future work, we want to study the work fluctuation (work statistics) [263] in our measurement-based finite time QOE model as mentioned in Chapter 3. The main interesting point is that, in our model, there remains quantum coherence in the energy eigenbasis when $\gamma \neq 0$. But, when $\gamma = 0$, there is no coherence in the energy eigenbasis. Our main goal is to show how coherence plays a role in work statistics [272]. We are also interested in seeing how the work statistics of a measurement-based QOE differs from a QOE that operates between two heat baths [263]. We will also explore the fundamental difference between two strategies of fueling a quantum heat engine: a heat bath vs the non-selective quantum measurement.

Also, a many-body Tavis Cummings model represents the interaction of a single-mode field with N number of two-level systems [273, 274]. This model shows a QPT at a critical coupling constant value. We want to study QHE operation with this model as a working system. We will investigate how the many-body working system plays a role and also what is the impact of the QPT on the QHE behaviour.

In recent years, simulations of QHE on quantum computers have gained attention because they provide a kind of experimental verification of the QHE models [142, 144, 275]. We want to simulate QHE operation on a quantum computer. We will consider our measurement-based QOE model where non-selective measurements are used for the isochoric heating process [147]. The isochoric cooling process is based on the concept that selective measurement leads the system to its ground state, which causes it to cool rapidly [223]. In this model, we don't require any heat bath

for the operation of the engine. So, this will help us to simulate the heat engine on a quantum computer.

References

[1] MARON FREITAS ANKA. Analysis of a Measurement-based Quantum Otto Cycle With a Single-bath. PhD thesis, Fluminense Federal University, 2020.

[2] Andrew Rex. Maxwell's demon—a historical review. Entropy, 19(6):240, 2017.

[3] Mark Waldo Zemansky and Richard Dittman. Heat and thermodynamics: an intermediate textbook. McGraw-Hill, 1968.

[4] Herbert B Callen. Thermodynamics and an Introduction to Thermostatistics. John wiley & sons, 1991.

[5] Dilip Kondepudi and Ilya Prigogine. Modern thermodynamics: from heat engines to dissipative structures. John Wiley & Sons, 2014.

[6] Sanjeev Chandra. Energy, Entropy and Engines: An Introduction to Thermodynamics. John Wiley & Sons, 2016.

[7] Walter Greiner, Ludwig Neise, and Horst Stöcker. Thermodynamics and statistical mechanics. Springer Science & Business Media, 2012.

[8] Andrea Solfanelli, Marco Falsetti, and Michele Campisi. Nonadiabatic single-qubit quantum otto engine. Physical Review B, 101(5):054513, 2020.

[9] Clebson Cruz, Hamid-Reza Rastegar-Sedehi, Maron F Anka, Thiago R de Oliveira, and Mario Reis. Quantum stirling engine based on dinuclear metal complexes. Quantum Science and Technology, 8(3):035010, 2023.

[10] Luca Peliti and Simone Pigolotti. Stochastic Thermodynamics: An Introduction. Princeton University Press, 2021.

[11] James Millen and André Xuereb. Perspective on quantum thermodynamics. New Journal of Physics, 18(1):011002, 2016.

[12] James Clerk Maxwell and Peter Pesic. Theory of heat. Courier Corporation, 2001.

[13] Harvey Leff and Andrew F Rex. Maxwell's Demon 2 Entropy, Classical and Quantum Information, Computing. CRC Press, 2002.

[14] Koji Maruyama, Franco Nori, and Vlatko Vedral. Colloquium: The physics of maxwell's demon and information. Reviews of Modern Physics, 81(1):1, 2009.

[15] Gonzalo Manzano Paule. Thermodynamics and Synchronization in Open Quantum Systems. Springer, 2018.

[16] Leo Szilard. Über die entropieverminderung in einem thermodynamischen system bei eingriffen intelligenter wesen. Zeitschrift für Physik, 53(11-12): 840–856, 1929.

[17] Leon Brillouin. The negentropy principle of information. Journal of Applied Physics, 24(9):1152–1163, 1953.

[18] Charles H Bennett. The thermodynamics of computation—a review. International Journal of Theoretical Physics, 21:905–940, 1982.

[19] Charles H Bennett. Demons, engines and the second law. Scientific American, 257(5):108–117, 1987.

[20] Rolf Landauer. Irreversibility and heat generation in the computing process. IBM journal of research and development, 44(1/2):261, 2000.

[21] Felix Binder, Luis A Correa, Christian Gogolin, Janet Anders, and Gerardo Adesso. Thermodynamics in the quantum regime. Fundamental Theories of Physics, 195:1–2, 2018.

[22] Patrick P Potts. Introduction to quantum thermodynamics (lecture notes). arXiv preprint arXiv:1906.07439, 2019.

[23] Mark T Mitchison. Quantum thermal absorption machines: refrigerators, engines and clocks. Contemporary Physics, 60(2):164–187, 2019.

[24] Sai Vinjanampathy and Janet Anders. Quantum thermodynamics. Contemporary Physics, 57(4):545–579, 2016.

[25] ASLI TUNCER ÖZDEMİR and ÖZGÜR ESAT MÜSTECAPLIOĞLU. Quantum thermodynamics and quantum coherence engines. Turkish Journal of Physics, 44(5):404–436, 2020.

[26] Manabendra N Bera, Arnau Riera, Maciej Lewenstein, and Andreas Winter. Generalized laws of thermodynamics in the presence of correlations. Nature Communications, 8(1):2180, 2017.

[27] Yohei Morikuni. Quantum Thermodynamics with Measurement Processes. PhD thesis, University of Tokyo, 2019.

[28] Mikio Nakahara. Lectures on quantum computing, thermodynamics and statistical physics, volume 8. World Scientific, 2013.

[29] Ken Funo, Masahito Ueda, and Takahiro Sagawa. Quantum fluctuation theorems. Thermodynamics in the Quantum Regime: Fundamental Aspects and New Directions, pages 249–273, 2018.

[30] Michael A Nielsen and Isaac Chuang. Quantum computation and quantum information, 2002.

[31] Emmanuel Desurvire. Classical and quantum information theory: an introduction for the telecom scientist. Cambridge university press, 2009.

[32] Massimiliano Esposito, Upendra Harbola, and Shaul Mukamel. Nonequilibrium fluctuations, fluctuation theorems, and counting statistics in quantum systems. Reviews of Modern Physics, 81(4):1665, 2009.

[33] H-H Hasegawa, J Ishikawa, K Takara, and DJ Driebe. Generalization of the second law for a nonequilibrium initial state. Physics Letters A, 374(8): 1001–1004, 2010.

[34] Massimiliano Esposito and Christian Van den Broeck. Second law and landauer principle far from equilibrium. Europhysics Letters, 95(4):40004, 2011.

[35] Sebastian Deffner and Eric Lutz. Information free energy for nonequilibrium states. arXiv preprint arXiv:1201.3888, 2012.

[36] Juan MR Parrondo, Jordan M Horowitz, and Takahiro Sagawa. Thermodynamics of information. Nature physics, 11(2):131–139, 2015.

[37] Herbert B Callen. Thermodynamics and an Introduction to Thermostatistics. American Association of Physics Teachers, 1998.

[38] Walther Nernst. The New Heat Theorem: Its foundations in theory and experiment. Methuen & Company Limited, 1926.

[39] Ronnie Kosloff. Quantum thermodynamics: A dynamical viewpoint. Entropy, 15(6):2100–2128, 2013.

[40] Lluís Masanes and Jonathan Oppenheim. A general derivation and quantification of the third law of thermodynamics. Nature Communications, 8(1):1–7, 2017.

[41] Harvey S Leff. Proof of the third law of thermodynamics for ising ferromagnets. Physical Review A, 2(6):2368, 1970.

[42] Michael Aizenman and Elliott H Lieb. The third law of thermodynamics and the degeneracy of the ground state for lattice systems. Statistical Mechanics: Selecta of Elliott H. Lieb, pages 333–351, 2004.

[43] Yair Rezek, Peter Salamon, Karl Heinz Hoffmann, and Ronnie Kosloff. The quantum refrigerator: The quest for absolute zero. Europhysics Letters, 85 (3):30008, 2009.

[44] Armen E Allahverdyan, Karen Hovhannisyan, and Guenter Mahler. Optimal refrigerator. Physical Review E, 81(5):051129, 2010.

[45] Ronnie Kosloff, Eitan Geva, and Jeffrey M Gordon. Quantum refrigerators in quest of the absolute zero. Journal of Applied Physics, 87(11):8093–8097, 2000.

[46] Amikam Levy, Robert Alicki, and Ronnie Kosloff. Quantum refrigerators and the third law of thermodynamics. Physical Review E, 85(6):061126, 2012.

[47] Amikam Levy and Ronnie Kosloff. Quantum absorption refrigerator. Physical Review Letters, 108(7):070604, 2012.

[48] Armen E Allahverdyan, Karen V Hovhannisyan, Dominik Janzing, and Guenter Mahler. Thermodynamic limits of dynamic cooling. Physical Review E, 84(4):041109, 2011.

[49] Lian-Ao Wu, Dvira Segal, and Paul Brumer. No-go theorem for ground state cooling given initial system-thermal bath factorization. Scientific Reports, 3 (1):1824, 2013.

[50] Carlo Di Franco and Mauro Paternostro. A no-go result on the purification of quantum states. Scientific Reports, 3(1):1387, 2013.

[51] Francesco Ticozzi and Lorenza Viola. Quantum resources for purification and cooling: fundamental limits and opportunities. Scientific Reports, 4(1):1–7, 2014.

[52] David Reeb and Michael M Wolf. An improved landauer principle with finite-size corrections. New Journal of Physics, 16(10):103011, 2014.

[53] Hai-Tao Quan, Yu-xi Liu, Chang-Pu Sun, and Franco Nori. Quantum thermodynamic cycles and quantum heat engines. Physical Review E, 76 (3):031105, 2007.

[54] Sai Vinjanampathy and Janet Anders. Quantum thermodynamics. Contemporary Physics, 57(4):545–579, 2016.

[55] Sourav Bhattacharjee and Amit Dutta. Quantum thermal machines and batteries. The European Physical Journal B, 94:1–42, 2021.

[56] Robert Alicki and Ronnie Kosloff. Introduction to quantum thermodynamics: History and prospects. Springer, 2018.

[57] Loris Maria Cangemi, Chitrak Bhadra, and Amikam Levy. Quantum engines and refrigerators. arXiv preprint arXiv:2302.00726, 2023.

[58] Henry ED Scovil and Erich O Schulz-DuBois. Three-level masers as heat engines. Physical Review Letters, 2(6):262, 1959.

[59] JE Geusic, EO Schulz-Du Bois, RW De Grasse, and HED Scovil. Three level spin refrigeration and maser action at 1500 mc/sec. Journal of Applied Physics, 30(7):1113–1114, 1959.

[60] Robert Alicki. The quantum open system as a model of the heat engine. Journal of Physics A: Mathematical and General, 12(5):L103, 1979.

[61] Ronnie Kosloff. A quantum mechanical open system as a model of a heat engine. The Journal of Chemical Physics, 80(4):1625–1631, 1984.

[62] Nathan M Myers, Obinna Abah, and Sebastian Deffner. Quantum thermodynamic devices: From theoretical proposals to experimental reality. AVS Quantum Science, 4(2):027101, 2022.

[63] Victor Mukherjee and Uma Divakaran. Many-body quantum thermal machines. Journal of Physics: Condensed Matter, 33(45):454001, 2021.

[64] Antonio Acín, Immanuel Bloch, Harry Buhrman, Tommaso Calarco, Christopher Eichler, Jens Eisert, Daniel Esteve, Nicolas Gisin, Steffen J Glaser, Fedor Jelezko, et al. The quantum technologies roadmap: a european community view. New Journal of Physics, 20(8):080201, 2018.

[65] Hideaki Okane, Shunsuke Kamimura, Shingo Kukita, Yasushi Kondo, and Yuichiro Matsuzaki. Quantum thermodynamics applied for quantum refrigerators cooling down a qubit. arXiv preprint arXiv:2210.02681, 2022.

[66] Jonatan Bohr Brask, Géraldine Haack, Nicolas Brunner, and Marcus Huber. Autonomous quantum thermal machine for generating steady-state entanglement. New Journal of Physics, 17(11):113029, 2015.

[67] Patrick P Hofer, Jonatan Bohr Brask, Martí Perarnau-Llobet, and Nicolas Brunner. Quantum thermal machine as a thermometer. Physical Review Letters, 119(9):090603, 2017.

[68] Mohsen Izadyari, M Tahir Naseem, and Özgür E Müstecaplıouglu. Enantiomer detection via quantum otto cycle. arXiv preprint arXiv:2211.06888, 2022.

[69] Jeongrak Son, Peter Talkner, and Juzar Thingna. Charging quantum batteries via otto machines: Influence of monitoring. Physical Review A, 106(5):052202, 2022.

[70] Tobias Denzler and Eric Lutz. Efficiency fluctuations of a quantum heat engine. Physical Review Research, 2(3):032062, 2020.

[71] Roie Dann, Ronnie Kosloff, and Peter Salamon. Quantum finite-time thermodynamics: insight from a single qubit engine. Entropy, 22(11):1255, 2020.

[72] Yair Rezek and Ronnie Kosloff. Irreversible performance of a quantum harmonic heat engine. New Journal of Physics, 8(5):83, 2006.

[73] Sangyun Lee, Meesoon Ha, Jong-Min Park, and Hawoong Jeong. Finite-time quantum otto engine: Surpassing the quasistatic efficiency due to friction. Physical Review E, 101(2):022127, 2020.

[74] Patrice A Camati, Jonas FG Santos, and Roberto M Serra. Coherence effects in the performance of the quantum otto heat engine. Physical Review A, 99 (6):062103, 2019.

[75] Selçuk Çakmak, Ferdi Altintas, Azmi Gençten, and Özgür E Müstecaplıoğlu. Irreversible work and internal friction in a quantum otto cycle of a single arbitrary spin. The European Physical Journal D, 71(3):1–10, 2017.

[76] Deniz Türkpençe and Ferdi Altintas. Coupled quantum otto heat engine and refrigerator with inner friction. Quantum Information Processing, 18(8):1–16, 2019.

[77] Barış Çakmak and Özgür E Müstecaplıoğlu. Spin quantum heat engines with shortcuts to adiabaticity. Physical Review E, 99(3):032108, 2019.

[78] Francesco Plastina, Antonio Alecce, Tony JG Apollaro, Giovanni Falcone, Gianluca Francica, Fernando Galve, N Lo Gullo, and Roberta Zambrini. Irreversible work and inner friction in quantum thermodynamic processes. Physical Review Letters, 113(26):260601, 2014.

[79] Yair Rezek. Reflections on friction in quantum mechanics. Entropy, 12(8): 1885–1901, 2010.

[80] Yun-Hao Shi, Hai-Long Shi, Xiao-Hui Wang, Ming-Liang Hu, Si-Yuan Liu, Wen-Li Yang, and Heng Fan. Quantum coherence in a quantum heat engine. Journal of Physics A: Mathematical and Theoretical, 53(8):085301, 2020.

[81] Marlan O Scully, M Suhail Zubairy, Girish S Agarwal, and Herbert Walther. Extracting work from a single heat bath via vanishing quantum coherence. Science, 299(5608):862–864, 2003.

[82] XL Huang, Tao Wang, XX Yi, et al. Effects of reservoir squeezing on quantum systems and work extraction. Physical Review E, 86(5):051105, 2012.

[83] Johannes Roßnagel, Obinna Abah, Ferdinand Schmidt-Kaler, Kilian Singer, and Eric Lutz. Nanoscale heat engine beyond the carnot limit. Physical Review Letters, 112(3):030602, 2014.

[84] Jan Klaers, Stefan Faelt, Atac Imamoglu, and Emre Togan. Squeezed thermal reservoirs as a resource for a nanomechanical engine beyond the carnot limit. Physical Review X, 7(3):031044, 2017.

[85] Nicolas Brunner, Marcus Huber, Noah Linden, Sandu Popescu, Ralph Silva, and Paul Skrzypczyk. Entanglement enhances cooling in microscopic quantum refrigerators. Physical Review E, 89(3):032115, 2014.

[86] Jung Jun Park, Kang-Hwan Kim, Takahiro Sagawa, and Sang Wook Kim. Heat engine driven by purely quantum information. Physical Review Letters, 111(23):230402, 2013.

[87] Tharon Holdsworth and Ryoichi Kawai. Heat pump driven entirely by quantum correlation. Physical Review A, 106(6):062604, 2022.

[88] Martin Josefsson, Artis Svilans, Heiner Linke, and Martin Leijnse. Optimal power and efficiency of single quantum dot heat engines: Theory and experiment. Physical Review B, 99(23):235432, 2019.

[89] Francisco J Peña, D Zambrano, Oscar Negrete, Gabriele De Chiara, PA Orellana, and P Vargas. Quasistatic and quantum-adiabatic otto engine for a two-dimensional material: The case of a graphene quantum dot. Physical Review E, 101(1):012116, 2020.

[90] L Chotorlishvili, M Azimi, S Stagraczyński, Z Toklikishvili, M Schüler, and J Berakdar. Superadiabatic quantum heat engine with a multiferroic working medium. Physical Review E, 94(3):032116, 2016.

[91] Victor Mukherjee, Uma Divakaran, Adolfo del Campo, et al. Universal finite-time thermodynamics of many-body quantum machines from kibble-zurek scaling. Physical Review Research, 2(4):043247, 2020.

[92] Keye Zhang, Francesco Bariani, and Pierre Meystre. Quantum optomechanical heat engine. Physical Review Letters, 112(15):150602, 2014.

[93] Andreas Dechant, Nikolai Kiesel, and Eric Lutz. All-optical nanomechanical heat engine. Physical Review Letters, 114(18):183602, 2015.

[94] Cyril Elouard, Maxime Richard, and Alexia Auffèves. Reversible work extraction in a hybrid opto-mechanical system. New Journal of Physics, 17 (5):055018, 2015.

[95] Keye Zhang, Francesco Bariani, and Pierre Meystre. Theory of an optomechanical quantum heat engine. Physical Review A, 90(2):023819, 2014.

[96] David Gelbwaser-Klimovsky and Gershon Kurizki. Work extraction from heat-powered quantized optomechanical setups. Scientific Reports, 5(1):7809, 2015.

[97] Tien D Kieu. The second law, maxwell's demon, and work derivable from quantum heat engines. Physical Review Letters, 93(14):140403, 2004.

[98] Rui Wang, Jianhui Wang, Jizhou He, and Yongli Ma. Efficiency at maximum power of a heat engine working with a two-level atomic system. Physical Review E, 87(4):042119, 2013.

[99] Ferdi Altintas, Ali ÜC Hardal, and Özgür E Müstecaplıoğlu. Rabi model as a quantum coherent heat engine: From quantum biology to superconducting circuits. Physical Review A, 91(2):023816, 2015.

[100] G Alvarado Barrios, F Albarrán-Arriagada, FA Cárdenas-López, G Romero, and JC Retamal. Role of quantum correlations in light-matter quantum heat engines. Physical Review A, 96(5):052119, 2017.

[101] Jianhui Wang, Zhaoqi Wu, and Jizhou He. Quantum otto engine of a two-level atom with single-mode fields. Physical Review E, 85(4):041148, 2012.

[102] Ali ÜC Hardal and Özgür E Müstecaplıoğlu. Superradiant quantum heat engine. Scientific Reports, 5(1):12953, 2015.

[103] Qiao Song, Swati Singh, Keye Zhang, Weiping Zhang, and Pierre Meystre. One qubit and one photon: The simplest polaritonic heat engine. Physical Review A, 94(6):063852, 2016.

[104] G Marchegiani, P Virtanen, F Giazotto, and M Campisi. Self-oscillating josephson quantum heat engine. Physical Review Applied, 6(5):054014, 2016.

[105] Carl M Bender, Dorje C Brody, and Bernhard K Meister. Quantum mechanical carnot engine. Journal of Physics A: Mathematical and General, 33(24):4427, 2000.

[106] Jianhui Wang and Jizhou He. Optimization on a three-level heat engine working with two noninteracting fermions in a one-dimensional box trap. Journal of Applied Physics, 111(4):043505, 2012.

[107] Xiao-Li Huang, DY Guo, SL Wu, and XX Yi. Multilevel quantum otto heat engines with identical particles. Quantum Information Processing, 17:1–14, 2018.

[108] Obinna Abah and Eric Lutz. Optimal performance of a quantum otto refrigerator. Europhysics Letters, 113(6):60002, 2016.

[109] Andrea Insinga, Bjarne Andresen, and Peter Salamon. Thermodynamical analysis of a quantum heat engine based on harmonic oscillators. Physical Review E, 94(1):012119, 2016.

[110] Jianhui Wang, Zhuolin Ye, Yiming Lai, Weisheng Li, and Jizhou He. Efficiency at maximum power of a quantum heat engine based on two coupled oscillators. Physical Review E, 91(6):062134, 2015.

[111] Jing Li, E Ya Sherman, and Andreas Ruschhaupt. Quantum heat engine based on a spin-orbit-and zeeman-coupled bose-einstein condensate. Physical Review A, 106(3):L030201, 2022.

[112] Enrique Munoz and Francisco J Pena. Quantum heat engine in the relativistic limit: The case of a dirac particle. Physical Review E, 86(6):061108, 2012.

[113] Francisco J Peña, Michel Ferré, PA Orellana, René G Rojas, and P Vargas. Optimization of a relativistic quantum mechanical engine. Physical Review E, 94(2):022109, 2016.

[114] Konstantin E Dorfman, Dmitri V Voronine, Shaul Mukamel, and Marlan O Scully. Photosynthetic reaction center as a quantum heat engine. Proceedings of the National Academy of Sciences, 110(8):2746–2751, 2013.

[115] Ferdi Altintas, Ali ÜC Hardal, and Özgür E Müstecaplıoglu. Quantum correlated heat engine with spin squeezing. Physical Review E, 90(3):032102, 2014.

[116] George Thomas and Ramandeep S Johal. Coupled quantum otto cycle. Physical Review E, 83(3):031135, 2011.

[117] Xiao-Li Huang, Xin-Ya Niu, Xiao-Ming Xiu, and Xue-Xi Yi. Quantum stirling heat engine and refrigerator with single and coupled spin systems. The European Physical Journal D, 68:1–8, 2014.

[118] S Lin and Z Song. Non-hermitian heat engine with all-quantum-adiabatic-process cycle. Journal of Physics A: Mathematical and Theoretical, 49(47):475301, 2016.

[119] Ali ÜC Hardal, Nur Aslan, CM Wilson, and Özgür E Müstecaplıoğlu. Quantum heat engine with coupled superconducting resonators. Physical Review E, 96(6):062120, 2017.

[120] Nicolás F Del Grosso, Fernando C Lombardo, Francisco D Mazzitelli, and Paula I Villar. Quantum otto cycle in a superconducting cavity in the nonadiabatic regime. Physical Review A, 105(2):022202, 2022.

[121] Marlan O Scully, Kimberly R Chapin, Konstantin E Dorfman, Moochan Barnabas Kim, and Anatoly Svidzinsky. Quantum heat engine power can be increased by noise-induced coherence. Proceedings of the National Academy of Sciences, 108(37):15097–15100, 2011.

[122] Konstantin E Dorfman, Dazhi Xu, and Jianshu Cao. Efficiency at maximum power of a laser quantum heat engine enhanced by noise-induced coherence. Physical Review E, 97(4):042120, 2018.

[123] HT Quan, P Zhang, and CP Sun. Quantum-classical transition of photon-carnot engine induced by quantum decoherence. Physical Review E, 73(3):036122, 2006.

[124] Raoul Dillenschneider and Eric Lutz. Energetics of quantum correlations. Europhysics Letters, 88(5):50003, 2009.

[125] Deniz Türkpençe, Ferdi Altintas, Mauro Paternostro, and Özgür E Müstecaplioğlu. A photonic carnot engine powered by a spin-star network. Europhysics Letters, 117(5):50002, 2017.

[126] O Fialko and DW Hallwood. Isolated quantum heat engine. Physical Review Letters, 108(8):085303, 2012.

[127] Nicole Yunger Halpern, Christopher David White, Sarang Gopalakrishnan, and Gil Refael. Quantum engine based on many-body localization. Physical Review B, 99(2):024203, 2019.

[128] David Von Lindenfels, Oliver Gräb, Christian T Schmiegelow, Vidyut Kaushal, Jonas Schulz, Mark T Mitchison, John Goold, Ferdinand Schmidt-Kaler, and Ulrich G Poschinger. Spin heat engine coupled to a harmonic-oscillator flywheel. Physical Review Letters, 123(8):080602, 2019.

[129] Gleb Maslennikov, Shiqian Ding, Roland Hablützel, Jaren Gan, Alexandre Roulet, Stefan Nimmrichter, Jibo Dai, Valerio Scarani, and Dzmitry Matsukevich. Quantum absorption refrigerator with trapped ions. Nature Communications, 10(1):1–8, 2019.

[130] Johannes Roßnagel, Samuel T Dawkins, Karl N Tolazzi, Obinna Abah, Eric Lutz, Ferdinand Schmidt-Kaler, and Kilian Singer. A single-atom heat engine. Science, 352(6283):325–329, 2016.

[131] J-W Zhang, J-Q Zhang, G-Y Ding, J-C Li, J-T Bu, B Wang, L-L Yan, S-L Su, L Chen, F Nori, et al. Dynamical control of quantum heat engines using exceptional points. Nature Communications, 13(1):6225, 2022.

[132] J-T Bu, J-Q Zhang, G-Y Ding, J-C Li, J-W Zhang, B Wang, W-Q Ding, W-F Yuan, L Chen, ŞK Özdemir, et al. Enhancement of quantum heat engine by encircling a liouvillian exceptional point. Physical Review Letters, 130(11): 110402, 2023.

[133] James Klatzow, Jonas N Becker, Patrick M Ledingham, Christian Weinzetl, Krzysztof T Kaczmarek, Dylan J Saunders, Joshua Nunn, Ian A Walmsley, Raam Uzdin, and Eilon Poem. Experimental demonstration of quantum effects in the operation of microscopic heat engines. Physical Review Letters, 122(11): 110601, 2019.

[134] Yueyang Zou, Yue Jiang, Yefeng Mei, Xianxin Guo, and Shengwang Du. Quantum heat engine using electromagnetically induced transparency. Physical Review Letters, 119(5):050602, 2017.

[135] Quentin Bouton, Jens Nettersheim, Sabrina Burgardt, Daniel Adam, Eric Lutz, and Artur Widera. A quantum heat engine driven by atomic collisions. Nature Communications, 12(1):2063, 2021.

[136] Jean-Philippe Brantut, Charles Grenier, Jakob Meineke, David Stadler, Sebastian Krinner, Corinna Kollath, Tilman Esslinger, and Antoine Georges. A thermoelectric heat engine with ultracold atoms. Science, 342(6159): 713–715, 2013.

[137] John PS Peterson, Tiago B Batalhão, Marcela Herrera, Alexandre M Souza, Roberto S Sarthour, Ivan S Oliveira, and Roberto M Serra. Experimental characterization of a spin quantum heat engine. Physical Review Letters, 123 (24):240601, 2019.

[138] VF Lisboa, PR Dieguez, JR Guimarães, JFG Santos, and RM Serra. Experimental investigation of a quantum heat engine powered by generalized measurements. Physical Review A, 106(2):022436, 2022.

[139] K Ono, SN Shevchenko, T Mori, S Moriyama, and Franco Nori. Analog of a quantum heat engine using a single-spin qubit. Physical Review Letters, 125 (16):166802, 2020.

[140] Martin Josefsson, Artis Svilans, Adam M Burke, Eric A Hoffmann, Sofia Fahlvik, Claes Thelander, Martin Leijnse, and Heiner Linke. A quantum-dot heat engine operating close to the thermodynamic efficiency limits. Nature nanotechnology, 13(10):920–924, 2018.

[141] Kunkun Wang, Ruqiao Xia, Léa Bresque, and Peng Xue. Experimental demonstration of a quantum engine driven by entanglement and local measurements. Physical Review Research, 4(3):L032042, 2022.

[142] Filipe V Melo, Nahum Sá, Itzhak Roditi, Alexandre M Souza, Ivan S Oliveira, Roberto S Sarthour, and Gabriel T Landi. Implementation of a two-stroke quantum heat engine with a collisional model. Physical Review A, 106(3): 032410, 2022.

[143] Feng-Jui Chan, Yi-Te Huang, Jhen-Dong Lin, Huan-Yu Ku, Jui-Sheng Chen, Hong-Bin Chen, and Yueh-Nan Chen. Maxwell's two-demon engine under pure dephasing noise. Physical Review A, 106(5):052201, 2022.

[144] Xinfang Nie, Xuanran Zhu, Keyi Huang, Kai Tang, Xinyue Long, Zidong Lin, Yu Tian, Chudan Qiu, Cheng Xi, Xiaodong Yang, et al. Experimental realization of a quantum refrigerator driven by indefinite causal orders. Physical Review Letters, 129(10):100603, 2022.

[145] Sei Suzuki, Jun-ichi Inoue, and Bikas K Chakrabarti. Quantum Ising phases and transitions in transverse Ising models, volume 862. Springer, 2012.

[146] John B Parkinson and Damian JJ Farnell. An introduction to quantum spin systems, volume 816. Springer, 2010.

[147] Chayan Purkait and Asoka Biswas. Measurement-based quantum otto engine with a two-spin system coupled by anisotropic interaction: Enhanced efficiency at finite times. Physical Review E, 107(5):054110, 2023.

[148] Heinz-Peter Breuer, Francesco Petruccione, et al. The theory of open quantum systems. Oxford University Press on Demand, 2002.

[149] Marco Cattaneo, Gian Luca Giorgi, Sabrina Maniscalco, and Roberta Zambrini. Local versus global master equation with common and separate baths: superiority of the global approach in partial secular approximation. New Journal of Physics, 21(11):113045, 2019.

[150] Eric Chitambar and Gilad Gour. Quantum resource theories. Reviews of Modern Physics, 91(2):025001, 2019.

[151] Matteo Lostaglio. An introductory review of the resource theory approach to thermodynamics. Reports on Progress in Physics, 82(11):114001, 2019.

[152] Nelly Huei Ying Ng and Mischa Prebin Woods. Resource theory of quantum thermodynamics: Thermal operations and second laws. In Thermodynamics in the quantum regime: Fundamental aspects and new directions, pages 625–650. Springer, 2019.

[153] Matteo Lostaglio. The resource theory of quantum thermodynamics. PhD thesis, Imperial College London, 2016.

[154] Fernando GSL Brandao, Michał Horodecki, Jonathan Oppenheim, Joseph M Renes, and Robert W Spekkens. Resource theory of quantum states out of thermal equilibrium. Physical Review Letters, 111(25):250404, 2013.

[155] Sai Vinjanampathy and Janet Anders. Quantum thermodynamics. Contemporary Physics, 57(4):545–579, 2016.

[156] Xiao-Li Huang, Xin-Ya Niu, Xiao-Ming Xiu, and Xue-Xi Yi. Quantum stirling heat engine and refrigerator with single and coupled spin systems. The European Physical Journal D, 68(2):1–8, 2014.

[157] Yong Yin, Lingen Chen, Feng Wu, and Yanlin Ge. Work output and thermal efficiency of an endoreversible entangled quantum stirling engine with one dimensional isotropic heisenberg model. Physica A: Statistical Mechanics and its Applications, 547:123856, 2020.

[158] Yu-Han Ma, Shan-He Su, and Chang-Pu Sun. Quantum thermodynamic cycle with quantum phase transition. Physical Review E, 96(2):022143, 2017.

[159] George Thomas, Debmalya Das, and Sibasish Ghosh. Quantum heat engine based on level degeneracy. Physical Review E, 100(1):012123, 2019.

[160] Sarbani Chatterjee, Arghadip Koner, Sohini Chatterjee, and Chandan Kumar. Temperature-dependent maximization of work and efficiency in a degeneracy-assisted quantum stirling heat engine. Physical Review E, 103(6): 062109, 2021.

[161] Yong Yin, Lingen Chen, and Feng Wu. Optimal power and efficiency of quantum stirling heat engines. The European Physical Journal Plus, 132: 1–10, 2017.

[162] Hasan Saygin and Altuğ Şişman. Quantum degeneracy effect on the work output from a stirling cycle. Journal of Applied Physics, 90(6):3086–3089, 2001.

[163] Giacomo Serafini, Stefano Zippilli, and Irene Marzoli. Optomechanical stirling heat engine driven by feedback-controlled light. Physical Review A, 102(5): 053502, 2020.

[164] Altuğ Şişman and Hasan Saygin. Efficiency analysis of a stirling power cycle under quantum degeneracy conditions. Physica Scripta, 63(4):263, 2001.

[165] Yong Yin, Lingen Chen, and Feng Wu. Performance of quantum stirling heat engine with numerous copies of extreme relativistic particles confined in 1d potential well. Physica A: Statistical Mechanics and its Applications, 503: 58–70, 2018.

[166] S Hamedani Raja, Sabrina Maniscalco, Gheorghe-Sorin Paraoanu, Jukka P Pekola, and N Lo Gullo. Finite-time quantum stirling heat engine. New Journal of Physics, 23(3):033034, 2021.

[167] Nikhil Gupt, Srijan Bhattacharyya, and Arnab Ghosh. Statistical generalization of regenerative bosonic and fermionic stirling cycles. Phys. Rev. E, 104:054130, Nov 2021.

[168] Kay Brandner, Michael Bauer, and Udo Seifert. Universal coherence-induced power losses of quantum heat engines in linear response. Phys. Rev. Lett., 119:170602, Oct 2017.

[169] Pritam Chattopadhyay, Ayan Mitra, Goutam Paul, and Vasilios Zarikas. Bound on efficiency of heat engine from uncertainty relation viewpoint. Entropy, 23(4), 2021. ISSN 1099-4300.

[170] Selçuk Çakmak. Benchmarking quantum stirling and otto cycles for an interacting spinsystem. J. Opt. Soc. Am. B, 39(4):1209–1215, Apr 2022.

[171] Yong Yin, Lingen Chen, and Feng Wu. Optimal power and efficiency of quantum stirling heat engines. The European Physical Journal Plus, 132(1): 1–10, 2017.

[172] Kay Brandner, Michael Bauer, and Udo Seifert. Universal coherence-induced power losses of quantum heat engines in linear response. Physical Review Letters, 119(17):170602, 2017.

[173] S Hamedani Raja, Sabrina Maniscalco, Gheorghe-Sorin Paraoanu, Jukka P Pekola, and N Lo Gullo. Finite-time quantum stirling heat engine. New Journal of Physics, 23(3):033034, 2021.

[174] Nikhil Gupt, Srijan Bhattacharyya, and Arnab Ghosh. Statistical generalization of regenerative bosonic and fermionic stirling cycles. Physical Review E, 104(5):054130, 2021.

[175] Feng Pan, Nan Ma, Xin Guan, and JP Draayer. First order quantum phase transitions of the xx spin-1/2 chain in a uniform transverse field. Physics Letters A, 367(6):450–453, 2007.

[176] Fang Zhao, Fu-Quan Dou, and Qing Zhao. Quantum battery of interacting spins with environmental noise. Physical Review A, 103(3):033715, 2021.

[177] Eduardo Mascarenhas, Helena Bragança, Ross Dorner, M França Santos, Vlatko Vedral, Kavan Modi, and John Goold. Work and quantum phase transitions: Quantum latency. Physical Review E, 89(6):062103, 2014.

[178] Michele Campisi and Rosario Fazio. The power of a critical heat engine. Nature Communications, 7(1):1–5, 2016.

[179] Suman Chand and Asoka Biswas. Critical-point behavior of a measurement-based quantum heat engine. Physical Review E, 98(5):052147, 2018.

[180] Michal Kloc, Pavel Cejnar, and Gernot Schaller. Collective performance of a finite-time quantum otto cycle. Physical Review E, 100(4):042126, 2019.

[181] Thomás Fogarty and Thomas Busch. A many-body heat engine at criticality. Quantum Science and Technology, 6(1):015003, nov 2020.

[182] Victor Mukherjee, Uma Divakaran, Adolfo del Campo, et al. Universal finite-time thermodynamics of many-body quantum machines from kibble-zurek scaling. Physical Review Research, 2(4):043247, 2020.

[183] Yang-Yang Chen, Gentaro Watanabe, Yi-Cong Yu, Xi-Wen Guan, and Adolfo del Campo. An interaction-driven many-particle quantum heat engine and its universal behavior. npj Quantum Information, 5(1):1–6, 2019.

[184] XL Huang, LC Wang, XX Yi, et al. Quantum brayton cycle with coupled systems as working substance. Physical Review E, 87(1):012144, 2013.

[185] Yunus A Cengel, Michael A Boles, and M Kanoglu. Thermodynamics: An Engineering Approach 9th Editon. The McGraw-Hill Companies, Inc., New York, 2019.

[186] Subir Sachdev. Quantum phase transitions. Cambridge university press, 2011.

[187] Xinhua Peng, Jiangfeng Du, and Dieter Suter. Quantum phase transition of ground-state entanglement in a heisenberg spin chain simulated in an nmr quantum computer. Physical review A, 71(1):012307, 2005.

[188] Jingfu Zhang, Fernando M Cucchietti, Raymond Laflamme, and Dieter Suter. Defect production in non-equilibrium phase transitions: experimental investigation of the kibble–zurek mechanism in a two-qubit quantum simulator. New Journal of Physics, 19(4):043001, 2017.

[189] R Islam, EE Edwards, K Kim, S Korenblit, C Noh, H Carmichael, G-D Lin, L-M Duan, C-C Joseph Wang, JK Freericks, et al. Onset of a quantum phase transition with a trapped ion quantum simulator. Nature Communications, 2 (1):1–6, 2011.

[190] Ping Lou, Wen-Chin Wu, and Ming-Che Chang. Quantum phase transition in spin-1 2 xx heisenberg chain with three-spin interaction. Physical Review B, 70(6):064405, 2004.

[191] G Lagmago Kamta, Andrei Y Istomin, and Anthony F Starace. Thermal entanglement of two interacting qubits in a static magnetic field. The European Physical Journal D, 44(2):389–400, 2007.

[192] Chen Shi-Rong, Xia Yun-Jie, and Man Zhong-Xiao. Quantum phase transition and entanglement in heisenberg xx spin chain with impurity. Chinese Physics B, 19(5):050304, 2010.

[193] Iulia M Georgescu, Sahel Ashhab, and Franco Nori. Quantum simulation. Reviews of Modern Physics, 86(1):153, 2014.

[194] Fang Zhao, Fu-Quan Dou, and Qing Zhao. Quantum battery of interacting spins with environmental noise. Physical Review A, 103(3):033715, 2021.

[195] Eduardo Mascarenhas, Helena Bragança, Ross Dorner, M França Santos, Vlatko Vedral, Kavan Modi, and John Goold. Work and quantum phase transitions: Quantum latency. Physical Review E, 89(6):062103, 2014.

[196] Feng Pan, Nan Ma, Xin Guan, and JP Draayer. First order quantum phase transitions of the xx spin-1/2 chain in a uniform transverse field. Physics Letters A, 367(6):450–453, 2007.

[197] MC Arnesen, S Bose, and V Vedral. Natural thermal and magnetic entanglement in the 1d heisenberg model. Physical Review Letters, 87(1): 017901, 2001.

[198] Tobias J Osborne and Michael A Nielsen. Entanglement in a simple quantum phase transition. Physical Review A, 66(3):032110, 2002.

[199] Xiaoguang Wang. Entanglement in the quantum heisenberg xy model. Physical Review A, 64(1):012313, 2001.

[200] G Lagmago Kamta and Anthony F Starace. Anisotropy and magnetic field effects on the entanglement of a two qubit heisenberg xy chain. Physical Review Letters, 88(10):107901, 2002.

[201] Guifre Vidal, José Ignacio Latorre, Enrique Rico, and Alexei Kitaev. Entanglement in quantum critical phenomena. Physical Review Letters, 90 (22):227902, 2003.

[202] Julien Vidal, Guillaume Palacios, and Rémy Mosseri. Entanglement in a second-order quantum phase transition. Physical Review A, 69(2):022107, 2004.

[203] Roya Radgohar and Afshin Montakhab. Global entanglement and quantum phase transitions in the transverse xy heisenberg chain. Physical Review B, 97(2):024434, 2018.

[204] AA Zvyagin. Thermal entanglement of spin chains with quantum critical behavior. Physical Review B, 80(14):144408, 2009.

[205] XL Huang, Huan Xu, XY Niu, and YD Fu. A special entangled quantum heat engine based on the two-qubit heisenberg xx model. Physica Scripta, 88(6): 065008, 2013.

[206] Y.A. Çengel, M.A. Boles, and M. Kanoglu. Thermodynamics: An Engineering Approach. McGraw-Hill series in mechanical engineering. McGraw-Hill Education, 2018.

[207] Rozhin Yousefjani and Abolfazl Bayat. Parallel entangling gate operations and two-way quantum communication in spin chains. Quantum, 5:460, May 2021.

[208] L Tian. Circuit qed and sudden phase switching in a superconducting qubit array. Physical Review Letters, 105(16):167001, 2010.

[209] Alexander van Oudenaarden and JE Mooij. One-dimensional mott insulator formed by quantum vortices in josephson junction arrays. Physical Review Letters, 76(26):4947, 1996.

[210] Cleverson Cherubim, Frederico Brito, and Sebastian Deffner. Non-thermal quantum engine in transmon qubits. Entropy, 21(6), 2019. ISSN 1099-4300. doi: 10.3390/e21060545.

[211] George Thomas and Ramandeep S Johal. Coupled quantum otto cycle. Physical Review E, 83(3):031135, 2011.

[212] Ferdi Altintas and Özgür E Müstecaplıoğlu. General formalism of local thermodynamics with an example: Quantum otto engine with a spin-1/2 coupled to an arbitrary spin. Physical Review E, 92(2):022142, 2015.

[213] XL Huang, Yang Liu, Zhen Wang, and XY Niu. Special coupled quantum otto cycles. The European Physical Journal Plus, 129(1):1–8, 2014.

[214] Arpan Das and Sibasish Ghosh. Measurement based quantum heat engine with coupled working medium. Entropy, 21(11):1131, 2019.

[215] Suman Chand, Shubhrangshu Dasgupta, and Asoka Biswas. Finite-time performance of a single-ion quantum otto engine. Physical Review E, 103 (3):032144, 2021.

[216] Paolo Abiuso and Vittorio Giovannetti. Non-markov enhancement of maximum power for quantum thermal machines. Physical Review A, 99(5): 052106, 2019.

[217] Arpan Das and Victor Mukherjee. Quantum-enhanced finite-time otto cycle. Physical Review Research, 2(3):033083, 2020.

[218] Saar Rahav, Upendra Harbola, and Shaul Mukamel. Heat fluctuations and coherences in a quantum heat engine. Physical Review A, 86(4):043843, 2012.

[219] Raam Uzdin, Amikam Levy, and Ronnie Kosloff. Equivalence of quantum heat machines, and quantum-thermodynamic signatures. Physical Review X, 5(3):031044, 2015.

[220] Selçuk Çakmak, Ferdi Altintas, and Özgür E Müstecaplıoğlu. Lipkin-meshkov-glick model in a quantum otto cycle. The European Physical Journal Plus, 131(6):1–9, 2016.

[221] Selçuk Çakmak, Deniz Türkpençe, and Ferdi Altintas. Special coupled quantum otto and carnot cycles. The European Physical Journal Plus, 132 (12):1–10, 2017.

[222] EA Ivanchenko. Quantum otto cycle efficiency on coupled qudits. Physical Review E, 92(3):032124, 2015.

[223] Suman Chand and Asoka Biswas. Measurement-induced operation of two-ion quantum heat machines. Physical Review E, 95(3):032111, 2017.

[224] Chayan Purkait and Asoka Biswas. Performance of heisenberg-coupled spins as quantum stirling heat machine near quantum critical point. Physics Letters A, 442:128180, 2022.

[225] AC Duriez, D Martínez-Tibaduiza, and AZ Khoury. Algebraic approach to a nonadiabatic coupled otto cycle. Physical Review A, 106(6):062212, 2022.

[226] AV Dodonov, D Valente, and T Werlang. Quantum power boost in a nonstationary cavity-qed quantum heat engine. Journal of Physics A: Mathematical and Theoretical, 51(36):365302, 2018.

[227] Gustavo Rigolin. Thermal entanglement in the two-qubit heisenberg xyz model. International Journal of Quantum Information, 2(03):393–405, 2004.

[228] L Zhou, HS Song, YQ Guo, and C Li. Enhanced thermal entanglement in an anisotropic heisenberg xyz chain. Physical Review A, 68(2):024301, 2003.

[229] Yang Guo-Hui, Gao Wen-Bin, Zhou Ling, and Song He-Shan. Entanglement in anisotropic heisenberg xyz chain with inhomogeneous magnetic field. Communications in Theoretical Physics, 48(3):453, 2007.

[230] ZN Hu, SH Youn, K Kang, and CS Kim. Entanglement of a two-qubit system with anisotropic couplings in nonuniform magnetic fields. Journal of Physics A: Mathematical and General, 39(33):10523, 2006.

[231] M Rojas, SM de Souza, and Onofre Rojas. Entangled state teleportation through a couple of quantum channels composed of xxz dimers in an ising-xxz diamond chain. Annals of Physics, 377:506–517, 2017.

[232] Ye Yeo, Tongqi Liu, Yu-En Lu, and Qi-Zhong Yang. Quantum teleportation via a two-qubit heisenberg xy chain—effects of anisotropy and magnetic field. Journal of Physics A: Mathematical and General, 38(14):3235, 2005.

[233] Yue Zhou and G-F Zhang. Quantum teleportation via a two-qubit heisenberg xxz chain–effects of anisotropy and magnetic field. The European Physical Journal D, 47(2):227–231, 2008.

[234] Saeed Haddadi, Mohammad Reza Pourkarimi, Youssef Khedif, and Mohammed Daoud. Tripartite measurement uncertainty in a heisenberg xxz model. The European Physical Journal Plus, 137(1):1–13, 2022.

[235] Srijon Ghosh, Aditi Sen, et al. Dimensional enhancements in a quantum battery with imperfections. Physical Review A, 105(2):022628, 2022.

[236] Srijon Ghosh, Titas Chanda, Aditi Sen, et al. Enhancement in the performance of a quantum battery by ordered and disordered interactions. Physical Review A, 101(3):032115, 2020.

[237] Tanoy Kanti Konar, Leela Ganesh Chandra Lakkaraju, and Aditi Sen De. Quantum battery with non-hermitian charging. arXiv preprint arXiv:2203.09497, 2022.

[238] Yair Rezek. Reflections on friction in quantum mechanics. Entropy, 12(8): 1885–1901, 2010.

[239] Lorenzo Buffoni, Andrea Solfanelli, Paola Verrucchi, Alessandro Cuccoli, and Michele Campisi. Quantum measurement cooling. Physical Review Letters, 122(7):070603, 2019.

[240] Cleverson Cherubim, Thiago R de Oliveira, and Daniel Jonathan. Nonadiabatic coupled-qubit otto cycle with bidirectional operation and efficiency gains. Physical Review E, 105(4):044120, 2022.

[241] Patrice A Camati, Jonas FG Santos, and Roberto M Serra. Coherence effects in the performance of the quantum otto heat engine. Physical Review A, 99 (6):062103, 2019.

[242] J Robert Johansson, Paul D Nation, and Franco Nori. Qutip: An open-source python framework for the dynamics of open quantum systems. Computer Physics Communications, 183(8):1760–1772, 2012.

[243] Wolfgang Niedenzu, David Gelbwaser-Klimovsky, and Gershon Kurizki. Performance limits of multilevel and multipartite quantum heat machines. Physical Review E, 92(4):042123, 2015.

[244] Victor Mukherjee, Wolfgang Niedenzu, Abraham G Kofman, and Gershon Kurizki. Speed and efficiency limits of multilevel incoherent heat engines. Physical Review E, 94(6):062109, 2016.

[245] XL Huang, LC Wang, XX Yi, et al. Quantum brayton cycle with coupled systems as working substance. Physical Review E, 87(1):012144, 2013.

[246] Cleverson Cherubim, Frederico Brito, and Sebastian Deffner. Non-thermal quantum engine in transmon qubits. Entropy, 21(6):545, 2019.

[247] Li-Mei Zhao and Guo-Feng Zhang. Entangled quantum otto heat engines based on two-spin systems with the dzyaloshinski–moriya interaction. Quantum Information Processing, 16(9):1–13, 2017.

[248] Sachin Sonkar and Ramandeep S. Johal. Spin-based quantum otto engines and majorization. Phys. Rev. A, 107:032220, Mar 2023.

[249] Abdelkader El Makouri, Abdallah Slaoui, and Mohammed Daoud. Enhancing the performance of coupled quantum otto thermal machines without entanglement and quantum correlations. Journal of Physics B: Atomic, Molecular and Optical Physics, 56(8):085501, 2023.

[250] Wolfgang Niedenzu and Gershon Kurizki. Cooperative many-body enhancement of quantum thermal machine power. New Journal of Physics, 20 (11):113038, 2018.

[251] Michal Kloc, Pavel Cejnar, and Gernot Schaller. Collective performance of a finite-time quantum otto cycle. Physical Review E, 100(4):042126, 2019.

[252] PW Hess, P Becker, HB Kaplan, A Kyprianidis, AC Lee, B Neyenhuis, G Pagano, Phil Richerme, C Senko, J Smith, et al. Non-thermalization in trapped atomic ion spin chains. Philosophical Transactions of the Royal Society A: Mathematical, Physical and Engineering Sciences, 375(2108): 20170107, 2017.

[253] Tobias Graß and Maciej Lewenstein. Trapped-ion quantum simulation of tunable-range heisenberg chains. EPJ Quantum Technology, 1(1):1–20, 2014.

[254] Christopher Monroe, Wes C Campbell, L-M Duan, Z-X Gong, Alexey V Gorshkov, PW Hess, R Islam, K Kim, Norbert M Linke, Guido Pagano, et al. Programmable quantum simulations of spin systems with trapped ions. Reviews of Modern Physics, 93(2):025001, 2021.

[255] C Monroe, WC Campbell, EE Edwards, R Islam, D Kafri, S Korenblit, A Lee, P Richerme, C Senko, and J Smith. Quantum simulation of spin models with trapped ions. In Proceedings of the International School of Physics 'Enrico Fermi,'Course, volume 189, pages 169–187, 2015.

[256] Hai Li, Jian Zou, Jun-Gang Li, Bin Shao, and Lian-Ao Wu. Revisiting the quantum szilard engine with fully quantum considerations. Annals of Physics, 327(12):2955–2971, 2012.

[257] Andrew N Jordan, Cyril Elouard, and Alexia Auffèves. Quantum measurement engines and their relevance for quantum interpretations. Quantum Studies: Mathematics and Foundations, pages 1–13, 2019.

[258] Suman Chand and Asoka Biswas. Single-ion quantum otto engine with always-on bath interaction. EPL (Europhysics Letters), 118(6):60003, 2017.

[259] Xiao-Li Huang, AN Yang, HW Zhang, SQ Zhao, and SL Wu. Two particles in measurement-based quantum heat engine without feedback control. Quantum Information Processing, 19(8):1–14, 2020.

[260] Juyeon Yi, Peter Talkner, and Yong Woon Kim. Single-temperature quantum engine without feedback control. Physical Review E, 96(2):022108, 2017.

[261] Zhiyuan Lin, Shanhe Su, Jingyi Chen, Jincan Chen, and Jonas FG Santos. Suppressing coherence effects in quantum-measurement-based engines. Physical Review A, 104(6):062210, 2021.

[262] Xiao-Li Huang, AN Yang, HW Zhang, SQ Zhao, and SL Wu. Two particles in measurement-based quantum heat engine without feedback control. Quantum Information Processing, 19(8):1–14, 2020.

[263] Guangqian Jiao, Shoubao Zhu, Jizhou He, Yongli Ma, and Jianhui Wang. Fluctuations in irreversible quantum otto engines. Physical Review E, 103(3): 032130, 2021.

[264] Juyeon Yi, Peter Talkner, and Yong Woon Kim. Single-temperature quantum engine without feedback control. Physical Review E, 96(2):022108, 2017.

[265] Nicolò Piccione, Gabriele De Chiara, and Bruno Bellomo. Power maximization of two-stroke quantum thermal machines. Physical Review A, 103(3):032211, 2021.

[266] Gershon Kurizki and Abraham G Kofman. Thermodynamics and Control of Open Quantum Systems. Cambridge University Press, 2022.

[267] Roie Dann, Amikam Levy, and Ronnie Kosloff. Time-dependent markovian quantum master equation. Physical Review A, 98(5):052129, 2018.

[268] Anthony J Leggett, SDAFMGA Chakravarty, Alan T Dorsey, Matthew PA Fisher, Anupam Garg, and Wilhelm Zwerger. Dynamics of the dissipative two-state system. Reviews of Modern Physics, 59(1):1, 1987.

[269] Tameem Albash, Sergio Boixo, Daniel A Lidar, and Paolo Zanardi. Quantum adiabatic markovian master equations. New Journal of Physics, 14(12):123016, 2012.

[270] Li-Zhen Hu, Zhong-Xiao Man, and Yun-Jie Xia. Steady-state entanglement and thermalization of coupled qubits in two common heat baths. Quantum Information Processing, 17(3):1–14, 2018.

[271] Jie-Qiao Liao, Jin-Feng Huang, Le-Man Kuang, et al. Quantum thermalization of two coupled two-level systems in eigenstate and bare-state representations. Physical Review A, 83(5):052110, 2011.

[272] Bao-Ming Xu, Jian Zou, Li-Sha Guo, and Xiang-Mu Kong. Effects of quantum coherence on work statistics. Physical Review A, 97(5):052122, 2018.

[273] Kingshuk Adhikary, Ozgur E Mustecaplioglu, and Bimalendu Deb. Dissipative phase transition in open tavis-cummings model with two-photon drive. Journal of Physics B: Atomic, Molecular and Optical Physics, 2023.

[274] Devvrat Tiwari and Subhashish Banerjee. Quantum chaos in the dicke model and its variants. arXiv preprint arXiv:2305.15505, 2023.

[275] Andrea Solfanelli, Alessandro Santini, and Michele Campisi. Experimental verification of fluctuation relations with a quantum computer. PRX Quantum, 2(3):030353, 2021.